Establishment of a fluorescence assay for characterization of protein-mediated vesicle fusion and acidification

Dissertation

for the award of the degree
„Doctor rerum naturalium”
of the Georg-August-Universität Göttingen

within the doctoral program: Chemistry
of the Georg-August-University School of Science (GAUSS)

submitted by
Miriam Schwamborn
from Göttingen

Göttingen, 2017

Betreuungsausschuss:

Prof. Dr. Claudia Steinem
Institut für Organische und Biomolekulare Chemie
Georg-August Universität Göttingen

Prof. Dr. Mikael Simons
Max-Planck Institut für Experimentelle Medizin, Göttingen
Institute of Neuronal Cell Biology, Technische Universität München
Deutsches Zentrum für Neurodegenerative Erkrankungen, München

Mitglieder der Prüfungskommission:

Referentin: Prof. Dr. Claudia Steinem

Korreferent: Prof. Dr. Mikael Simons

Weitere Mitglieder der Prüfungskommission:

Prof. Dr. Burkard Geil
Institut für Physikalische Chemie
Georg-August Universität Göttingen

Dr. Sebastian Kruss
Institut für Physikalische Chemie
Georg-August Universität Göttingen

Prof. Dr. Michael Meinecke
European Neuroscience Institute
Georg-August-Universität Göttingen

Prof. Dr. Silvio O. Rizzoli
Universitätsmedizin Göttingen
Georg-August Universität Göttingen

Tag der mündlichen Prüfung: 24.05.2017

Declaration

I, Miriam Schwamborn, hereby certify that my doctoral thesis entitled "Establishment of a fluorescence assay for characterization of protein-mediated vesicle fusion and acidification" has been written independently and with no other sources and aids than quoted.

Göttingen, 2017

Miriam Schwamborn

Meiner Familie

Wir leben nicht, um zu glauben,

sondern um zu lernen.

XIV. Dalai Lama

Abstract. Membrane proteins mediate a manifold of essential transport processes across the lipid membrane of cells and organelles, therewith representing important drug targets. To investigate protein-mediated transport in vitro, model membrane systems separating two aqueous compartments are required.

Pore-spanning lipid bilayers consist of an array of defined cavities in a solid substrate, sealed by a solvent-free lipid membrane, thus meeting the condition for observation of membrane protein mediated active transport. In the current preparation of pore-spanning lipid bilayers physiological conditions, which are crucial to retain the functionality of most membrane proteins, are not permanently maintained. SNARE-proteins mediate membrane fusion and may be used for protein reconstitution into pore-spanning lipid bilayers under physiological conditions. Therefore, the feasibility of a physiological reconstitution method based on SNARE-protein mediated fusion was examined in this work. For this approach the robust F_0F_1-ATPase (ATP synthase) from a thermophilic bacterium was chosen as an exemplary proton pumping protein.

After isolation of the recombinant protein from *Escherichia coli*, its reconstitution efficiency into lipid vesicles was characterized and the ATPase induced vesicle acidification was detected with a membrane-permeable fluorophore. The lipid-coupled fluorophore Oregon Green 488 allowed to quantify the average luminal pH-value of acidified vesicles to $\Delta pH = -0.45$ (pH 7.3 → pH 6.85).

After successful detergent-mediated ATPase reconstitution, a combined fusion and acidification assay for small proteoliposomes, based on the lipid-coupled Oregon Green 488, was introduced. First, the fusion of SNARE-ATPase-vesicles with SNARE-Oregon Green 488-vesicles was monitored by a dequenching of the fluorophore. This phenomenon resulted from the fluorophore dilution by fusion and allowed to quantify the lipid mixing efficiency to 59 %. Through successful fusion the F_0F_1-ATPase should come in contact with the Oregon Green 488, thus allowing to detect acidification in the fusion products. However, acidification of the fusion products was not detectable with Oregon Green 488 in any case, while a general ATPase activity after the fusion process could be proven with the membrane permeable fluorophore.

To assess whether a heterogeneous protein distribution in the fusing vesicle populations might explain the undetectable acidification of fusion products, a fluorescence microscopy based single vesicle assay was established. In this assay, F_0F_1-ATPase was reconstituted into biotinylated, Oregon Green 488-doped vesicles that were immobilized on a NeutrAvidin functionalized glass surface. Only 5 % of all singles vesicles showed a clearly distinguishable ATPase-induced acidification ($\Delta pH = -0.5$ to -2.0, average: $\Delta pH \approx -1$). Averaging the luminal acidification of all immobilized vesicles resulted in $\Delta pH = -0.47$, which was in good agreement with the average luminal pH decrease ($\Delta pH = -0.45$) obtained from the bulk acidification experiments. In order to use SNARE-protein mediated fusion as a reconstitution tool, the functional reconstitution of ATPase itself has to be improved towards a more homogeneous distribution of active protein. For this purpose, the established single vesicle assay will be very helpful.

Zusammenfassung. Membranproteine vermitteln eine Vielzahl von essentiellen Transportprozessen über die Lipidmembran von Zellen und Organellen und stellen wichtige Angriffspunkte für Medikamente dar. Um die Funktion dieser Proteine in einem *in vitro* System untersuchen zu können, müssen zwei getrennte wässrige Volumina vorliegen.

Porenüberspannende Lipidmembranen bestehen aus einer Anordnung von definierten Poren in einem festen Trägermaterial, welche von einer lösungsmittelfreien Lipiddoppelschicht verschlossen werden und stellen somit ein potentielles Modellmembran-System für die Beobachtung des Protein-vermittelten aktiven Transports dar. Derzeit erfolgt die Präparation von porenüberspannenden Lipidmembranen unter nicht physiologischen Bedingungen, welche aber für den Erhalt der Funktionalität der meisten Membranproteine essentiell sind. SNARE-Protein vermittelte Membranfusion könnte als physiologische Rekonstitutionsmethode für andere Membranproteine in die porenüberspannenden Lipidmembranen dienen. Daher wurde in dieser Arbeit die Realisierbarkeit von Membranfusion als physiologische Rekonstitutionsmethode für die F_0F_1-ATPase (ATP Synthase), stellvertretend für andere Membranproteine, untersucht.

Dazu wurde zunächst die F_0F_1-ATPase eines thermophilen Bakteriums rekombinant aus *Escherichia coli* isoliert und die Rekonstitutionseffizienz in Lipidvesikel charakterisiert. Die aus der Protonenpumpen Aktivität resultierende Acidifikation der Vesikel Lumina wurde zunächst mit Hilfe eines membranpermeablen, pH-sensitiven Fluorophors nachgewiesen und anschließend mittels des lipidgebundenen Fluorophors Oregon Green 488 quantifiziert ($\Delta \mathrm{pH} = -0.45$, pH 7.3 → pH 6.85).

Nach erfolgreicher Detergenz-vermittelter Rekonstitution der F_0F_1-ATPase wurde ein kombinierter Fusions- und Acidifikations-*Assay* auf Basis des lipidgebundenen Oregon Green 488 etabliert. Zuerst lässt sich damit die Membranfusion zwischen zwei Vesikel Populationen – SNARE-ATPase-Vesikel und SNARE-Oregon Green 488-Vesikel – über ein Dequenching des Fluorophors beobachten. Dieser Effekt resultiert aus der Verdünnung des Fluorophors durch die Fusion und ermöglichte es, die Lipidvermischungseffizienz auf 59 % zu quantifizieren. Durch eine erfolgreiche Fusion hätte die F_0F_1-ATPase mit dem Oregon Green 488 in Verbindung kommen sollen, um somit eine Detektion von ATPase-verursachter Acidifikation in den Fusionsprodukten zu ermöglichen. Die Acidifikation der Fusionsprodukte ließ sich in keinem Experiment detektieren, jedoch konnte mit Hilfe des membran-permeablen Fluorophors eine generelle ATPase Aktivität nach dem Fusionsprozess nachgewiesen werden.

Um zu untersuchen, ob eine heterogene Proteinverteilung in den fusionierenden Vesikel Populationen, eine Ursache für die nicht messbare ATPase Aktivität sein könnte, wurde ein Mikroskopie basierter *Single vesicle assay* entwickelt. Hierfür wurde nur die F_0F_1-ATPase in biotinylierte, Oregon Green 488 haltige Vesikel rekonstituiert, welche mittels NeutrAvidin auf einer Glasoberfläche immobilisiert wurden. Von allen immobilisierten ATPase-Vesikeln zeigten nur 5 % eine eindeutige Acidifikation ($\Delta \mathrm{pH} = -0.5$ bis -2.0, Durchschnitt: $\Delta \mathrm{pH} \approx -1$). Eine Mittelung der pH-Werte aller einzelnen Vesikel resultierte in $\Delta \mathrm{pH} = -0.47$, was gut mit der durchschnittlichen Acidifikation ($\Delta \mathrm{pH} = -0.45$) aus den Küvetten Messungen übereinstimmt. Bevor also eine Proteinrekonstitution mittels Membranfusion weiterverfolgt wird, muss zunächst die direkte F_0F_1-ATPase Rekonstitution hinsichtlich einer homogenen Verteilung aktiven Proteins verbessert werden. Dafür stellt der etablierte *single vesicle assay* eine wertvolle Methode dar.

CONTENT

1 Introduction 1

1.1 Proton gradients across biological membranes 1

1.2 Structure and function of F_0F_1-ATPase 4

1.2.1 The proton motive force provides energy for ATP synthesis 7

1.3 Model membrane systems for actively induced electrochemical gradients 9

1.3.1 Small and giant proteoliposomes 10

1.3.2 Pore-spanning lipid bilayers 13

2 Scope of thesis 17

3 Materials and methods 19

3.1 Protein chemical methods 19

3.1.1 Expression and purification of TF_0F_1-ATPase in *Escherichia coli* 19

3.1.2 Quantification of protein concentration 21

3.1.3 SDS-Polyacrylamide gel electrophoresis 22

3.2 Lipid chemical and reconstitution methods 24

3.2.1 Preparation of large unilamellar vesicles 24

3.2.2 Protein reconstitution 26

3.2.2.1 Reconstitution by the direct method 27

3.2.2.2 Reconstitution by the co-micellization method 28

3.2.3 Determination of proteoliposome size by dynamic light scattering 28

3.2.4 Determination of the ATPase reconstitution efficiency by density gradient centrifugation 28

3.2.5 Phosphate determination assay 29

3.3 Fluorescence based proteoliposome acidification assays 29

3.3.1 pK_a determination of Oregon Green 488-DHPE and intensity-pH calibration for acidified vesicles in ATPase buffer 35

3.4 Quantitative fusion assay based on OG488-DHPE dequenching 35

3.5 Microscopy based single vesicle assay 36

3.5.1 Principle of fluorescence microscopy ... 36

3.5.2 Silanization & PEGylation of glass slides ... 37

3.5.3 Conduction of the single vesicle assay ... 38

3.5.4 Analysis of the recorded time series ... 39

3.5.5 Characterization of vesicle immobilization strategy ... 41

4 Results ... 43

4.1 Expression and isolation of TF_0F_1-ATPase from *E. coli* DK8 ... 43

4.2 Detergent-mediated reconstitution of the TF_0F_1-ATPase into liposomes ... 45

4.3 Investigation of TF_0F_1-ATPase activity in liposomes with a membrane permeable fluorophore ... 49

4.4 Analysis of the TF_0F_1-ATPase activity with the lipid-coupled pH-sensor Oregon Green 488-DHPE ... 53

4.4.1 Characterization of the pH-dependent Oregon Green 488-DHPE fluorescence ... 54

4.4.2 Results of the Oregon Green 488-DHPE based TF_0F_1-ATPase activity assay ... 58

4.5 Combined fusion and acidification assay based on Oregon Green 488-DHPE ... 61

4.5.1 Characterization of SNARE-mediated vesicle fusion ... 62

4.5.2 Acidification assay after fusion ... 65

4.6 Microscopy-based 2D-single vesicle assay for observation of TF_0F_1-ATPase activity ... 74

4.6.1 Characterization of the vesicle immobilization ... 74

4.6.2 Conduction and analysis of the single vesicles experiments ... 75

4.6.3 Analysis of single vesicle acidification ... 78

5 Discussion ... 83

5.1 Purification of recombinant TF_0F_1-ATPase from *E. coli* DK8 ... 83

5.2 Detergent-mediated ATPase reconstitution into large unilamellar vesicles ... 84

5.3 Monitoring of the ATPase proton pumping activity with ACMA ... 88

5.4 Quantitative Oregon Green 488-DHPE based acidification assay ... 90

5.5 Combined fusion and acidification assay based on Oregon Green 488-DHPE ... 94

5.5.1 Fusion efficiency and acidification assay ... 94

5.5.2 Influence of the ΔN49-complex on the OG488-DHPE fluorescence emission intensity 95

5.5.3 Possible protein heterogeneities in the liposomes 98
5.6 Single vesicle assay 101
5.6.1 ATPase-liposome immobilization 102
5.6.2 TF_0F_1-ATPase activity in attached liposomes 103
6 Conclusion 105
7 Bibliography 107
8 Appendix 125
8.1 List of Figures 125
8.2 Symbols 128
8.3 Abbreviations 129
8.4 Chemicals and consumables 132
8.5 Devices 134
8.6 Software 136
8.7 Calculation of ATPase molecules per vesicle 136
8.8 Matlab Script 138

1 INTRODUCTION

1.1 Proton gradients across biological membranes

Lipid membranes result from the self-assembly of amphiphilic molecules and represent an indispensable prerequisite for the existence of life, as they act as a diffusion barrier allowing to separate a defined aqueous volume from the environment.[1] In a cell, a variety of proteins spanning the membrane enables controlled exchange of chemical substances with the surrounding. These transmembrane proteins may act as receptors and transporters, functioning as channels and carriers for passive transport or as pumps for active transport. These controlled transport processes also allow an energy storage in form of electrochemical gradients.[2] The organization of biological membranes is very complex and the widely-known fluid mosaic model, proposed by Singer and Nicholson in 1972, only represents a very simplified model assuming that the membrane spanning proteins freely diffuse in a homogeneous and fluid lipid bilayer. Today it is known that membrane-associated or membrane spanning proteins account for approx. half of the cell membrane's mass and the organization is not homogeneous at all, but rather patchy with protein and lipid nanoclusters.[3–5] These dynamic nanoscale assemblies, composed of certain lipids (sphingolipids and cholesterol) and proteins, play important roles in membrane trafficking, signaling and virus infection.[4]

Protein-protein as well as protein-lipid interactions allow the formation of protein clusters also in bacterial and mitochondrial membranes like the so-called supercomplexes of the respiratory chain complexes. Formerly, a free diffusion of the proteins involved in the respiratory chain and oxidative phosphorylation was assumed. Recently, it was possible to resolve the detailed organization of these supercomplexes by means of high resolution cryo-electron microscopy. The predominantly found supercomplex with a molecular mass of 1.7 MDa consists of the proton pumps complex I (NADH:ubiquinone oxidoreductase), a complex III dimer (cytochrome bc_1 complex) and complex IV (cytochrome *c* oxidase). Lipids such as cardiolipin, phosphatidylcholine (PC) and phosphatidylethanolamine (PE) were also found to be involved in the supercomplex assembly. Advantages of such a protein assembly might be a stabilization of the electron transport chain and the control of reactive oxygen species production.[6–9]

Besides the protein complexes I, III and IV of the respiratory chain, several other proton pumps exist in prokaryotic and eukaryotic cells that convert energy into proton gradients. Figure 1.1 gives a categorized overview of several proton pumping proteins. Marine bacteria and halobacteria, for example, use light empowered proton pumps like proteorhodopsin and bacteriorhodopsin.[10]

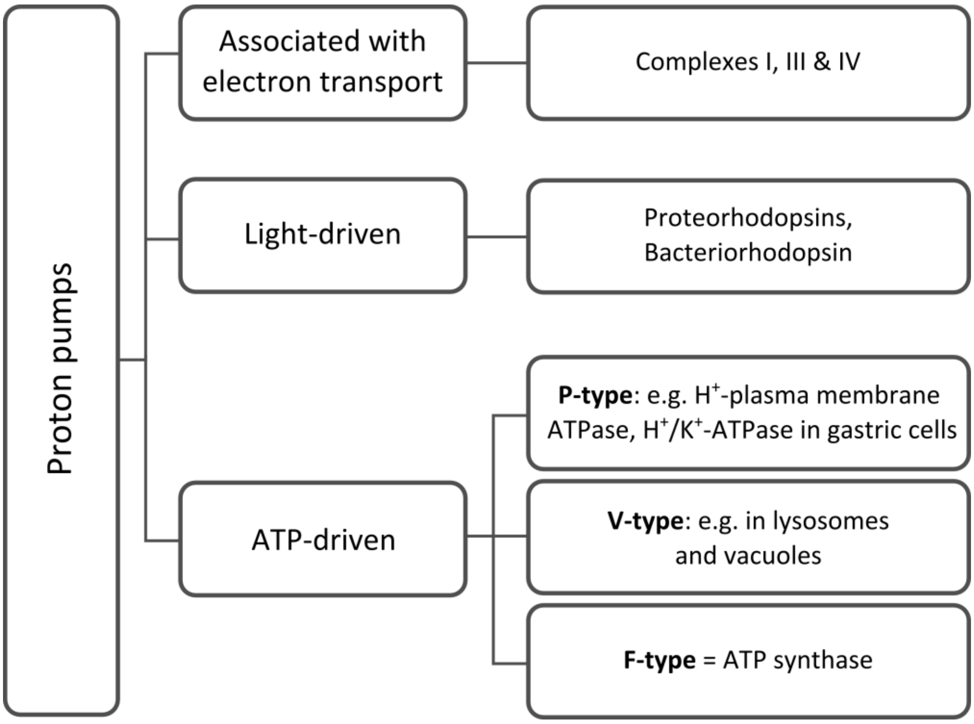
Proton pumps
Associated with electron transport
Complexes I, III & IV
Light-driven
Proteorhodopsins, Bacteriorhodopsin
ATP-driven
P-type: e.g. H+-plasma membrane ATPase, H+/K+-ATPase in gastric cells
V-type: e.g. in lysosomes and vacuoles
F-type = ATP synthase

Figure 1.1. Overview of proton pumping proteins. Besides the proton translocating proteins associated with electron transport in the respiratory chain, a prominent example for a light-driven proton pump is bacteriorhodopsin. ATP-driven proton (and ion) pumps are found among the large P-type ATPase family, as well as in the V-type and F-type ATPase family, although the latter primarily synthesises ATP.

ATP-powered proton pumps, like the H^+-ATPase AHA2 are for example found in plant and fungal cell membranes, where they maintain the membrane potential, which may reach approx. – 300 mV. This is very high compared to the membrane potential of mammalian cells (about – 70 mV), which is generated by the Na^+/K^+-ATPase. Both, H^+-ATPase and Na^+/K^+-ATPase are members of the large P-type ATPase family. A further member of this family is the H^+/K^+-ATPase, which is responsible for production of the strongly acidic gastric acid.[11] Despite transporting different substrates, either as a uniporter or as an antiporter, the basic structure and function of all members of the P-type ATPase family is the same. With energy obtained from ATP hydrolysis, they change between two conformations E1 and E2, with E1 having a high affinity for the substrate to be taken-up from the cytosol. In E2 this affinity is strongly reduced, allowing the substrate to leave the binding pocket and to bind a substrate for transport into the opposite direction, in case of an antiport (Figure 1.2).[12,13]

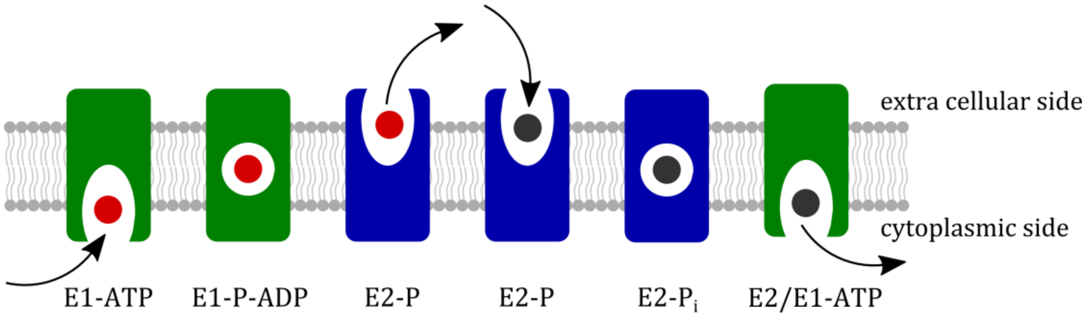

Figure 1.2. Schematic overview of antiport by P-type ATPases. In the E1-state (green), the affinity for the ion to be transported from the cytoplasm to the extracellular side of the membrane (red sphere) is high. In the ion bound E1 state, phosphorylation of an aspartate residue results in a high energy E1-P-ADP state that leads to a conformational change into the E2 state (blue). In this state, the enzyme is open towards the extracellular side, releasing the ion and binding a counter-transport ion (grey). Binding induces a change to the closed conformation and dephosphorylation. ATP binding then leads to a return to the E1 state, where the counter-transport ion is released to the cytoplasm. Modified from Palmgren *et al.*[12,13]

In contrast to the manifold of P-type ATPases, the V-type ATPase only generates proton gradients in the organelles of eukaryotic cells, in order to energize the specific membrane for secondary active sym- or antiport processes or channel-mediated transport. For instance, the neurotransmitter uptake in synaptic vesicles is enabled by a H^+/neurotransmitter antiport, fueled by V-type ATPase. Furthermore, V-type ATPase is present in the vesicles of exo- and endocytosis, Golgi vesicles, lysosomes, endosomes and vacuoles.[14] While the P-type ATPases interchange between two conformations, E1 and E2, for substrate transport, the structure and function of V-ATPase is strikingly different, resembling two coupled rotary motor proteins. Briefly, the water-soluble V_1-part consists of a hexameric ring of three alternating subunits that undergoes conformational changes upon ATP hydrolysis. These changes set the central stalk, which is embedded in the center of the hexameric ring, into rotation, which is transferred to the membrane spanning c-ring. This oligomeric ring belongs to the water insoluble V_0-part and transports protons through the hydrophobic membrane core by rotational motion.[15]

The F-type ATPase, also referred to as F_0F_1-ATPase or ATP synthase, is structurally and functionally related to the V-type ATPase, but *in vivo* preliminary responsible for ATP synthesis from proton gradients, e.g. in the oxidative phosphorylation in mitochondria. However, if the proton gradient depletes, F_0F_1-ATPase is capable of reversing its function, hence, hydrolyzing ATP in order to prevent a collapse of the proton gradient. More detailed information on the F-type ATPase will be given in the subsequent Chapter 1.2.

Figure 1.3 compares the structures of P-type, V-type and F-type ATPase. While P-type ATPases (Figure 1.3 A) consist of one amino acid chain folding into at least five essential domains, V- and F-type ATPases (Figure 1.3 B and C) are large protein assemblies of eight and more subunits.

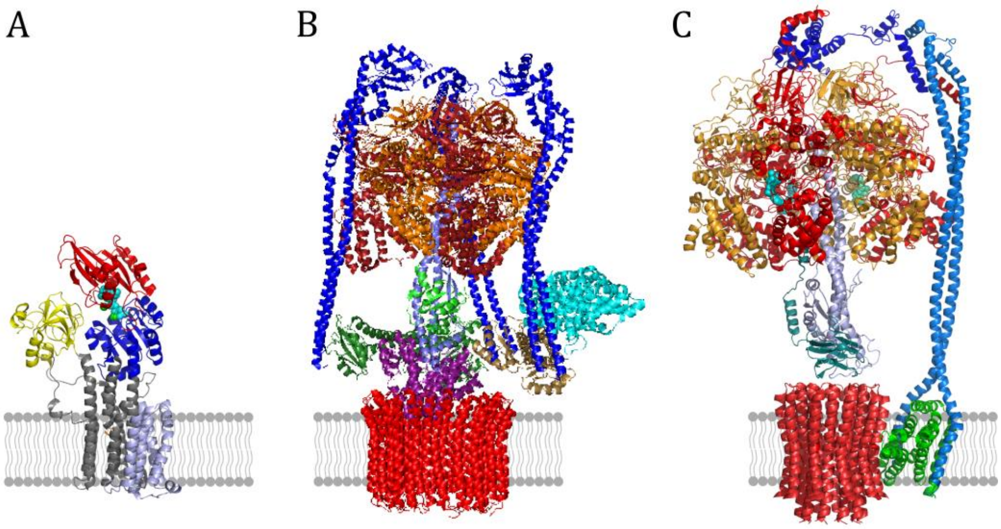

Figure 1.3. Structural comparison of different ATPase families. The crystal structure of a V-type ATPase plasma membrane proton pump (PDB ID: 5ksd) is shown in (A), the cyro-electron microscopy structures of a yeast V-ATPase (PDB ID: 3j9t) and of an *E. coli* F-type ATPase (PDB ID: 5t4o) are shown in (B) and (C), respectively. In P-type ATPases (A), conformational changes allow the entering and expelling of a diversity of substrates into the binding pocket, which is located in between the membrane spanning helices. By contrast, V- and F-type ATPases (B and C) are structurally similar, rotatory machines that use ATP hydrolysis to build-up proton gradients (V-type) or convert the energy stored in proton gradients into chemical energy by synthesizing ATP (F-type).

1.2 Structure and function of F_0F_1-ATPase

ATP synthase or F_0F_1-ATPase is a unique molecular machine that is highly conserved among all species and allows the production of ATP from energy stored in an electrochemical proton gradient and, *vice versa* the generation of proton gradients from the energy of ATP hydrolysis. This interconversion between a proton electrochemical potential ($\Delta\bar{\mu}_{\mathrm{H}^+}$) and chemical energy ($\Delta G$) is mediated by a rotational motion, i.e. mechanical energy. This is possible through the coupling of two autonomously working enzymes: the membrane-spanning F_0 (~120 kDa), mediating proton translocation through the lipid bilayer, and the water soluble F_1 (~380 kDa), responsible for ATP synthesis or hydrolysis, respectively. Both F_1 and F_0 consist of a stator and a rotary part. In bacteria, F_1 is composed of three alternating α- and β-subunits each, forming a hexameric structure with a central bearing for the γ-stalk. δ and ε are subunits connecting F_1 with F_0. The F_0 consists of the monomeric a- and the dimeric b-

subunits that are stators and the oligomeric c-ring rotor, composed of 10–15 c-subunit monomers, depending on the species (Figure 1.4 A). The δ-subunit acts as a connector between the b_2-subunit of F_0 and the α- and β-subunits of F_1. A connection between the rotary subunits γ of F_1 and the c-ring are accomplished by the ε-subunit that additionally acts as an inhibitor of ATP hydrolysis/synthesis.[16,17] Coupling between γ-subunit and c-ring is accomplished by the N-terminal β-sandwich domain of the ε-subunit, while the inhibition is regulated by the C-terminal α-helical domain, which undergoes a drastic conformational change, from a closed hairpin to an open conformation with the α-helical domain stretched out to the N-terminus of the γ-subunit.[17,18]

The downstream translocation of protons through the c_{10-15}-ring, with the a-subunit functioning as an entrance and exit for the protons to the c-subunit H^+-binding site, results in a rotation of oligomeric ring. This motion is transferred to the γ-stalk that induces conformational changes in the α- and β-subunits. Here, ATP synthesis or hydrolysis is catalyzed. α- and β-subunits are composed of an N-terminal domain located towards the membrane plane (bottom), a centrally located nucleotide binding domain and C-terminal domain located at the top. The nucleotides bind between the α- and β-interfaces, while the catalytic sites are located in the β-subunits. While the N-terminal domains form a smooth cavity for the γ-stalk, the C-terminal domains show asymmetric interactions with γ that lead to a cyclic alternating opening and closing of the nucleotide binding cleft or, reversely, conformational changes through ATP hydrolysis set the γ-stalk into rotation.

The so-called binding-change mechanism describes the interplay of γ-rotation and conformational changes of α- and β-subunits that are associated with open and closed states. Figure 1.4 B shows the binding-change mechanism for ATP hydrolysis. In particular, three different α-β-conformations are distinguished: open (O), half-closed (C') or closed (C).[19] During one anticlockwise revolution of the γ-stalk, an ATP is bound at 0° (O-conformation), hydrolyzed at 200° (C-conformation), the ADP released at 240° (C'-conformation) and release of phosphate occurs at 320° (O-conformation) (Figure 1.4 B). First only three different angles (0°, 120° and 240°) of the γ-stalk were found, but single molecule experiments with higher resolution revealed sub-steps of 80° and 40°. The 80° sub-step is induced by ATP binding, while ATP hydrolysis and phosphate release trigger the 40° sub-step. Consequently, the angle of the γ-stalk before the 80° movement is denoted as the binding or waiting angle and that before the 40° movement as the catalytic angle. So for one 360° rotation of the γ-stalk, each of the three catalytic sites consumes one ATP, in particular at angles of 0°, 120° and 240°.[20]

The catalytic mechanism for ATP hydrolysis could be uncovered by observing the rotary movement of single immobilized F_1 molecules with the help of an actin-filament or a small bead attached to the γ-stalk.[21,22] For proving that the ATP synthesis mechanism equals a reversion of the hydrolysis mechanism, a single F_1-molecule was enclosed in femtoliter chamber and a forced clockwise rotation of the γ-stalk by magnetic tweezers resulted in accumulation of a detectable amount of ATP in the chamber. Interestingly, the $\alpha_3\beta_3\gamma$-subcomplex only yielded a low coupling ratio (10 %) between γ-stalk rotation and ATP synthesis, while the $\alpha_3\beta_3\gamma\varepsilon$-subcomplex resulted in a much higher coupling ratio (80 %). Thus, the ε-subunit may also act stabilizing on the γ-stalk.[23]

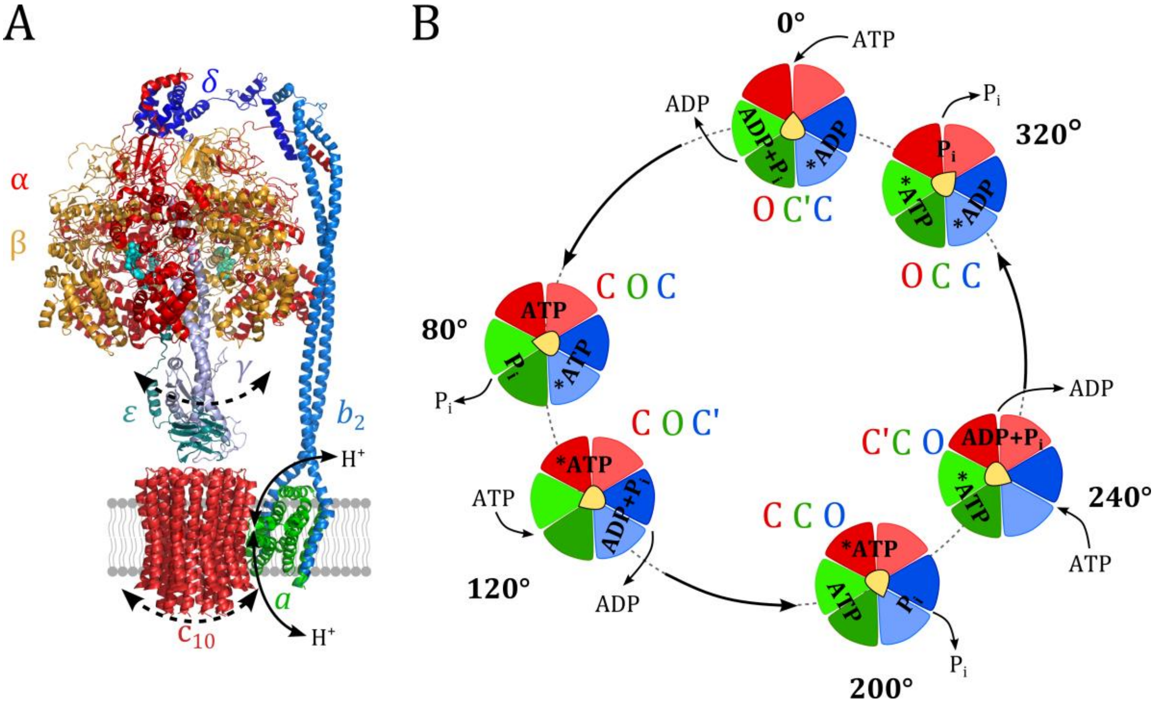

Figure 1.4. (A) Structure of *E. coli* ATP synthase obtained from cryo-electron microscopy (PDB ID: 5t4o). F_0F_1-ATPase is composed of a water soluble F_1-part responsible for ATP synthesis or hydrolysis, respectively. The F_0-part is embedded in the membrane and mediates proton translocation through a rotation of decameric *c*-ring (indicated by dashed arrow). This rotational motion is coupled to the γ-stalk, inducing or resulting from conformational changes in the α- and β-subunits. (B) Scheme of the binding change mechanism of ATP hydrolysis. The two red, green and blue units each correspond to an α-β-subunit pair. Energy from ATP hydrolysis results in conformational changes of the catalytic site on the β-subunits, e.g. referred to as open (O), half-closed (C’) and closed (C). These changes lead to anticlockwise 80° and 40° rotations of the γ-stalk (viewing from the membrane plane), which is coupled to the *c*-ring rotation.[19,20]

For the proton translocation induced rotation of the *E. coli* c_{10}-ring, 36° steps were found under ATP hydrolyzing conditions, but not much about the dynamics of the *c*-ring rotation is known.[20] Generally, it is assumed that protons enter and exit the *c*-ring through two half-channels located in the *a*-subunit, which consists of four membrane embedded α-helices tilted 20°–30° to the membrane plane. A conserved arginine residue at the end of the entering half channel most likely protonates a conserved aspartate residue on position 61 (Asp61) in the *c*-subunits. Upon the protonation the negative charge of Asp61 is neutralized allowing a rotation into the hydrophobic membrane core. Simultaneously, a subunit with protonated Asp61 reaches the second half-channel were the proton can be expelled to the other side of the membrane.[24,25]

In the following a closer look is taken on the electrochemical proton gradient that powers the ATP synthesis or can be generated by ATP hydrolysis activity of F_0F_1-ATPase.

1.2.1 The proton motive force provides energy for ATP synthesis

In 1961 Peter Mitchel published the chemiosmotic theory, postulating that electron transport and adenosine triphosphate (ATP) synthesis are coupled via a proton gradient across the inner mitochondrial membrane. According to this theory, protons are pumped into the mitochondrial intermembrane space by the proteins of the respiratory chain, eventually resulting in an electrochemical potential difference.[26] The electrochemical potential difference $\Delta\bar{\mu}_{\mathrm{H}^+}$ resulting from the proton gradient is composed of an electric potential $\Delta\psi$ and a chemical concentration gradient between a high proton concentration $[\mathrm{H}^+]_\mathrm{p}$ on one side of the membrane and a lower concentration $[\mathrm{H}^+]_\mathrm{n}$ on the other side. Equation 1.1 describes the electrochemical potential, with the Faraday constant F = 96,485 C mol^{-1}, [27] the universal gas constant R = 8.3145 J K^{-1} mol^{-1} [27] and the absolute temperature T.[28]

$$\Delta\bar{\mu}_{\mathrm{H}^+} = \mathrm{F} \cdot \Delta\psi + \mathrm{R}T \cdot \ln\frac{[\mathrm{H}^+]_\mathrm{p}}{[\mathrm{H}^+]_\mathrm{n}} \qquad 1.1$$

$\Delta\mu_{\mathrm{H}^+}$ has the units of J mol^{-1}, considering that the pH-value is the negative decadic logarithm of the proton concentration and dividing by F results in the so-called proton motive force (PMF) Δp in Volts (Equation 1.2). For example at a temperature of 298 K, ΔpH = 1 corresponds to Δp = 60 mV or $\Delta\mu_{\mathrm{H}^+}$ = 5.7 kJ mol^{-1}.[28]

$$\Delta p = \frac{\Delta\bar{\mu}_{\mathrm{H}^+}}{\mathrm{F}} = \Delta\psi - 2.3 \cdot \mathrm{R}T\mathrm{F}^{-1} \cdot \Delta\mathrm{pH} \qquad 1.2$$

The PMF is not only the driving force for ATP synthesis in mitochondria and chloroplasts of eukaryotic cells, but also prokaryotes make use of the energy stored in the electrochemical proton gradient between their cytoplasm and the environment.[29,30]

For ATP synthesis, the PMF needs to be slightly larger than the Gibbs free energy required for the synthesis of ATP, which is $\Delta G_{\mathrm{ADP}\rightarrow\mathrm{ATP}} \approx 50$ kJ mol under physiological conditions (under standard conditions: $\Delta G^0_{\mathrm{ADP}\rightarrow\mathrm{ATP}} \approx 30.5$ kJ/mol).[31]

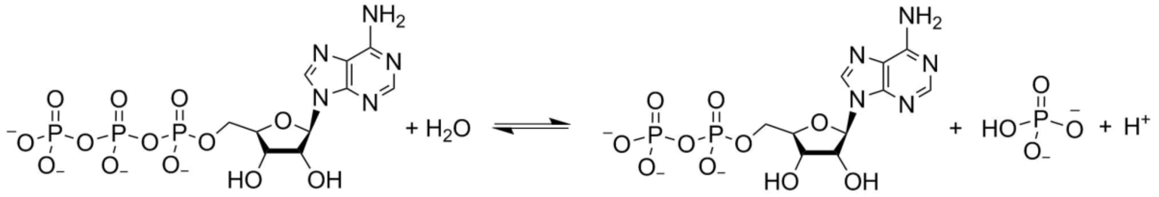

Figure **1.5.** Hydrolysis of adenosine triphosphate (ATP) to adenosine diphosphate (ADP) yields $\Delta G^0_{\mathrm{ADP \to ATP}} = -30.5\ \mathrm{kJ\ mol^{-1}}$ under standard conditions.[31]

In Equation 1.3, the PMF is equated with the Gibbs free energy of ATP synthesis $\Delta G_{\mathrm{ADP \to ATP}}$, with *n* being the stoichiometric ratio of protons translocated per ATP synthesized or hydrolyzed.[32] Depending on the number of monomeric units of the proton translocating oligomeric *c*-ring, $n = \mathrm{H^+/ATP}$ can vary from two to four between ATP synthases of different species, e.g. for the chloroplast ATP synthase $n = 4$ and for the mitochondrion ATP synthase $n = 3$.[33]

$$n \cdot \Delta p = n \cdot \frac{\Delta \bar{\mu}_{\mathrm{H^+}}}{\mathrm{F}} = \Delta G_{\mathrm{ADP \to ATP}} = \Delta G^0_{\mathrm{ADP \to ATP}} + \mathrm{R}T \cdot \ln \frac{[\mathrm{ATP}]}{[\mathrm{ADP}] \cdot [\mathrm{P_i}]} \qquad 1.3$$

With knowledge of the ΔpH between mitochondrial matrix (pH ≈ 8) and the cytosol (pH = 7.2), it is thus possible to estimate the minimum of the PMF needed for ATP synthesis.[34] The Gibbs free energy of ATP synthesis is $\Delta G_{\mathrm{ADP \to ATP}} \approx 50\ \mathrm{kJ\ mol^{-1}}$, corresponding to a PMF of $\Delta p = 173$ mV (for $n = 3$). With a known ΔpH of 0.8, the electrical potential difference $\Delta\psi$ would account for 124 mV.

If the PMF decreases below $\Delta G_{\mathrm{ADP \to ATP}}$, the function of the ATP synthase is reversed to ATP hydrolysis in order to prevent a collapse of the proton gradient (Equation 1.4).[25]

$$\mathrm{ADP} + \mathrm{P_i} + n\ \mathrm{H^+}_{\mathrm{out}} + m\ \mathrm{H^+} \underset{\Delta G_{\mathrm{ATP}} > n \cdot \Delta p}{\overset{n \cdot \Delta p\ > \Delta G_{\mathrm{ATP}}}{\rightleftharpoons}} \mathrm{ATP} + \mathrm{H_2O} + n\ \mathrm{H^+}_{\mathrm{in}} \qquad 1.4$$

The number of transported protons *n* per ATP is between two and four, *m* is the stoichiometric quotient for scalar proton consumption and close to one at pH > 7.5, depending mainly on the pH and the concentration of $\mathrm{Mg^{2+}}$, which stabilizes ATP and ADP.[35]

1.3 Model membrane systems for actively induced electrochemical gradients

A variety of proton pumping proteins is found in all forms of life (see Figure 1.1, Chapter 1.1), allowing (temporary) energy storage in form of electrochemical proton gradients. Furthermore, the specific pH-values of organelles, which are essential for their function, are induced by proton pumps.[36,37] With their abundance, it is not surprising that proton pumps are often drug targets. For example, health issues associated with the gastric acid are often treated with inhibitors of the H^+/K^+-ATPase.[38] Furthermore, in tumors the control of pH through proton transporters and exchangers is often disturbed, resulting in an acidic microenvironment around the tumor. This low pH protects the cancer cells from body reactions and also renders cytotoxic drugs useless, as they are not taken up by the cancer cells in their protonated state. For this reason, proton pump inhibitors might be promising in cancer treatment.[39]

In order to investigate the structural and functional features of a membrane-spanning transport protein and to test potential inhibitors or drugs, it is helpful to observe the isolated protein in a defined artificial, biomimetic environment. Therefore, isolated membrane proteins, which are kept in solution by amphiphilic detergents, have to be inserted into an artificial lipid membrane. In the following, a rough overview on artificial or model membranes is given, which are more or less suited for the investigation of membrane proteins. Several model membrane systems rely on a solid support, which is critical in context with membrane-spanning proteins because they might lose functionality upon contact with the solid support. Nanodisks, consisting of a small lipid bilayer area (8–13 nm in diameter) assembled around the membrane protein, represent a contact-free system. However, they do not separate two aqueous compartments what disqualifies them for the investigation of substrate transport.[40] Lipid vesicles represent a well-established model systems for membrane protein investigation, as they separate an aqueous volume from the surrounding bulk solution and a diversity of reconstitution protocols is available.[41,42] Furthermore, it is possible to immobilize vesicles on a solid support, e.g. via the biotin-avidin interaction or DNA-linkers, allowing to obtain high statistics.[40] A more advanced system are so-called pore-spanning lipid bilayers that consists of a solid supported membrane that spans cavities in a solid support.[43–45] Both, vesicles and pore-spanning lipid bilayers, enable a separation of two aqueous compartments, therewith meeting the condition for the observation of transport processes.

1.3.1 Small and giant proteoliposomes

Since many years, membrane proteins isolated from their original membranes, are reconstituted into lipid vesicles by the use of detergent, allowing to investigate passive, secondary active and active transport.[46] Basically, two reconstitution methods are established, the insertion of proteins into preformed lipid vesicles or the generation of proteoliposomes from a ternary mixture of lipids, detergent and protein by detergent removal. Depending on the characteristics of the protein, the type of detergent used and the method of detergent removal, one of both reconstitution methods might be more successful than the other. The applied reconstitution method also has an influence on the orientation of the protein and a nearly uniform orientation is desired for efficient transport. A favored orientation results especially when an asymmetric protein, e.g. with a water soluble part like the F_0F_1-ATPase, is inserted into detergent destabilized vesicles, as it is energetically very unfavorable for the hydrophilic part to cross the hydrophobic membrane core. When the vesicles are formed from a ternary mixture of lipids, detergent and protein, it is more likely to obtain a less uniform orientation of proteins.[41] The proteoliposomes obtained from these reconstitution procedures have diameters in the range of approx. 80-500 nm, depending on the type of detergent and the method used for detergent removal.[47–49]

Unlike membrane protein reconstitution into small liposomes, the functional reconstitution into giant unilamellar vesicles (GUVs, diameter: ~1-100 μm) is more challenging, but yet very desirable because GUVs are in the same size range as cells.[50] Typically, GUVs are produced by electroformation.[51] In this method, a chloroform solution of the desired lipid mixture is deposited on electrically conducting indium tin oxide coated glass slides and dried to form a multilamellar lipid film, which is then rehydrated in an ion-free sucrose solution under an applied electric field.[52] This non-physiological procedure hampers the functional reconstitution of membrane proteins, so that in recent years several strategies for membrane protein reconstitution into GUVs have been developed. Among them are rehydration of (partially) dried small proteoliposomes in an electric field,[53,54] detergent-mediated reconstitution into preformed GUVs [50,55,56] and a variety of fusion-based methods.[57–60] For example, the sarcoplasmic reticulum Ca^{2+}-ATPase, the light-driven H^+-pump bacteriorhodopsin and SNARE-proteins have all been successfully reconstituted into GUVs by drying of small proteoliposomes on a conducting surface and rehydration in the presence of an electric field.[53,54] In case of bacteriorhodopsin, two thirds of GUVs showed a preferential orientation that lead to GUV acidification, while one third showed a pH increase inside the GUVs. The preferential orientation of Ca^{2+}-ATPase was not specified. However, ATP-dependent Ca^{2+}-transport into the GUVs was found, indicating a certain amount of protein was orientated with the ATP hydrolyzing moiety towards the bulk solution.[53] Kreir *et al*. and Battle *et al*. have reconstituted the porin OmpF and mechanosensitive ion channel proteins into preformed GUVs, respectively. While Kreir *et al*. obtained GUVs with the electroformation, Battle *et al*. produced GUVs by hydration of a lipid film. The detergent stabilized proteins were incubated with the GUVs and detergent was removed by adsorption to a hydrophobic resin.[55,56] A very interesting approach was made by Dezi *et al*. who prepared GUVs in sucrose solution by electroformation from a film of lipids and detergent. The detergent-doped GUVs were permeable so the interior sucrose solution could be exchanged for a buffer solution and allowed the insertion of detergent-stabilized membrane proteins bacteriorhodopsin and bacterial porin. After detergent removal by hydrophobic adsorption or complexation, the membrane permeability was strongly reduced.[50] Another approach for membrane protein reconstitution into GUVs under physiological conditions is based on membrane fusion. The fusion of sub-micron sized proteoliposomes with GUVs can be induced by electrostatic forces, fusogenic peptides or SNARE-proteins, which are responsible for exocytosis *in vivo*.[58–61] Charge induced fusion has been successfully used to reconstitute enzymes of the respiratory chain, bo_3-oxidase and ATP synthase, from positively charged small proteoliposomes into negatively charged GUVs. However, the use of non-natural positively charged lipids is inevitable in this method.[59,60] Membrane fusion of small proteoliposomes with GUVs has been mediated by fusogenic peptides and SNARE-proteins. While a fusogenic peptide can be coupled to preformed vesicles,[58] the α-helical SNARE-proteins have to be reconstituted into GUVs, e.g. via the de- and rehydration of small proteoliposomes. However, the SNARE-proteins retain their functionality during this process, which might not be the case for other membrane proteins.[61] Many membrane proteins mediate a directional substrate transport, so their orientation in vesicles is an important issue. The formation of proteo-GUVs from dehydrated proteoliposomes most likely yields a mixed final protein orientation, while the insertion of proteins into detergent-doped GUVs yields a more uniform orientation, which is comparable to protein reconstitution into performed small vesicles.[50] In case of fusion, the predominating orientation present in the small proteoliposomes will be retained, because during the merging of the vesicle membranes the outer and inner membrane leaflets connect (Figure 1.6).[62]

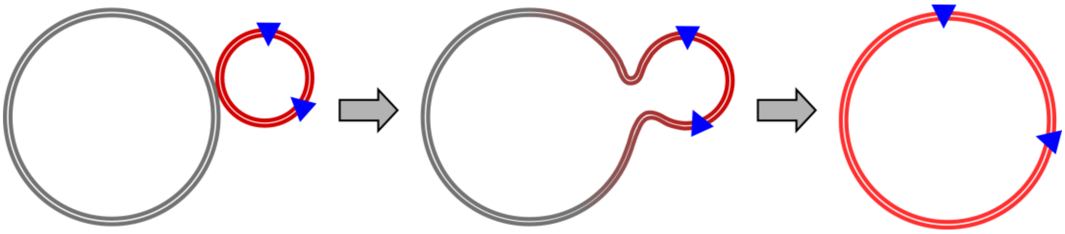

Figure 1.6. The orientation of membrane proteins (blue triangles) retained upon fusion of a small proteoliposomes with GUVs.

In addition to protein orientation, also the amount of reconstituted protein has to be considered. The rates of active transport are relatively slow, e.g. for bacterial F_0F_1-ATPase, hydrolysis rates are in the range of approx. 1–2.3 μmol · min^{-1} · mg^{-1},[63,64] corresponding to proton translocation rates of 28-64 $H^+ \cdot s^{-1}$ per ATP molecule (assuming M = 550 kDa and that n = 3 H^+).[19,65] Thus, for the observation of a single transport protein a small vesicle volume is required (vesicle with d = 130 nm → V = 10^{-18} L).[66] With increasing vesicle diameter, the volume increases tremendously, thus, for observation of active transport processes in GUVs, many proteins have to be active in parallel in order to accumulate a detectable amount of substrate inside the GUVs (GUV with d = 10 μm → V = 10^{-13} L). Concerning the accumulation of transported protons inside a GUV, it is important to consider that the proton permeability P_{H^+} of lipid bilayers is similar to that of water, and several magnitudes above that of other monovalent cations ($P_{\mathrm{H}^+} \approx 10^{-2}$–$10^{-5}$ cm · s^{-1}, $P_{\mathrm{Na}^+/\mathrm{K}^+} \approx 10^{-12}$ cm · s^{-1}).[67,68] Thus, for observation of active proton transport it is even more important to have a large number of active proteins, that for transport of other substrates. However, only few studies quantified the amount of protein reconstituted into GUVs. Girard *et al.* could reconstitute bacteriorhodopsin and Ca^{2+}-ATPase at protein/lipid ratios of up to 1:160 and 1:680 (n/n) by dehydration of small proteoliposomes and rehydration in an electric field, which corresponds to approx. $3 \cdot 10^6$ bacteriorhodopsin molecules or $6.5 \cdot 10^5$ Ca^{2+}-ATPase molecules in a 20 μm diameter GUV (~9,500 bacteriorhodopsin/μm^2 or ~2,000 Ca^{2+}-ATPase/μm^2).[53] Bacteriorhodopsin reconstitution was also quantified by Dezi *et al.*, who used detergent-mediated reconstitution into GUVs. However, they obtained a much smaller protein/lipid ratio (~1:2,000 (n/n), ~1,800 proteins/μm^2) than Girard *et al.*[50] This shows that the reconstitution efficiency varies between the reconstitution methods. A study comparing the reconstitution of a voltage-gated K^+-channel from dehydrated proteoliposomes under physiological buffer condition and high AC-frequency or non-physiological low salt concentration and low AC-frequency, showed that the latter yielded a much more homogenous protein distribution in the resulting GUVs.[69]

To detect the substrate transport into vesicles, fluorescent indicators are commonly used. For monitoring proton transport, for example, three possibilities exist: a water soluble pH-sensitive dye can be encapsulated in small proteoliposomes or proteo-GUVs, lipids with a pH-sensitive head group label can be included in the lipid mixture or a membrane permeable fluorescent pH-indicator (like acridine derivatives) can be used.[70–72] Besides measuring the active transport in a bulk experiment, small proteoliposomes and proteo-GUVs can also be immobilized on a surface allowing to observe transport activity of individual vesicles with fluorescence microscopy techniques.[73]

1.3.2 Pore-spanning lipid bilayers

A more sophisticated model system for fluorescence microscopic studies than immobilized vesicles are the so-called pore-spanning lipid bilayers (PSLBs). This model system consists of a lipid membrane sealing an array of pico- to attoliter sized cavities in a solid substrate.[45] As the membrane separates the cavities from the surrounding bulk, the system is predestined for the observation of transport processes in a highly parallel manner. In 2013, Frese *et al.* could induce proton gradients across pore-spanning lipid bilayers by passive transport with the K^+/H^+-antiporter nigericin, suggesting the applicability of the model system for the observation of active, protein-mediated proton transport.[74]

The formation of the PSLBs is accomplished by spreading GUVs on the hydrophilically functionalized substrate, which has been immersed into an aqueous solution (Figure 1.7).[52]

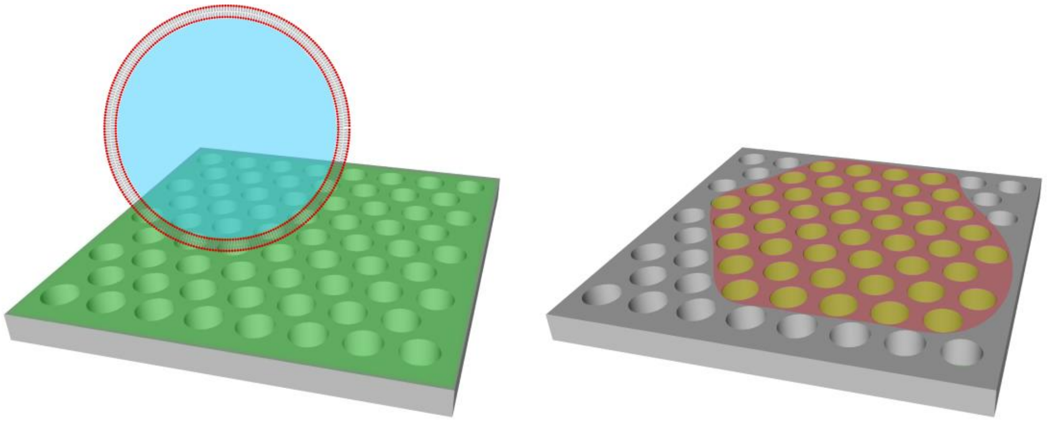

Figure 1.7. Spreading of a GUV on a porous substrate results in formation of a membrane patch, sealing the pores. Fluorophores can conveniently be entrapped inside the pores, by spreading the GUVs in the desired solution and rinsing with another solution afterwards.

This allows to encapsulate a defined solution, e.g. with an indicator dye, inside the pores. After the spreading process, the porous substrate can be rinsed with another solution, allowing to remove non-encapsulated indicator dye or to establish a concentration gradient, for example.

The most obvious preparation of protein containing PSLBs is spreading of proteo-GUVs. This approach has already been used to span single pores in planar patch clamp measurements[55,57] and Schwenen *et al.* were the first to prepare SNARE-protein containing PSLBs by spreading of proteo-GUVs.[75] The spreading process is described by the so-called receding-top mechanism, where a GUV adsorbs on the surface, then ruptures at the side and spreads out so that the former outer membrane leaflet now forms the bottom leaflet of the PSLB.[76] For GUVs with preferentially orientated protein this spreading mechanism is important to consider. For example, if the majority of proteins is orientated in a way that substrates are transported into the GUV lumen, the resulting PSLBs would have a favored protein orientation for transport from the pores into the bulk solution (Figure 1.8).

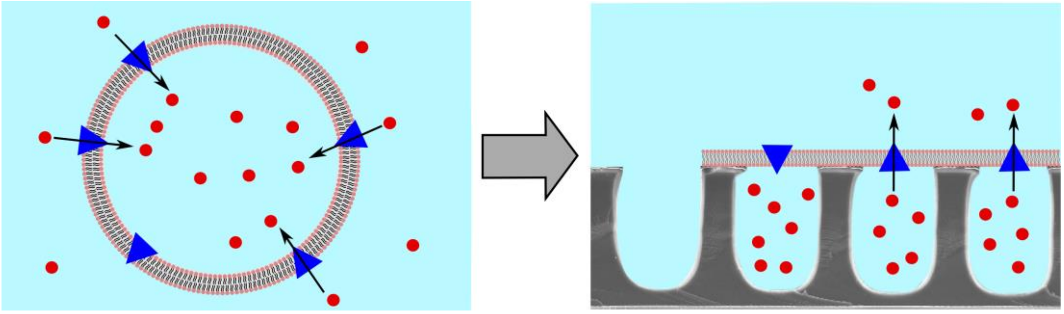

Figure 1.8. Scheme of protein orientation in a GUV and the resulting orientation in PSLBs. If proteins (blue triangles) are preferentially orientated in a GUV, e.g. transporting substrates into the lumen, the PSLB would have the proteins orientated in a way that they would transport substrate out of the pores.

F_0F_1-ATPase can act as an ATP-powered proton pump or can use the proton motive force of a proton gradient for ATP synthesis. Depending on the protein's orientation in the membrane, either an acidification of the underlying cavities upon ATP hydrolysis or an ATP production upon imposition of a proton gradient would be feasible. In the first case (cf. Figure 1.9 A), the ATP hydrolyzing F_1-part would stick out of the membrane into the bulk solution, so that ATP addition would result in a proton transport into the pores, which would be detectable by an entrapped pH-sensitive fluorescent dye. In the second case (cf. Figure 1.9 B), the F_1-part would point inside the pores, thus, an acidification of the outside buffer would enable ATP synthesis from ADP and phosphate inside the pores, which could be detected by the luciferin luciferase bioluminescence.[77]

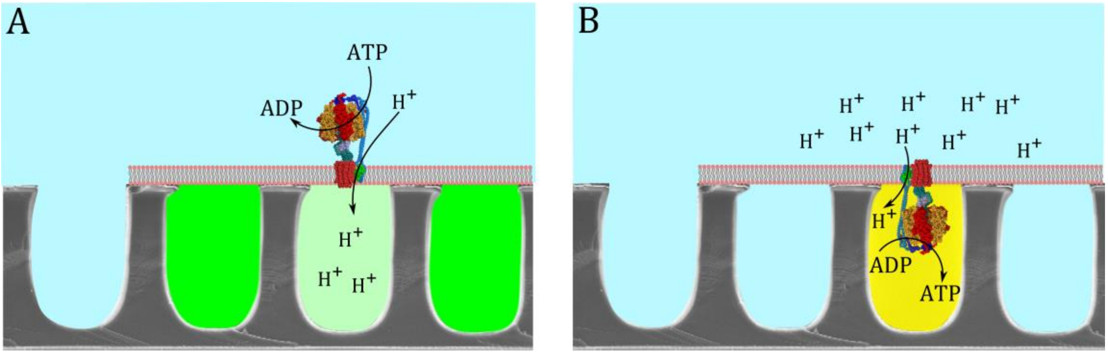

Figure 1.9. Depending on the orientation of F_0F_1-ATPase in the pore-spanning lipid bilayer, an acidification or ATP synthesis inside the pores would be achievable. (A) If the ATP hydrolyzing F_1-part pointed into the bulk solution, the sealed cavities would be acidified. (B) If the F_1-part pointed into the pore, an imposed proton gradient would result in ATP production inside the pore. A fluorescent indicator (indicated in green in A) or the bioluminescent luciferin luciferase system (indicated in yellow in B) would allow to detect acidification or ATP synthesis, respectively.

In addition to the proteins' orientation in the PSLBs, the amount of protein and the pore volume have to be taken into account. Like described in the previous chapter, rates of active transport are slow compared to passive transport. Therefore, a small pore volume in the attoliter range (comparable with that of 100-200 nm diameter vesicles) would presumably allow to monitor the activity of single active transporters. Larger pore volumes in the femto- to picoliter range by contrast, would require several active proteins for a detectable amount of translocated substrate within a minute time range. Especially for proton transport, the time it might take to achieve a measurable pH-change is important to consider, as lipid membranes are about a 10^7-fold more permeable for protons than for Na^+ or K^+.[68]

A comparable system to PSLBs was published in 2014 by Wanatabe *et al*. Their system of arrayed lipid bilayer chambers (V = 7 fL , ALBICs) in a hydrophobic fluorinated polymer substrate, allowed to monitor passive and active protein-mediated transport (α-hemolysin and F_0F_1-ATPase, respectively).[78] The striking difference between the systems of ALBICs and the PSLBs is the presence of residual solvent in the lipid bilayer. While the PSLBs obtained from spreading of GUVs are completely solvent-free, the lipid bilayers of the ALBIC-system were produced *in situ* from lipids dissolved in organic solvent (chloroform, decane or hexadecan).[66,78]

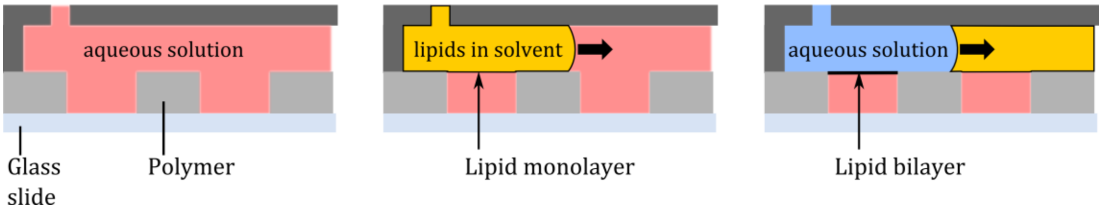

Figure 1.10. Preparation scheme of arrayed lipid bilayer chambers (ALBICs) in a microfluidic device. First, the chambers are filled with aqueous solution (red). Then a solution of lipids in an organic solvent are flushed through the device, covering the femtoliter chambers with a lipid monolayer. A second aqueous solution (blue) is flushed through the microfluidic device, leading to a bilayer formation. Modified from Wanatabe *et al*.[78]

Residual solvent might remain in the lipid bilayers and influence the membrane properties. For example, chloroform is expected to have an effect on lateral and transversal membrane organization,[79,80] while residual hydrocarbon solvents like decane or hexadecane are known to increase the membrane thickness and alter the lateral membrane tension and diffusion coefficient.[81,82] Consequently, residual solvent may also have an impact on membrane proteins in those lipid bilayers. To reconstitute the proton pump F_0F_1-ATPase under physiological conditions into the ALBICs, Wanatabe *et al.* fused ATPase-proteoliposomes with the preformed ALBICs mediated by 5 % of polyethylene glycol.[78,83] Within approx. 1.5 h some of the chambers experienced a ATP-induced pH-decrease ($\Delta pH \approx -1.7$). However, the ALBICs were nearly impermeable for protons, as an imposed ΔpH of 2.1 was retained for 2 h, which does not pertain to the proton permeability of solvent-free lipid bilayers.[68,78] As it took more than 15 min to detect the proton pumping activity, the authors suggested to decrease the chamber volume to attoliter size. Indeed, a year later the authors were able to decrease the volume of the ALBICs to a minimum of 200 aL (diameter: 3 µm, depth: 30 nm). However, only passive transport by α-hemolysin was monitored with these attoliter sized chambers.[66]

2 SCOPE OF THESIS

Membrane-spanning proteins enable active transport processes across lipid membranes and are pivotal for all organisms, e.g. as they build-up electrochemical gradients to store energy and drive ATP synthesis empowered by those gradients. Since these proteins occur in variety and are crucial for a functioning metabolism, they are also important drug targets. To investigate membrane protein mediated transport and the potential of drugs *in vitro*, artificial membrane systems consisting of two aqueous compartments are of great importance. Pore-spanning lipid bilayers (PSLBs) consist of a well-defined pore array in a solid substrate that is sealed by a lipid membrane and are therewith predestined for observation of transport processes into or from the pores. PSLBs are prepared by spreading of GUVs that are formed in an electric field under non-physiological conditions. Hence, the reconstitution of membrane-spanning transport proteins into PSLBs under physiological conditions is a challenge. Recently, Schwenen *et al.* have established SNARE-protein mediated fusion of small vesicles with PSLBs. As a long-term objective, the small fusing vesicles could be envisaged as transporters for sensitive proteins, merging their cargo into preformed PSLBs under physiological conditions.

This work aims at investigating the potential of SNARE-protein mediated membrane fusion as a reconstitution tool on the level of small proteoliposome experiments. F_0F_1-ATPase will be used as an exemplary proton-pumping protein. First, the F_0F_1-ATPase will be isolated and its proton pumping activity in proteoliposomes will be qualified. Luminal pH-values reached by the ATPase liposomes will be quantified by an acidification assay based on the pH-sensitivity of the lipid-coupled fluorophore Oregon Green 488. To test for the feasibility of the SNARE-protein mediated reconstitution approach, a combined fusion and acidification assay, based on the lipid-coupled fluorophore Oregon Green 488-DHPE (OG488-DHPE), will be introduced. In its first stage, this assay will allow to monitor vesicle fusion and in the second stage, ATP driven acidification by ATPase will be detectable in successfully fused vesicle.

3 MATERIALS AND METHODS

3.1 Protein chemical methods

3.1.1 Expression and purification of TF_0F_1-ATPase in *Escherichia coli*

TF_0F_1-ATPase expression in *Escherichia coli* (*E. coli*)

TF_0F_1-ATPase, with a His_{10}-tag on the *N*-terminus of the *β*-subunit, was expressed in *E. coli* DK8 harboring the plasmid pTR19-ASDS, encoding for the ATPase of the thermophilic *Bacillus* PS3.[84] The expression and purification was carried out very similar to the protocol of Schenck and coworkers.[85]

From cryostocks (−80 °C, 50 % glycerol) overnight cultures in 30 mL terrific broth (TB) medium, supplemented with 100 mg/mL ampicillin, were grown at 37 °C and 120 rpm. The next morning eight main cultures, 250 mL TB medium with 100 mg/mL ampicillin each, were inoculated with 5 mL of the overnight culture and incubated at 37 °C and 120 rpm. When an optical density of 0.6–0.7 at λ = 600 nm (OD_{600}) was reached, 1 mM isopropyl *β*-D-1-thiogalactopyranoside (IPTG) was added. At an OD_{600} in the range of 1.3–1.7, cells were harvested by centrifugation for 15 min at 4,000 *g* and 4 °C. All cell pellets were collected in one 50 mL conical centrifuge tube and frozen at −80 °C.

Preparation of TB medium:

12 g tryptone, 24 g yeast extract, 4 mL glycerol were solved in 900 mL MilliQ water and autoclaved. After cooling down, 100 mL of filter sterilized 23.1 g/L KH_2PO_4 and 125.4 g/L K_2HPO_4 were added.

Purification of TF_0F_1-ATPase

The frozen pellets were resuspended in 150 mL lysis buffer and incubated for 30 min at 37 °C. $MgCl_2$ (5 mM) and 150 µL DNase I buffer were added. After 30 min of stirring at room temperature, the cell-suspension was mechanically lysed by three cycles in the ice cooled Microfluidizer LM10 (1,000 bar) (Microfluidics, Westwood, USA). Na_2SO_4 and sodium cholate were added to final concentrations of 250 mM and 0.7 % (*w*/*v*), respectively and stirred for 20 min at room temperature. After centrifugation at 20,000 *g* and 4 °C (30 min), the supernatant was discarded and the pellet resuspended in HEPES buffer and stirred for 45 min at room temperature. The supernatant resulting from a further centrifugation at 20,000 *g* and 4 °C (30 min) was batch incubated with equilibrated TALON Metal Affinity Resin (Clontech, Takara Bio Europe, Saint-Germain-en-Laye, France) for 2 h at 4 °C, while gently agitated on a tube roller. For equilibration, 5 mL of suspended TALON Metal Affinity Resin (corresponding to a bed volume of ~2.5 mL) was transferred into a 50 mL conical centrifuge tube, centrifuged for 2 min at 700 *g* and 4 °C and the supernatant was discarded. The equilibration buffer (25 mL) was added and removed by centrifugation (2 min, 700 *g*, 4 °C), this step was repeated once more. The incubated resin was centrifuged (2 min, 700 *g*, 4 °C) and separated from the supernatant, 20 mL wash buffer were added and the tube was incubated for 10 min on ice under slight movement. After centrifugation (5 min, 700 *g*, 4 °C) the supernatant was discarded, and the step was repeated. 2.5 mL of wash buffer were used to suspend and transfer the resin into a gravity-flow column, where it was rinsed with further 7.5 mL of wash buffer. Subsequently, the TF_OF_1-ATPase was eluted with 12.5 mL (5 bed volumes) elution buffer. The TALON Metal Affinity Resin was rinsed with regeneration buffer (12.5 mL), MilliQ water (12.5 mL) and stored in 20 % ethanol supplemented with 0.1 % (*w*/*v*) NaN_3.

After dialysis against buffer A the sample's concentration was increased by performing an anion exchange chromatography (MonoQ 5/50, ÄKTA Purifier 10, GE Healthcare Europe, Freiburg, Germany). For elution, the amount of buffer B was increased for the first four column volumes (CV, 1 CV = 1 mL) from 0–18 %, the next three CV from 18-60 % and for 11 CV from 60–100 %.

Table 3-1 List of buffers used for TF_OF_1-ATPase isolation.

Lysis buffer	50 mM Tris, 0.5 mM EDTA, 1 mg/mL lysozyme*, 1 tablet/50 mL c*O*mplete™ protease inhibitor cocktail* (Roche), pH 8.0 * add immediately before use
DNase I buffer	5 mg/mL DNase I in 50 % glycerol (*w*/*v*), 20 mM Tris, 1 mM $MgCl_2$, pH 7.5)
Microfluidizer buffer	50 mM Tris, 0.5 mM EDTA, 5 mM $MgCl_2$, pH 8.0
DNase I buffer	50 % (*w*/*v*) glycerol, 20 mM Tris, 1 mM $MgCl_2$, pH 7.5
HEPES buffer	20 mM HEPES, 100 mM KCl, 20 mM imidazole, 5 mM $MgCl_2$, 1 % (*w*/*v*) *n*-dodecyl *β*-D-maltoside (DDM), pH 7.6

Wash buffer	20 mM HEPES, 100 mM KCl, 20 mM imidazole, 5 mM $MgCl_2$, 0.08 % (*w*/*v*) *n*-dodecyl *β*-D-maltoside (DDM), pH 7.6
Elution buffer	20 mM HEPES, 50 mM KCl, 250 mM imidazole, 5 mM $MgCl_2$, 0.05 % (*w*/*v*) *n*-dodecyl *β*-D-maltoside (DDM), pH 7.4
Equilibration buffer	50 mM Na_3PO_4, 300 mM NaCl, pH 7.4
Regeneration buffer	20 mM MES, 300 mM NaCl, pH 5.0
Buffer A	20 mM NaCl, 20 mM HEPES, 5 mM $MgCl_2$, 0.05 % (*w*/*v*) DDM*, pH 7.5 *to be omitted for dialysis
Buffer B	100 mM NaCl, 20 mM HEPES, 5 mM $MgCl_2$, 0.05 % (*w*/*v*) DDM, pH 7.5

3.1.2 Quantification of protein concentration

The bicinchoninic acid (BCA) assay is a well-established, detergent compatible method for protein quantification. In an alkaline solution, the peptide bonds reduce Cu^{2+}- to Cu^+-ions, which form a purple chelate complex with the BCA (Figure 3.1). In a range of 0.02–2.0 mg the absorption of the complex at 562 nm increases almost linearly.[86,87]

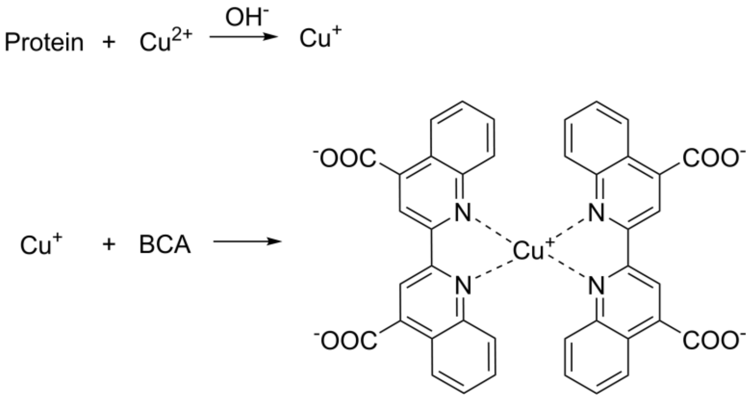

Figure 3.1. Reaction scheme of the bicinchoninic acid (BCA) assay. In an alkaline medium, peptide bonds reduce Cu^{2+} to Cu^+, which then forms a purple colored chelate complex with BCA, exhibiting a strong absorbance at 562 nm.

In this work, the Pierce BCA Protein Assay Kit was used for determination of TF_OF_1-ATPase concentration in a 96-well plate. Therefore, a working reagent was prepared by mixing reagent A (Na_2CO_3, $NaHCO_3$, bicinchoninic acid, Na^+-tartrate in 0.1 M NaOH) and reagent B (4 %

(w/v) $CuSO_4$) in a ratio of 50:1 (5.88 mL and 120 µL). A calibration curve with replicates of 0, 25, 125, 250, 500, 750, 1000, 1500 and 2000 µg/mL bovine serum albumin (BSA) was prepared by pipetting 20 µL of each standard and 200 µL of the working reagent into the wells and accordingly, 25 µL replicates of the protein sample of unknown concentration were mixed the working reagent (200 µL). The 96-well plate was covered, shaken for 30 s and incubated at 37 °C for 30 min. After cooling to room temperature, the absorption at 578 nm was measured with a microplate reader (Biochrom® Anthos 2010, Anthos Mikrosysteme GmbH, Krefeld, Germany). The software ADAP 2.0 plus allowed to assign the standards and samples to the wells, as well as an automated calibration curve fitting and concentration output of the TF_0F_1-ATPase samples.

3.1.3 SDS-Polyacrylamide gel electrophoresis

The SDS-PAGE (sodium dodecyl sulfate polyacrylamide gel electrophoresis) was used to analyze the purified TF_0F_1-ATPase. The denaturing anionic detergent SDS unfolds the protein structure by attaching to the amino acid chain, thereby masking the amino acids' charges and thus, creating a constant mass-to-charge ratio. Consequently, proteins are separated according to their masses in a voltage field.

The gel is composed of two parts, the stacking gel and the resolving gel, which differ in their mesh sizes and pH-values. The stacking gel, to which the samples are applied, has a larger mesh size and a lower pH (5 % acrylamide, pH 6.8) than the resolving gel (17% acrylamide, pH 8.8). The stacking gel allows a concentration of the protein sample. Here, the glycine, which diffuses into the gel from the tank buffer, is zwitterionic and thus does not move much in the electric field (trailing ions), the chloride ions by contrast have a high mobility and migrate towards the anode (leading ions). The resulting potential difference between leading and trailing ions leads to a generation of equally fast migrating protein stacks, eventually increasing the protein concentration at the border to the resolving gel. In the higher pH resolving gel, zwitterionic glycine is deprotonated to its anionic form, thus moving a lot faster in the electric field. Consequently, the potential difference between chloride and glycine is dissipated, allowing the SDS-complexed proteins to be separated according to their mass/charge ratio in the smaller meshes of the resolving gel. Polyacrylamide is obtained by radical polymerization of the monomers acrylamide and bisacrylamide, with ammonium peroxosulfate (APS) being the initiator and *N*,*N*,*N*',*N*'-tetramethylethylendiamine (TEMED) the catalyst. The gel's mesh size can be regulated by the monomer concentration.[88]

First, the resolving gel was prepared according to Table 3-2, pipetted into the gel chamber, covered with some isopropanol and was allowed to polymerize for 45 min. After removing the isopropanol, the stacking gel was pipetted on top of the resolving gel and a Teflon comb was inserted into the solution for formation of sample chambers. After 45 min, the stacking gel was polymerized and the gel chamber was mounted to the electrophoresis device, which was inserted into a tank and filled with tank buffer. The comb was pulled out carefully from the stacking gel, allowing to pipette the samples and a molecular weight standard (LMW-SDS Marker Kit, GE Healthcare Europe GmbH, Freiburg, Germany) into the chambers. 2 x sample buffer (10 µL) was added to each sample (10 µL) and incubated in an Eppendorf® *Thermomixer Compact* (Eppendorf AG, Hamburg, Germany) at 85 °C and 300 rpm for 5 min. The reducing agent dithiothreitol (DTT) contained in 2 x sample buffer assures a breaking of disulfide bonds, thus allowing the SDS to completely unfold the proteins. The electrophoresis was performed with 220 V for approx. 45 min. After disassembling the electrophoresis device, gels were stained with solvent-free Coomassie Brilliant Blue G-250. Therefore, the SDS was removed from the gel by microwaving it for 1 min in ~100 mL MilliQ water with subsequent shaking for 1 min. This step was repeated once. Then 20 mL staining solution (Table 3-2) were added and microwaved for 30 s, until the solution almost boiled. After shaking for 5 min, the staining solution was discarded and the gel was washed with 100 mL MilliQ water for ~10 min on a platform shaker and was then photographed.[89]

Table 3-2 Solutions used for the SDS-PAGE.

2 x sample buffer	125 mM Tris/HCl, 100 mM DTT, 20 % (*v*/*v*) glycerol, 2 % (*w*/*v*) SDS, 0.02 % (*w*/*v*) bromophenol blue, pH 6.8 (HCl)
tank buffer	25 mM Tris base, 192 mM glycine, 0.1 % (*w*/*v*) SDS, pH 8.3 (NaOH)
Stacking gel (5 %)	0.33 mL acrylamide/bisacrylamide (29:1, 30 %), 1.4 mL H_2O, 0.25 mL 1 M Tris/HCl, 20 µL 10 % (*w*/*v*) SDS, 20 µL 10 % (*w*/*v*) APS, 2 µL TEMED, pH 6.8
Resolving gel (17 %)	2.3 mL acrylamide/bisacrylamid (29:1, 30 %), 0.65 mL H_2O, 1.0 mL 1 M Tris/HCl, 40 µL 10 % (*w*/*v*) SDS, 40 µL 10 % (*w*/*v*) APS, 2 µL TEMED, pH 8.8
Staining solution	0.8 % (*w*/*v*) Coomassie Brilliant Blue G-250, 35 mM HCl

3.2 Lipid chemical and reconstitution methods

3.2.1 Preparation of large unilamellar vesicles

Large unilamellar vesicles (LUVs) were prepared by the extrusion through a polycarbonate membrane (LiposoFast-Basic, Avestin, Ottawa, Canada). The desired lipid mixture was pipetted from chloroform stock solutions into a small test tube with a total weight of 0.5 mg lipid. The solvent was evaporated under a nitrogen stream and the resulting lipid film was dried *in vacuo* for 3 h. When fluorophores were contained, the lipid films were protected from light. The test tubes were sealed with Parafilm and stored at 4 °C.
For vesicle preparation, the lipid film was allowed to swell in 0.5 mL ATPase buffer (0.5 mM MOPS, 100 mM KCl, 2 mM $MgCl_2$, pH 7.3) for 30 min at room temperature. Then the mixture was vortexed three times for 30 s in a 5 min interval, producing an opaque solution of multilamellar vesicles. Extrusion through a polycarbonate membrane with nominal diameters of 100 nm or 200 nm (31x) resulted in a clear solution of unilamellar vesicles.
The basic lipid mixture used was DOPC/POPE/POPS/cholesterol in a molar ratio of 50:20:10:20, resembling the lipid composition of synaptic vesicles.[90] An overview of all lipid used is presented in Table 3-3.

Table 3-3 Overview of lipids used in this work.

Lipid	Molecular mass
1,2-dioleoyl-*sn*-glycero-3-phosphocholine, DOPC 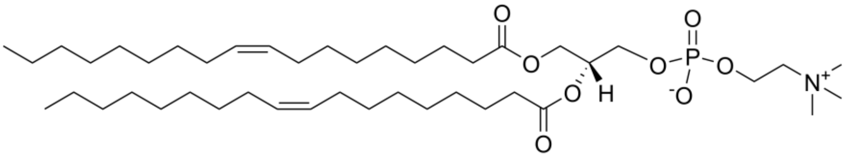	786.1 g/mol
1-palmitoyl-2-oleoyl-*sn*-glycero-3-phospho-L-serine, POPS 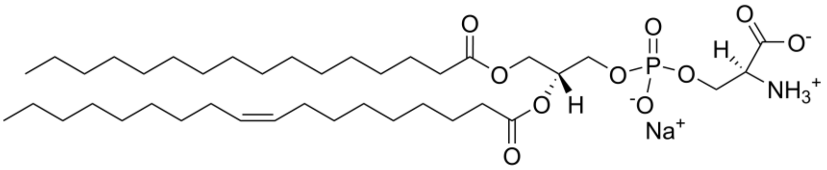	784.0 g/mol
1-palmitoyl-2-oleoyl-sn-glycero-3-phosphoethanolamine, POPE 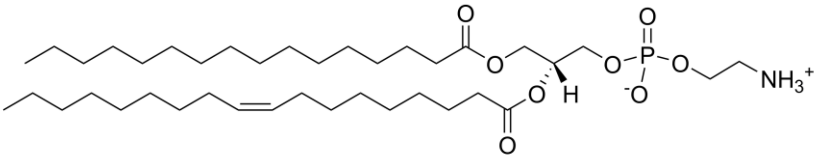	718.0 g/mol

Cholesterol 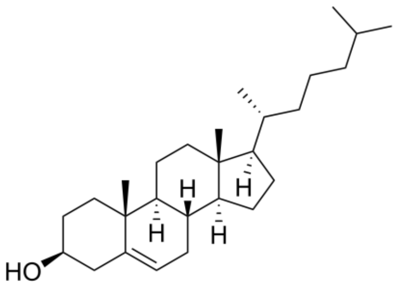	386.7 g/mol
Oregon Green 488 1,2-Dihexadecanoyl-*sn*-Glycero-3-phosphoethanolamine, OG488-DHPE, $\lambda_{\mathrm{ex/em}}$ = 508/534 nm 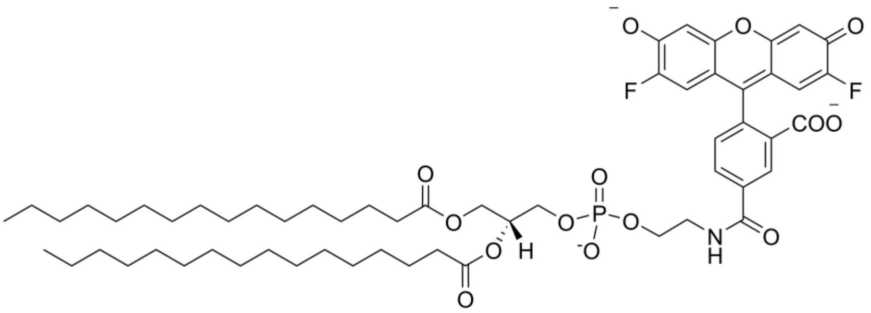	1086.3 g/mol
1,2-dioleoyl-*sn*-glycero-3-phosphoethanolamine-N-(cap biotinyl), biotin-cap-DOPE 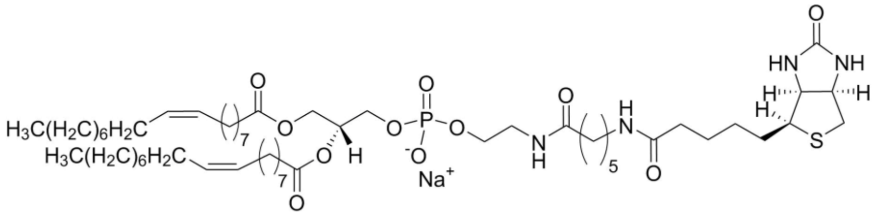	1105.5 g/mol
Texas Red 1,2-Dihexadecanoyl-*sn*-Glycero-3-Phosphoethanolamine, Texas Red DHPE, $\lambda_{\mathrm{ex/em}}$ = 595/615 nm 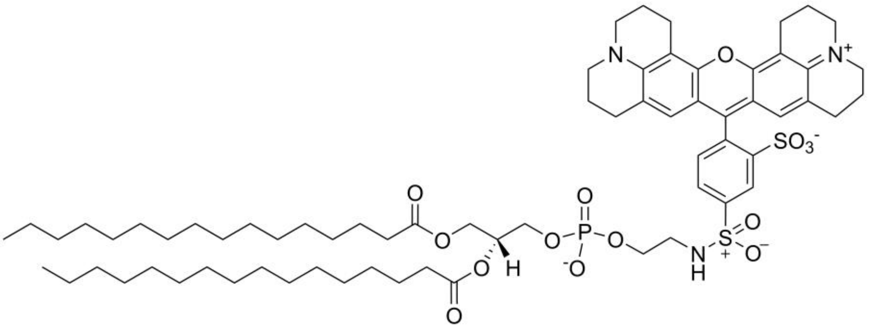	1381.9 g/mol

3.2.2 Protein reconstitution

Isolated membrane proteins are solubilized by detergents. These amphiphilic molecules assemble into micelles that harbor the transmembrane domains (TMD), mimicking the hydrophobic core of the lipid bilayer and therewith ensuring the proteins' solubility.[91] Protein reconstitution is a reversing of the membrane solubilization process, i.e. the protein is reinserted into a lipid membrane. For this purpose two strategies exist: in the direct method (also step-by-step reconstitution), the protein is inserted into preformed lipid vesicles that were destabilized by a detergent, followed by detergent removal, whereas in the co-micellization method, detergent is depleted from mixed lipid-detergent-protein micelles, which leads to proteoliposome formation. For membrane proteins with a water soluble part, the direct method yields a more uniform protein orientation in the membrane, because it is energetically unfavorable for the hydrophilic part to cross the hydrophobic membrane core. This effect does not occur in the co-micellization method.[42]

To remove detergents with a high critical micelle concentration (cmc) and/or a low micellar weight, dialysis or gel filtration can be applied. A high cmc corresponds to a high monomer concentration and a low micellar weight to small micelle sizes, so that in either case the detergent can be removed by gel filtration and/or dialysis. Detergents with low cmc and high micellar weight can only be removed by adsorption to hydrophobic resins like Bio-Beads® or by complexation with cyclodextrins.[91]

In this work, the direct method has been used for the reconstitution of TF_0F_1-ATPase and the co-reconstitution of the ATPase and the ΔN49-complex. Synaptobrevin 1-116 was reconstituted by the co-micellization method. The ΔN49-complex and synaptobrevin 1-116 were kindly provided by the colleagues J. Kuhlmann, R. Hubrich and L. Schwenen. In both methods, the non-ionic detergent *n*-octyl-*β*-D-glucoside (*n*OG) was used. Due to its high cmc of 20–25 mM it is well removable by dialysis or gel filtration. The SNARE proteins synaptobrevin and ΔN49-complex were stabilized by 3-[(3-Cholamidopropyl)dimethylammonio]-1-propanesulfonate (CHAPS), which is also removable by dialysis or gel filtration (cmc: 6.5 mM, micellar weight: 6 kDa). However, the *n*-dodecyl-*β*-D-maltoside (DDM) used to stabilize the ATPase has a low cmc of 0.15 mM and thus was removed by complexation with heptakis(2,6-di-*O*-methyl)-*β*-cyclodextrin (*β*CD). The overview of detergents used in this work are summarized in Table 3-4.

Table 3-4 Overview of detergents used for protein solubilization and reconstitution.[91]

Detergent	Molecular mass/ micellar weight	cmc at 25 °C
n-octyl-*ß*-D-glucoside, *n*OG 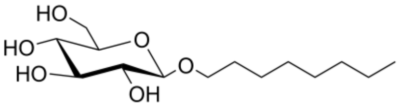	292.4 g/mol 25 kDa	20–25 mM
n-dodecyl-*β*-D-maltoside, DDM 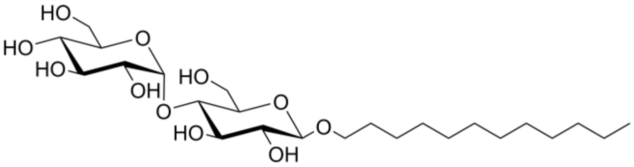	510.6 g/mol 70 kDa	0.15 mM
3-[(3-Cholamidopropyl)dimethylammonio]-1-propanesulfonate, CHAPS 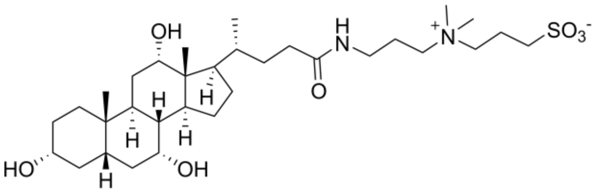	614.9 g/mol 6 kDa	6.5 mM

3.2.2.1 Reconstitution by the direct method

This reconstitution method was applied for the TF_0F_1-ATPase and the co-reconstitution of TF_0F_1-ATPase and the ΔN49-complex. The preformed LUVs (Chapter 3.2.1, nominal diameter: 200 nm) were destabilized with *n*OG. The concentration was chosen to fit an *R*-value of 1 ($R = (c_{\text{detergent}} - \text{cmc})/c_{\text{lipid}}$) (cf. Chapter 5.2), usually corresponding to a final concentration of 26 mM. Unless otherwise indicated, the ATPase was added in a molar protein/lipid ratio of 1:20,000 (~ 1:25 (*w*/*w*) assuming a molecular weight of 550 kDa[19]) and incubated for 10 min at room temperature, followed by dialysis over night at 4 °C against ATPase-buffer (0.5 mM MOPS, 100 mM KCl, 2 mM $MgCl_2$, pH 7.3) supplemented with Bio-Beads®. To complex the DDM, with which the ATPase was stabilized, the sample was incubated with an equimolar amount of heptakis(2,6-di-*O*-methyl)-*β*-cyclodextrin (*β*CD) for 1 h on ice. Gel filtration through a Sephadex G-25 prepacked illustra NAP-25 column (GE Healthcare Life Science) was used to remove the complexed DDM.[49]

For a co-reconstitution, ΔN49-complex (41.0 kDa) was added besides the ATPase in a molar protein/lipid ratio of 1:500.

3.2.2.2 Reconstitution by the co-micellization method

The co-micellization method was used for reconstitution of the synaptobrevin 1-116 (12.7 kDa). To obtain mixed micelles of lipid and detergent, a lipid film (0.5 mg) was incubated with 50 µL ATPase buffer (0.5 mM MOPS, 100 mM KCl, 2 mM $MgCl_2$, pH 7.3) containing 3.0 % (*w/v*) (or 103 mM) *n*OG for 30 min at room temperature. After subsequent vortexing, synaptobrevin was added in a molar protein/lipid ratio of 1:500 and incubated for 30 min. Detergent removal from the resulting ternary mixed micelles was accomplished by gel filtration (Sephadex G-25, illustra NAP-25 column, GE Healthcare Life Science), resulting in detergent free proteoliposomes.

3.2.3 Determination of proteoliposome size by dynamic light scattering

To obtain a size distribution of the proteoliposomes, dynamic light scattering (photon correlation spectroscopy) measurements were performed. When monochromatic and coherent light hits a small particle it is scattered and in a solution containing many particles the scattered light interferes. As the particles move, this interference leads to fluctuations in the scattering intensity. An analysis of these time dependent fluctuations allows to obtain information about the particles' velocity and their diffusion coefficients. The Stokes-Einstein equation then allows to correlate the diffusion constant to a hydrodynamic diameter.[92–94]
In this work, the intensity weighted size-distribution was determined with a Zetasizer NanoS (laser wavelength: 633 nm) (Malvern Instruments, Herrenberg, Germany) in the group of Prof. Dr. P. Vana (Institute of Physical Chemistry, Georg-August-University Göttingen). The proteoliposome sample was diluted tenfold to a final concentration of approx. 0.6 µM phospholipids in ATPase buffer at 25 °C.

3.2.4 Determination of the ATPase reconstitution efficiency by density gradient centrifugation

To analyze the amount of protein reconstituted into vesicles, a density gradient centrifugation was performed. Intact proteoliposomes and protein-free vesicles have an aqueous lumen and float on top of the density gradient, whereas non-reconstituted or denatured protein has a much higher density and therefore accumulates at the bottom of the gradient. Fractions taken from the gradient can be analyzed by SDS-PAGE to quantify the protein. Here, the reconstitution efficiency for nominal protein/lipid ratios of 1:40,000, 1:20,000 and 1:8,000 was determined.

For preparation of the gradient, the non-ionic Nycodenz ($M = 821$ g/mol, Axis-shield Alere Technologies AS, Oslo, Norway) was used.[95] An 80 % (*w*/*v*) and a 30 % (*w*/*v*) solution of Nycodenz in ATPase buffer (0.5 mM MOPS, 100 mM KCl, 2 mM $MgCl_2$, pH 7.3) were prepared. 40 µL of the 80 % solution were carefully mixed with 40 µL of the proteoliposome sample and pipetted into a small centrifuge tube resulting in a bottom layer of 40 % (*w*/*v*) Nycodenz. Then a 40 µL of the 30 % solution were pipetted on top, followed by 20 µL pure ATPase buffer. After centrifugation at 45,000 rpm for 2.5 h at 4 °C, seven 20 µL fractions were pipetted carefully from top of the gradient. Together with ATPase standards of 1.0 mg, 0.5 mg, 0.25 mg and 0.1 mg, the fractions were applied to an SDS-PAGE (Chapter 3.1.3). A calibration curve was obtained from the standards by reading out the grey value with the ImageJ feature *Analyze Gel* (Version 1.45s, W. Rasband, NIH, USA). Thus, allowing an assignment of protein mass to the gel band of the density gradient fractions. Proteoliposomes were only supposed to be in the three top fractions. A determination of the lipid concentration of the proteoliposomes was accomplished by a phosphate quantification assay (Chapter 3.2.5).

3.2.5 Phosphate determination assay

A calibration curve with 0, 0.25, 0.5, 1.0, 1.5 and 2.0 µg phosphate was prepared by evaporation of NaH_2PO_4 solution for 60 min at 200 °C. Perchloric acid (70 %, 200 µL) was added to the vesicle sample (30 µL) and heated to 220 °C for 60 min to produce inorganic phosphate. After cooling to room temperature, 700 µL of a solution of 0.45 % (*w*/*v*) NH_4MoO_4 and 12.6 % (*w*/*v*) $HClO_4$ and 700 µL of a 1.7 % (*w*/*v*) ascorbic acid solution were added. Absorption at 820 nm was measured after incubation of all samples for 10 min at 80 °C. The phospholipid concentrations of the vesicle samples were calculated by means of the calibration curve.[96]

3.3 Fluorescence based proteoliposome acidification assays

The principle of fluorescence

The proton pumping activity of the reconstituted TF_0F_1-ATPase was monitored by pH-sensitive fluorophores, allowing to perform fluorescence spectroscopic and microscopic experiments. When a fluorophore is excited by light absorption, electrons are elevated from the electronic ground state (S_0) to an electronically excited singlet state (S_1, S_2, ...). Figure 3.2 A shows the potential curves of S_0 and S_1 with their vibrational states *v*'' and *v*'. As the excitation process of electrons (timescale: 10^{-15} s) is much faster than the displacement of the heavy nuclei, the nuclear geometry does not change during the excitation. Consequently, a vertical transition into an excited vibrational state in which the nuclear geometry can stay the same is most likely (Franck-Codon principle). Through vibrational relaxation (timescale: 10^{-15} s to 10^{-12} s), resulting from collisions with solvent molecules, the vibrational ground state *v*'' = 0 of S_0 is reached. Electrons that were excited to a higher electronically state can reach S_1 through internal conversion, a non-radiative relaxation process. From the lowest vibrational state of the first electronically excited state (S_1, *v*' = 0, Kasha's rule), energy is released in form of spontaneous emission, known as fluorescence (timescale: 10^{-9} s). Here, also the Franck-Condon principle applies, resulting in vibrational excited states of S_0 and not directly in *v*'' = 0 of S_0. As a result, the emission spectrum often is a mirror image of the part of the absorption spectrum that accounts for the $S_0 \rightarrow S_1$ transitions. Again vibrational relaxation leads to a return to the vibrational ground state *v*'' = 0 of the electronic ground state S_0. As a result, from the energy lost through the vibrational relaxation, the emitted fluorescence is always of lower energy, i.e. longer wavelength, than the absorbed light (Figure 3.2B). This wavelength difference of absorption or excitation and fluorescence emission is called Stokes shift. Generally, the closer the energies of the S_1 and S_0 state are, the more internal conversion occurs instead of fluorescence.[97–99]

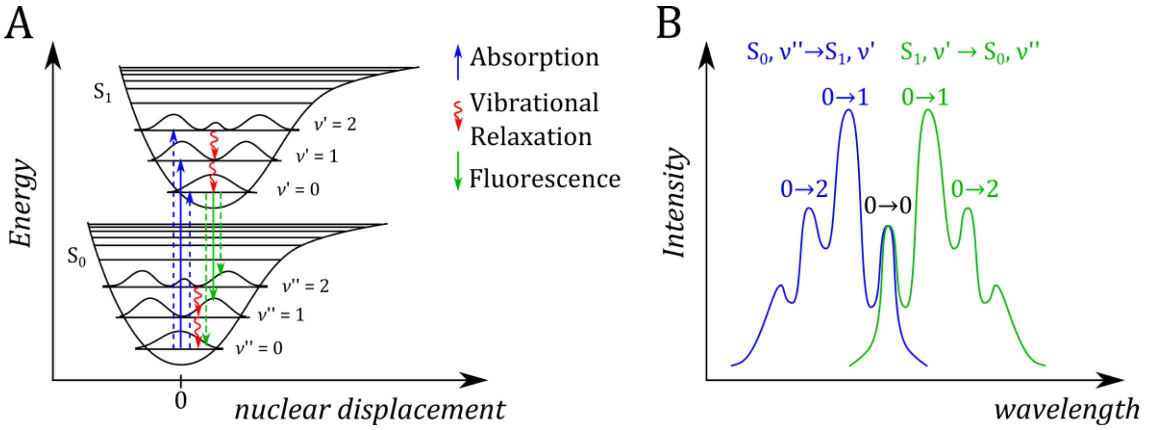

Figure 3.2. (A) Potential curves for molecules in the electronic ground state S_0 and the electronically excited S_1 state. The horizontal lines indicate the vibrational states v'' of S_0 and v' of S_1, with the curves displaying the probability densities of the nuclei to be at a certain place. The energy of the absorbed light (blue arrows) leads to an excitation of electrons to vibrational states of S_1. During this fast process (10^{-15} s) the heavy nuclei remain stationary, leading to vertical transitions (Franck-Condon principle). Fluorescence emission always occurs from S_1, $v' = 0$ into different vibrational states of S_0. (B) The transitions into different vibrational states reflect in the absorption and emission spectra. Due to the transition from S_1, $v' = 0$ into higher vibrational states of S_0, the emission spectrum is a mirror image of the excitation transitions.[97–99]

In some cases, the emission spectrum does not show the mirror image of the absorption spectrum. For example, the pK_a-values of fluorophores can be different in their ground and electronically excited states, like for pyranine (1-hydroxypyrene-3,6,8-trisulfonate). At a low pH, the molecule is protonated and shows an absorption spectrum with the vibrational structure of a hydrocarbon compound. However, the corresponding emission spectrum shows a large Stokes-shift and has completely different shape. This is because the electronically excited molecule has a lower pK_a-value, thus the emission results from a different molecular species, the deprotonated form of pyranine. Beside pK_a changes, also excimer (= excited-state dimer) and exciplex (= excited-state complex) formation can result is largely differing emission spectra. Examples are pyrene which forms excimers and anthracene, forming exciplexes with diethylaniline.[97]

pH-sensitive fluorophores 9-amino-6-chloro-2-methoxyacridine and Oregon Green 488-DHPE

To monitor TF_OF_1-ATPase mediated vesicular acidification, the pH-sensitive membrane permeable fluorophore 9-amino-6-chloro-2-methoxyacridine (ACMA) was used (Figure 3.3 A). ACMA has several protonation states: di-cationic ⇌ mono-cationic ⇌ neutral ⇌ anionic, with pK_a-values of -8.6, 8.6 and 18.0, respectively.[100] However, in the physiological pH-range only the equilibrium between the mono-cationic and neutral species is relevant (pK_a = 8.6, Figure 3.3 A).

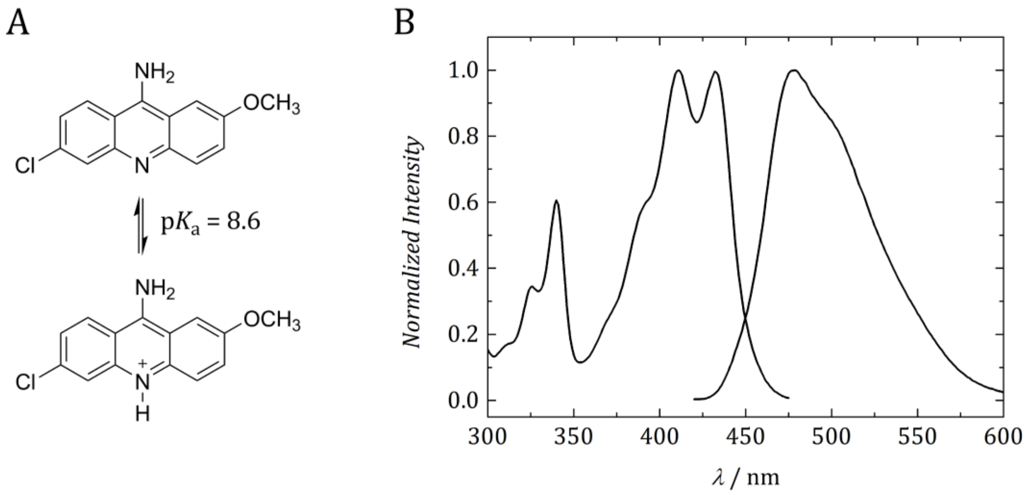

Figure 3.3. (A) Structures of 9-amino-6-chloro-2-methoxyacridine neutral and monocationic form, which both occur at neutral pH (pK_a = 8.6).[100] (B) Excitation and emission spectrum of ACMA in ATPase buffer (0.5 mM MOPS, 100 mM KCl, 2 mM $MgCl_2$, pH 7.3). At this pH, the mono-cationic species is predominat.

At pH 7.3, the mono-cationic and the neutral form coexist in a ratio of about 20:1, allowing the neutral dye molecules to permeate the membrane of lipid vesicles. Figure 3.3 B shows the excitation and emission spectrum, measured at pH 7.3 (ATPase buffer: 0.5 mM MOPS, 100 mM KCl, 2 mM $MgCl_2$, pH 7.3), thus resulting from a mixture of the intensely fluorescing neutral and the less intense fluorescing mono-cationic species of ACMA.[101] Vesicular acidification then leads to an increase of that ratio, e.g. to 400:1 at pH 6.0, resulting in changes of the partition equilibria at the membrane-buffer interfaces and eventually in a redistribution of fluorophores entailing fluorescence quenching.[72]

Oregon Green 488-DHPE

Besides membrane permeable fluorescent pH-indicators, lipid-coupled pH-sensitive fluorophores can be used to monitor vesicle acidification.[71] In this work, Oregon Green 488-DHPE (see Table 3-3) has been included in the lipid mixtures used for ATPase reconstitution (concentration: 1 mol%, unless otherwise indicated). Oregon Green 488 (OG 488) (Figure 3.4 A) can occur in four protonation states: di-anionic ⇌ mono-anionic ⇌ neutral ⇌ mono-cationic, with pK_a-values of 4.7, 3.6 and 1.0, respectively.[102,103] Thus, in a solution of neutral pH the di-anionic species is predominant. Figure 3.4 B shows the excitation and emission spectra of Oregon Green 488-DHPE in vesicles composed of (DOPC/POPE/POPS/cholesterol/OG488-DHPE (49:20:10:20:1) (solid line) and of OG488-DHPE in a 1 M KOH methanolic solution (dashed line). However, it has to be considered that the pK_a-values of OG488 change, when the fluorophore is coupled to a lipid and anchored to a lipid bilayer.[104]

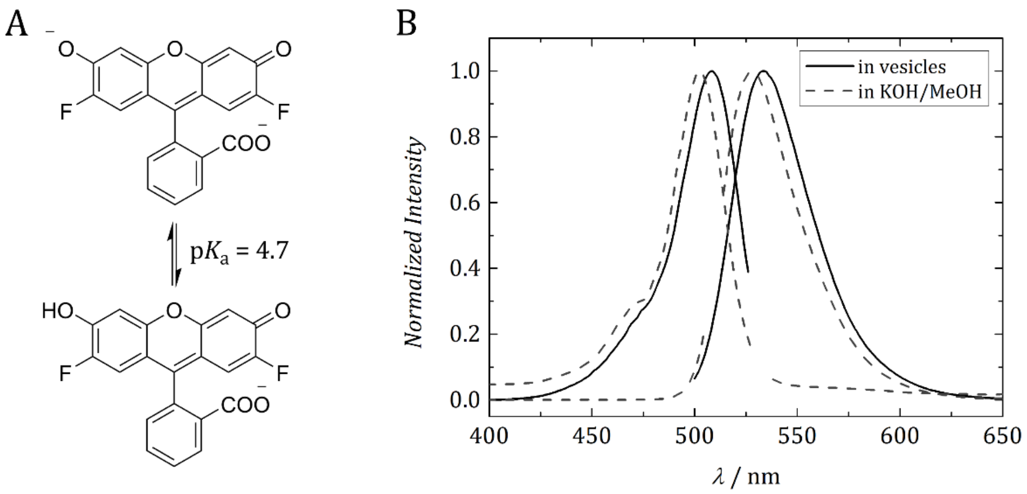

Figure 3.4. (A) In the physiological pH range the di-anionic Oregon Green 488 is predominant and with increasingly acidic pH the mono-anionic species emerges (pK_a = 4.7).[102,103] (B) Excitation and emission spectra of Oregon Green 488-DHPE (structure see Table 3-3) in vesicles in ATPase buffer (0.5 mM MOPS, 100 mM KCl, 2 mM $MgCl_2$, pH 7.3) (solid line) and dissolved in 1 M methanolic KOH solution (dashed line). The excitation and emission peaks are slightly red-shifted for the fluorophore in vesicles ($\lambda_{ex/em}$ (sol.) = 502/528 nm, $\lambda_{ex/em}$ (vesicles) = 508/534 nm).

Instrumentation

To measure excitation and emission spectra as well as fluorescence emission over time a fluorescence spectrometer (FP-6500, JASCO Germany GmbH, Gross-Umstadt, Germany), equipped with a magnetic stirrer and a heatable sample cell, was used.

Generally, a broad band light source is split into a spectrum of wavelengths by a diffraction grating. Focusing the desired wavelength onto a slit allows to excite the sample with a distinct wavelength. Through a lens the beam might be additionally focused onto the sample cell. The emitted fluorescence is collected by a lens and spectrally separated by a further monochromator, allowing the detection of a specified wavelength.[98]

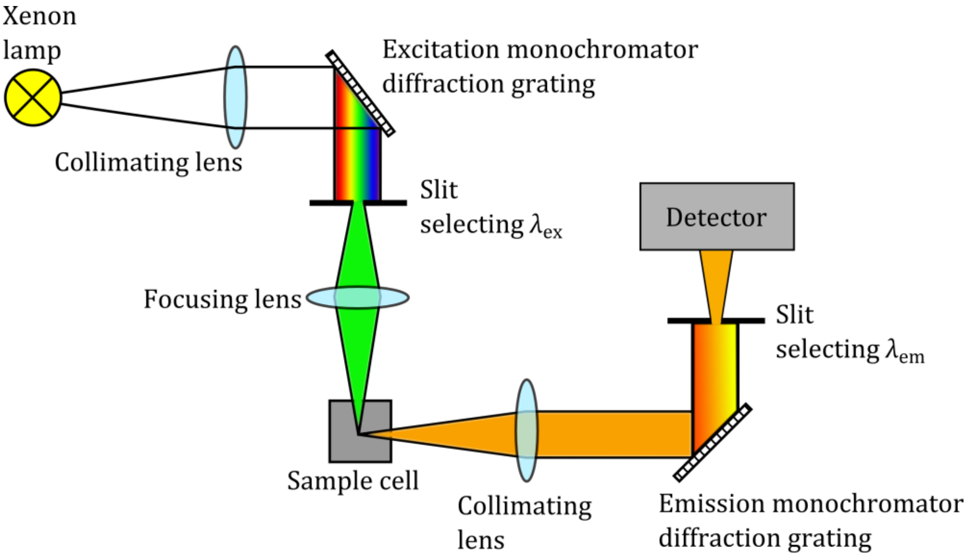
Xenon lamp
Excitation monochromator diffraction grating
Collimating lens
Slit selecting λ_{ex}
Detector
Focusing lens
Slit selecting λ_{em}
Sample cell
Collimating lens
Emission monochromator diffraction grating

Figure 3.5. Typical setup of a fluorescence spectrometer. An excitation monochromator allows to obtain the desired excitation wavelength from a broad band light source, e.g. a xenon lamp, which is focused on the sample. The emitted fluorescence is collected orthogonally to the excitation beam and focused on an emission monochromator to select the emission wavelength to be detected.

Conduction of the acidification assays

The OG488-DHPE and ACMA based acidification assays were performed at 37 °C with a Jasco FP-6500 fluorescence spectrometer. Basically, the experimental course of the acidification assays with either ACMA or OG488-DHPE does not differ. Thus, the experiment is generally described and the specifications for the particular assay are listed in Table 3-5.

680 µL ATPase buffer (0.5 mM MOPS, 100 mM KCl, 2 mM $MgCl_2$, pH 7.3) were preheated to 37 °C, unless otherwise indicated. Then 100 µL proteoliposomes ($c_{\text{phospholipid}} \approx 64$ µM) were added, followed by ACMA addition (omitted for the OG488-DHPE assay). Subsequently, the K^+-ionophore valinomycine (5.0 nM, 4.4 µL of 0.9 µM stock in DMSO) was added to allow a charge equilibration. ATP (1.2 mM, 7.8 µL of 120 mM stock in ATPase buffer, pH of stock was adjusted to 7.3) was added to induce proton pumping. To dissipate the proton gradient, the proton uncoupler carbonyl cyanide 3-chlorphenylhydrazone (CCCP) was added (0.4 µM, 1.6 µL of a 0.2 mM stock in DMSO). Inhibition of ATP hydrolysis could be achieved by adding 1 mM NaN_3 prior to ATP addition. A magnetic stirrer ensured complete mixing of the added substances.

Table 3-5 Specification of substances used for the ACMA or OG488-DHPE acidification assays, respectively.

	ACMA Assay	OG488-DHPE assay
$\lambda_{ex/em}$	410/490 nm	508/534 nm
Fluorophore	0.9 µM ACMA (3.5 µL of 0.2 mM in DMSO)	Included in proteoliposome membrane

3.3.1 pK_a determination of Oregon Green 488-DHPE and intensity-pH calibration for acidified vesicles in ATPase buffer

As indicated above, the pK_a-value of OG488-DHPE is dependent on the lipid composition of the membrane the fluorophore is anchored to.[104] To determine the pK_a-value of OG488-DHPE in the lipid composition used in this work, the fluorescence intensity of OG488-DHPE doped LUVs was measured at different pH-values. LUVs of DOPC/POPE/POPS/cholesterol/OG488-DHPE (49:20:10:20:1) with a nominal diameter of 100 nm were prepared in ATPase-buffer (0.5 mM MOPS, 100 mM KCl, 2 mM $MgCl_2$) with pH-values of 4.3, 5.3, 6.3 and 7.3 (LUV preparation see Chapter 3.2.1). The phospholipid concentration of each sample was quantified and kept constant in each measurement ($c_{\text{phospholipid}}$ = 64 µM). The samples were excited with λ_{ex} = 508 nm and emission was recorded from λ_{em} = 510–650 nm. The emission maxima ($\lambda_{em,max}$ = 534 nm) were plotted against the pH-values. Fitting the data with a variant of the Henderson-Hasselbalch equation allowed to determine the pK_a-value (Equation 4.2, Chapter 4.4.1).[105]

To obtain an intensity-pH calibration curve of acidified vesicles in a buffered bulk solution, the same measurements were performed, but samples of pH 4.3, 5.3 and 6.3 were injected into ATPase buffer of pH 7.3.

3.4 Quantitative fusion assay based on OG488-DHPE dequenching

With increasing concentration of lipid-coupled fluorophores in lipid vesicles so-called self-quenching occurs, i.e. the fluorescence intensity decreases.[106,107] This phenomenon can be exploited for measuring lipid mixing: when a vesicle population with a high fluorophore concentration fuses with colorless vesicles, lipid mixing leads to a dilution of the fluorophore resulting in a dequenching or a fluorescence intensity increase, respectively. Furthermore, a calibration curve for the self-quenching allows to quantify the lipid-mixing resulting from vesicle fusion.[108]

For preparation of the calibration curve, LUVs of DOPC/POPE/POPS/cholesterol/OG488-DHPE (50 − x:20:10:20:x, x = 0.7 mol%, 1.4 mol%, 2.8 mol%, 4.1 mol%, 5.5 mol%, 6.9 mol% and 8.3 mol%) were prepared according to Chapter 3.2.1. First, their fluorescence intensity F_{quench} was measured in ATPase buffer (0.5 mM MOPS, 100 mM KCl, 2 mM $MgCl_2$, pH 7.3). Subsequently, Triton X-100 (1 mM) was added to lyse the vesicles to eliminate the self-quenching effect. As a result, the maximum intensity F_{max} was obtained. For the calibration curve ratios of $F_{\text{max}}/F_{\text{quench}}$ were plotted against the OG488-DHPE concentration.

To quantify the amount of lipid mixing resulting from SNARE-mediated vesicle fusion, equimolar amounts ($c_{\text{phospholipid}}$ = 65 µM) of Sb1-116-liposomes (nominal p/l = 1:500) doped with 5.5 mol% OG488-DHPE and ATPase-ΔN49-liposomes (ATPase: nominal p/l = 1:20,000, ΔN49: nominal p/l = 1:500) were mixed in a fluorescence spectrometer at 37 °C (reconstitution methods see Chapters 3.2.2.1 and 3.2.2.2). The sample was excited with λ_{ex} = 508 nm and the emission was read out at $\lambda_{\text{em, max}}$ = 534 nm. The fluorescence intensity of the very beginning was denoted as $F_{\text{quench-start}}$. When no further intensity increase was observed the measurement was ended, obtaining $F_{\text{quench-end}}$. Then Triton X-100 (1 mM) was added to lyse the vesicles and to obtain the maximum possible fluorescence intensity F_{max} ($\lambda_{\text{em, max}}$ = 534 nm). By correlating the ratios of $F_{\text{max}}/F_{\text{quench-start}}$ and ratios of $F_{\text{max}}/F_{\text{quench-end}}$ to the calibration curve, the concentration of OG488-DHPE in the unfused Sb1-116 vesicles and in the resulting fusion products can be determined.

3.5 Microscopy based single vesicle assay

3.5.1 Principle of fluorescence microscopy

For the observation of single, immobilized fluorescently labeled vesicles, the methods of widefield fluorescence microscopy, confocal laser scanning microscopy (CLSM) and spinning-disk confocal microscopy (SDCM) have been used. Figure 3.6 shows schemes of the basic principles of the three methods.[109] In case of widefield microscopy, excitation light is focused onto the sample and the emitted light of the entire sample depth is collected (Figure 3.6 A).[99] In CLSM, an excitation laser beam scans the sample and only the emitted light of a defined focal plane is detected, which is achieved by a pinhole in front of the detector (Figure 3.6 B).

This also allows to obtain precise three-dimensional images of a specimen. However, scanning a larger area results in long image acquisition times that are even extended when several focal planes are scanned and assembled to a 3D-image.[110]

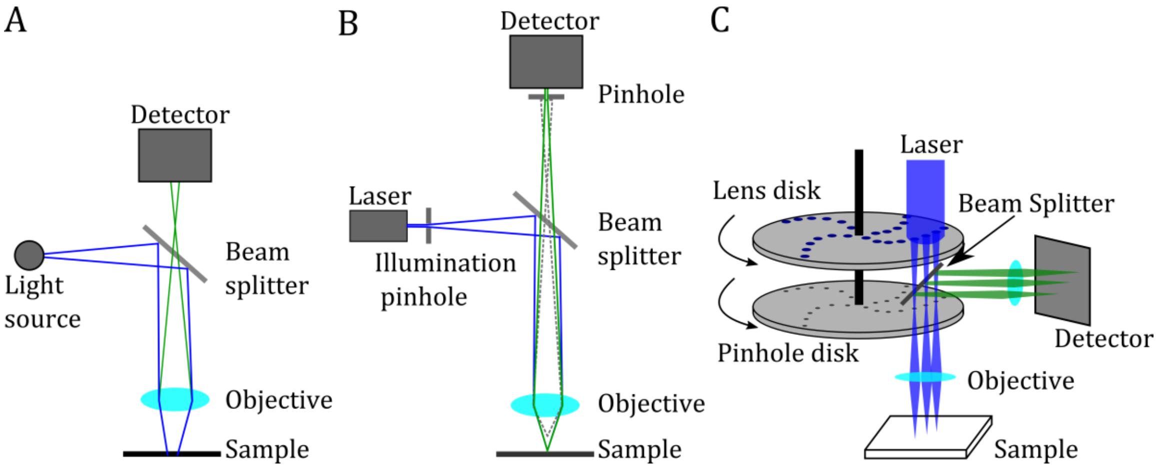

Figure 3.6. (A) Scheme of a widefield fluorescence microscope. As the fluorescence of the total specimen depth is detected, the resulting images are often blurry. (B) In confocal laser scanning microscopy only fluorescence emitted from the focal plane is detected. However, image acquisition of larger areas is slow due to the pointwise scanning of the sample. (C) The spinning disk confocal microscope allows a very fast image acquisition because an array of spinning pinholes allows to excite and detect the fluorescence of larger areas simultaneously.[109]

To monitor fast process, possibly also in a three-dimensional manner, image acquisition by CLSM might be too slow. The SDCM overcomes this problem by replacing the scanning process and the detection through a single pinhole by an array of pinholes that rotate. This allows an almost instant illumination of the whole sample and accordingly, an immediate image acquisition of the specimen (Figure 3.6 C). Using a piezo objective scanner allows to change the focal plane during image acquisition, thus enabling the measurement of z-stacks.[111]

3.5.2 Silanization & PEGylation of glass slides

To enable a vesicle immobilization via the NeutrAvidin-biotin interaction glass slides were functionalized with a mixture of biotin-PEG/methoxy-PEG. The glass slides (24 x 50 mm, #1, ThermoFisher Scientific Gerhard Menzel, Brunswick, Germany) were cleaned with ultra-pure water and ethanol p.a. and were subsequently treated with oxygen plasma (30 s, 0.2 mbar, 60 % power) (Zepto LF PC, Diener electronic, Ebhausen, Germany). The pure 3-glycidyloxipropyltrimethoxysilane (GOPTS, bottle was kept under argon atmosphere) was applied between two glass slides. The resulting "sandwiches" were placed in a glass weighing bottle and incubated for 1 h at 80 °C. During incubation, α-methoxy-ω-amino-PEG (methoxy-PEG, 2,000 Da) and α-amino-ω-biotin-PEG (biotin-PEG, 3,000 Da) were equilibrated from −21 °C to room temperature, mixed in a ratio of 9:1 (n/n) and molten in a Thermomixer at 85 °C and

1400 rpm. After incubation, the glass slides were carefully separated and thoroughly rinsed with dry acetone and dried under a nitrogen stream. Placing the glass slides on an aluminum block preheated to 80 °C allowed to apply the molten mixture of methoxy-PEG and biotin-PEG between two silanized glass slides without solidification of the PEG mixture. The glass-PEG "sandwiches" were placed in a weighting bottle and incubated at 80 °C for 4 h. After separating the glass slides they were intensely washed with ultra-pure water and dried under a nitrogen stream. The functionalized substrates were kept under argon atmosphere at 4 °C and were used for up to two weeks.[112]

3.5.3 Conduction of the single vesicle assay

For immobilization of biotinylated proteoliposomes, a PEGylated glass slide was mounted to a custom build microscopy flow chamber developed by Johannes Schumacher (Figure 3.7), which was heated to 37 °C. The objective (UPlanSApo, 60 x, 1.2 NA, Olympus, Hamburg, Germany) was also heated to 37 °C and thermally insulated with adapters SM1A3TS and RMSA1 (Thorlabs GmbH, Dachau/Munich, Germany). The ATPase buffer (0.5 mM MOPS, 100 mM KCl, 2 mM $MgCl_2$, pH 7.3) was preheated to 37 °C, degassed and then keep at that temperature. Preheated ATPase buffer (952 µL) was mixed with NeutrAvidin stock solution (10 µL of a 1 mg/mL solution) to yield a 10 µg/mL solution, which was immediately rinsed through the flow chamber for 10 min. After rinsing with ATPase buffer for approx. 3 min, TF_OF_1-ATPase vesicles doped with 0.4 mol% biotinyl-cap-DOPE and 1 mol% OG488-DHPE (10 µL proteoliposome sample + 990 µL ATPase buffer, $c_{\text{phospholipid}} \approx 0.6$ µM) were flushed through the flow chamber for about 10 min. Subsequently, non-bound vesicles were washed away by rinsing with ATPase buffer (~5 min). The image acquisition was started and ATPase buffer with 5 nM valinomycine was pumped through the chamber. To add ATP (1.2 mM) to the buffer reservoir the pumping was shortly interrupted, which resulted in a loss of focus for that time. After about 5 min of rinsing ATP solution through the chamber, the pumping was again interrupted for CCCP (0.4 µM) addition.

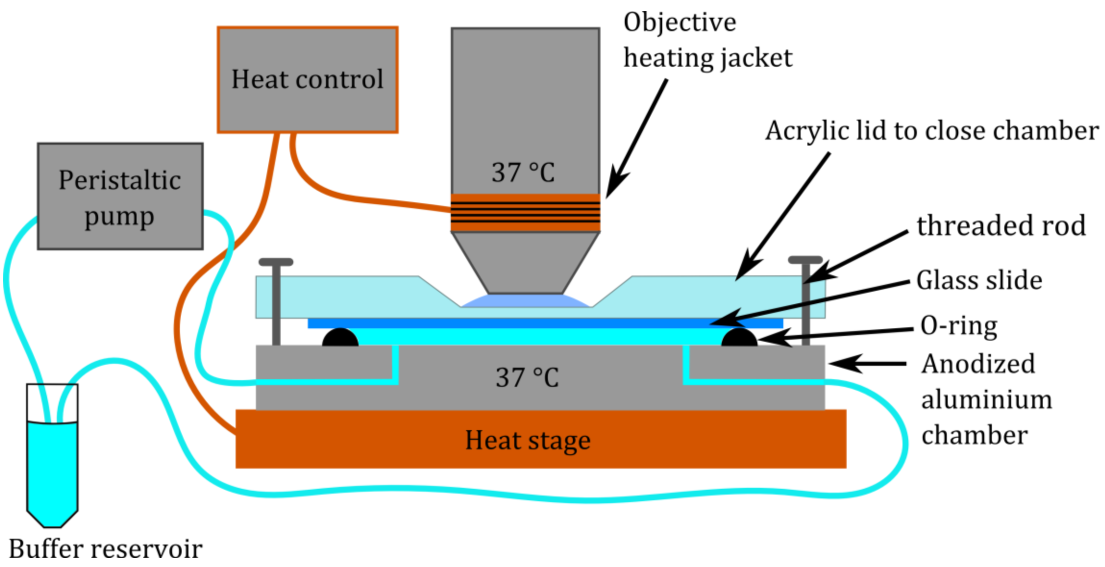

Figure 3.7. Scheme of the heatable measuring setup. The anodized aluminum heating chamber was mounted onto the microscope's heat stage (heat paste was applied to ensure good thermal conduction) and the PEGylated glass slide was put onto the chamber's O-ring. The acrylic lid was placed on top of the glass slide. By screwing knurled nuts onto the threaded rods the chamber was closed and immobilized on the heat stage.

The image series were either acquired with an upright Olympus BX60 WI, FluoView FV1200 confocal microscope using its total internal reflection (TIRF) module to evenly illuminate the sample, corresponding to a widefield microscopy setup (camera: Zyla 5.5, Andor Technology Ltd., Belfast, UK, acquisition settings: 4×4 binning, rolling shutter, frame rate: 4.65 fps) or with an upright spinning disc confocal microscope setup (spinning disc: Yokogawa CSU-X, Rota Yokogawa GmbH & Co. KG, Wehr, Germany; stand: Olympus custom-made, Olympus Deutschland GmbH, Hamburg, Germany; camera: iXON 897Ultra, Andor Technology Ltd., Belfast, UK). In both setups, OG488-DHPE fluorescence was excited at λ_{ex}= 488 nm and the emission was selected with a 496/LP BrightLine HC longpass emission filter (AHF Analysentechnik AG, Tübingen, Germany). To compensate for focal drift in z-direction, time series of z-stacks (5 µm in 26 planes or 6.8 µm in 35 planes) were recorded with the spinning disc confocal microscope (objective was moved with an P721.CLQ piezo objective nanopositioning system, Physik Instrumente GmbH & Co., Karlsruhe, Germany). With both cameras a dark image was recorded in order to correct for the cameras' dark currents.

3.5.4 Analysis of the recorded time series

To correct for the intensity counts resulting from the dark current of the camera, a dark image was subtracted from each image of the time series prior to further image processing (ImageJ plug-in *Calculator plus*). Figure 3.8 gives an overview of the image processing described in the following. When z-stack time series were recorded, the images of each stack were added up to a hyperstack (image sequence with slices assigned to time and z-position) with the ImageJ feature *Stack to hyperstack*, i.e. z-position information was assigned to the time frames. To obtain a two-dimensional time series, with the accumulated intensities compensating for the z-drifts, the images of each z-stack were added up with the *Sum Slices* ImageJ feature (resulting in a frame rate of 0.17 fps). These time processed image series and those obtained from the upright Olympus BX60 WI microscope were corrected for xy-drifts with the ImageJ plug-in *Template Matching: Align Slices in Stack* .[113]

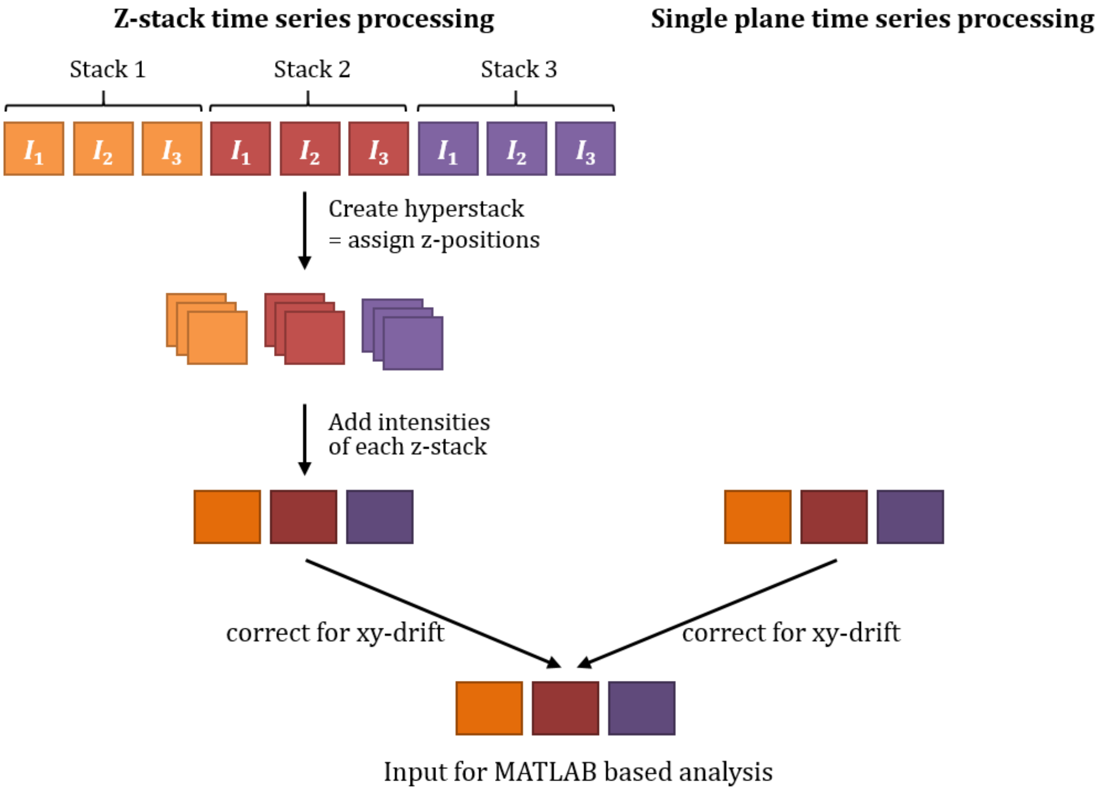
Z-stack time series processing
Single plane time series processing
Stack 1
Stack 2
Stack 3
I_1
I_2
I_3
Create hyperstack
= assign z-positions
Add intensities
of each z-stack
correct for xy-drift
correct for xy-drift
Input for MATLAB based analysis

Figure 3.8. Scheme of image series processing with ImageJ. The image series (I) obtained from z-stack measurements were converted into so-called hyperstacks by assigning z-positions to the time series. Then the images were added up for each z-stack of the time series, resulting in pictures corresponding to the time series obtained by single plane measurements. After a correction for xy-drifts, the image series were analyzed with a custom written Matlab script.

The recorded image series were background corrected and single vesicles were located by a custom Matlab script written by Jeremias Sibold (see Appendix 8.8). A region of interest (ROI, 7×7 pixels^2) was defined for each vesicle and the intensities were read out for each time frame. The time courses of the intensities of each detected vesicle were manually screened for a decrease after ATP addition and a fast intensity recovery after CCCP addition. A decrease after ATP addition and a 50 % recovery after CCCP addition was taken as the criterion of an

ATPase-mediated acidification, i.e. an active ATPase in the vesicle. After normalizing the intensities to the value at ATP addition (t = 0 s), they were converted into luminal pH-values by correlation with the intensity-pH calibration curve (Chapter 3.3.1).

3.5.5 Characterization of vesicle immobilization strategy

In order to evaluate the vesicle immobilization strategy Texas Red DHPE doped liposomes (DOPC/POPE/POPS/cholesterol/Texas Red DHPE/biotin-cap-PE (49.5:20:10:20:0.1:0.4) filled with a green fluorescing pyranine solution were attached as described in Chapter 3.5.3. Vesicles with a nominal diameter of 100 nm were prepared as described in Chapter 3.2.1, with 0.5 mM pyranine added to the ATPase buffer (0.5 mM MOPS, 100 mM KCl, 2 mM $MgCl_2$, pH 7.3). A colocalization of Texas Red DHPE and pyranine fluorescence will indicate intact vesicles.

To obtain a surface density of attached vesicles, two channel images were taken with an Olympus BX60 WI, FluoView FV1200 confocal laser scanning microscope (Channel 1 pyranine: λ_{ex} = 488 nm, λ_{em} = 500-550 nm, Channel 2 Texas Red DHPE λ_{ex} = 561 nm, λ_{em} = 570-670 nm).

In order to analyze the colocalization of green and red fluorescence the *Colocalization Analysis* plug-in of ImageJ was used, resulting in an RGB-image with the blue pixels representing the colocalization of green and red fluorophore. After thresholding this image, the *Analyze Particle* feature of ImageJ was used to count the particles of colocalized fluorescence.

4 RESULTS

4.1 Expression and isolation of TF_0F_1-ATPase from *E. coli* DK8

When developing a new assay or model system that aims on the observation of protein activity, it is essential to choose a stable, well characterized protein that is easy to purify. In this work, the active generation of proton gradients across lipid membranes should be monitored. ATP synthases, also known as F-type ATPases, present a well-characterized group of membrane proteins that are capable of synthesizing ATP from energy stored in proton gradients, but also function as proton pumps when ATP is provided as energy source.[114] The TF_0F_1-ATPase from the *thermophilic bacillus* PS3 (physiological temperature ~ 60 °C) is an exceptionally stable ATPase. An expression system for His-tagged TF_0F_1-ATPase in *E. coli* has been established in 2002 by Suzuki *et al*. and was used in several studies since then.[65,84,85,115–119] With its characteristics, the TF_0F_1-ATPase is a well-suited membrane protein for the generation of proton gradients in this work.

The expression system from Suzuki *et al.*, which was used here, is based on the *E. coli* strain DK8. This strain has no genes for an own F-type ATPase, but instead has the plasmid TR19-ASDS encoding for the TF_0F_1-ATPase.[84]

As mentioned in Chapter 1.2, TF_0F_1-ATPase consists of eight different protein units: three α- and three β-units, one γ-unit, one δ-unit and one ε-unit represent the water-soluble F_1-part, while one a-unit, one b-unit dimer and the c-unit decamer form the membrane-anchored F_0-part. Magnesium ions have to be present in each buffer used for protein purification and storage, because both parts are reversibly detached from each other when magnesium ions are removed.[84] The expression in *E. coli* DK8 was carried out in terrific broth medium at 37 °C. After yielding the bacterial pellets, cell lysis was performed enabling to purify the enzyme by means of immobilized metal ion chromatography (IMAC) (TALON® Metal Affinity Resin), since the β-units carry an *N*-terminal polyhistidine tag.

An SDS-PAGE gel of the elution fractions revealed, that no significant impurities were contained but the elution profile was broad, i.e. the protein concentration was low. Therefore, the total elution volume (14 mL) was subjected to an anion exchange chromatography (Mono Q 5/50 column, ÄKTA Purifier, GE Healthcare Life Science) to increase the protein concentration.

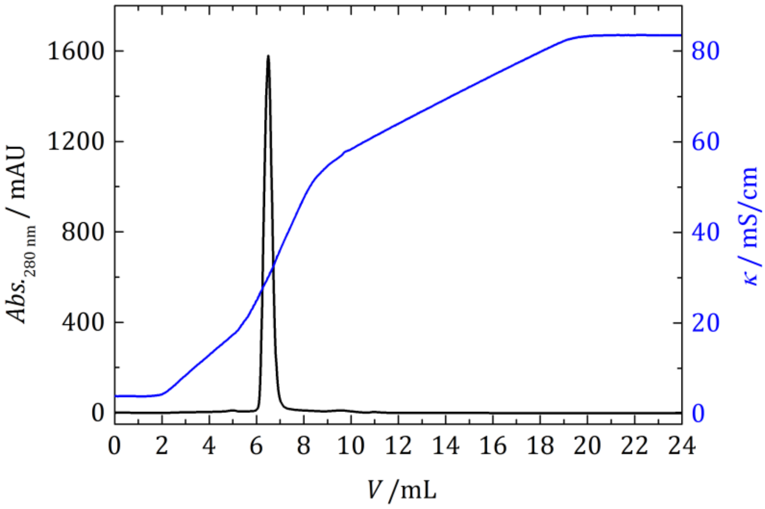

Figure 4.1. The chromatogram shows the elution profile of TF_OF_1-ATPase (indicated by absorption at 280 nm) and the conductivity of the NaCl-gradient, ranging from 20 mM to 1.0 M. The anion exchange chromatography (Mono Q 5/50 column, ÄKTA Purifier, GE Healthcare Life Science) increased the protein concentration to 2.2 µM in a volume of 1.2 mL. The course of the conductance indicates an elution at 30 mS/cm corresponding to a fraction of 30 % buffer B (≙ 314 mM NaCl). Buffer A: 20 mM NaCl, 20 mM HEPES, 5 mM $MgCl_2$, 1 mM DDM, pH 7.5, buffer B: 1 M NaCl, 20 mM HEPES, 5 mM $MgCl_2$, 1 mM DDM, pH 7.5.

The chromatogram in Figure 4.1 shows the elution profile of the TF_OF_1-ATPase, indicated by the absorption at 280 nm, and the increase in ion strength of the NaCl-gradient, indicated by the conductivity κ. The gradient was started at 20 mM NaCl (100 % buffer A) and was increased to 1.0 M NaCl (100 % buffer B) and the TF_OF_1-ATPase eluted at a conductance of approximately 30 mS/cm, which corresponds to a concentration of 30 % buffer B or 314 mM NaCl, respectively.

An SDS-PAGE gel (Figure 4.2) of the fractions corresponding to the protein peak (V_{elution} = 6.0–7.2 mL, fractions 9–12) shows that the protein was efficiently concentrated. Furthermore, the bands of the eight subunits of the TF_OF_1-ATPase were very well assignable when compared to literature.[84]

By means of a bicinchoninic acid (BCA) assay (Chapter 3.1.2) of the pooled peak-fractions a final concentration of 1.2 mg/mL was determined (2.2 µm, assuming a molecular weight of 550 kDa[19]), which corresponds to a yield of 1.49 mg protein per 2 L culture. The protein was stabilized by the detergent *n*-dodecyl-*β*-d-maltoside (DDM), which was present in the elution buffers (1 mM) and stored at 4 °C for several weeks.

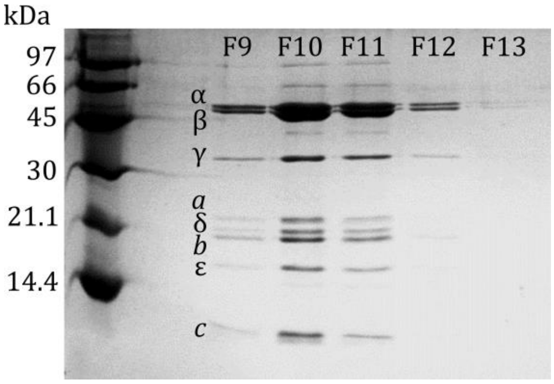

Figure 4.2. SDS-PAGE gel showing the bands of the eight single units of the TF_0F_1-ATPase in the elution fractions F9 to F13, corresponding to the elution volume from 6 mL to 7.2 mL, of the anion exchange chromatography. The TF_0F_1-ATPase subunits were assigned to the SDS-PAGE gel bands according to Suzuki *et al.*[84]

4.2 Detergent-mediated reconstitution of the TF_0F_1-ATPase into liposomes

- Parts of this Chapter have been published: M. Schwamborn, J. Schumacher, J. Sibold, N. K. Teiwes, C. Steinem, Monitoring ATPase induced pH changes in single proteoliposomes with the lipid-coupled fluorophore Oregon Green 488, *Analyst* **2017**, *accepted,* DOI: 10.1039/C7AN00215G.

Detergents serve for the solubilization of membrane proteins from their native membranes, and often maintain their functionality.[120] However, to monitor the activity of transporting membrane proteins, such as the TF_0F_1-ATPase, a reconstitution into an artificial membrane is indispensable.[41,42,121] The ATP-induced proton pumping of the ATPase will only work, when the protein is reconstituted with the right orientation into a membrane system that separates two aqueous compartments from each other.

Thus, the detergent stabilized membrane-protein TF_0F_1-ATPase was reconstituted into lipid vesicles, making it feasible to observe an acidification of the vesicular lumen due to ATPase-mediated proton pumping. The protein reconstitution was performed by the direct method (Chapter 0). In the first step, large unilamellar vesicles (LUVs) with a lipid composition of DOPC/POPE/POPS/cholesterol (50:20:10:20) and a diameter of about 200 nm were prepared by extrusion. Subsequently, the LUVs were destabilized with the detergent *n*-octyl-*β*-d-glucoside (*n*OG), allowing an insertion of the DDM-stabilized ATPase with a preferred orientation of the F_1-unit pointing outwards. Finally, the detergents were removed to ensure stable, non-leaky vesicle membranes.

To examine the reconstitution efficiency of the TF_0F_1-ATPase into the vesicles' lipid bilayer, a density gradient centrifugation was performed (Chapter 3.2.4). In this method, the samples with nominal protein/lipid (p/l) ratios of 1:40,000, 1:20,000 and 1:8,000 (n/n) were applied to a density gradient of 0 %–40 % (w/v) of the nonionic gradient medium Nycodenz in ATPase-buffer.

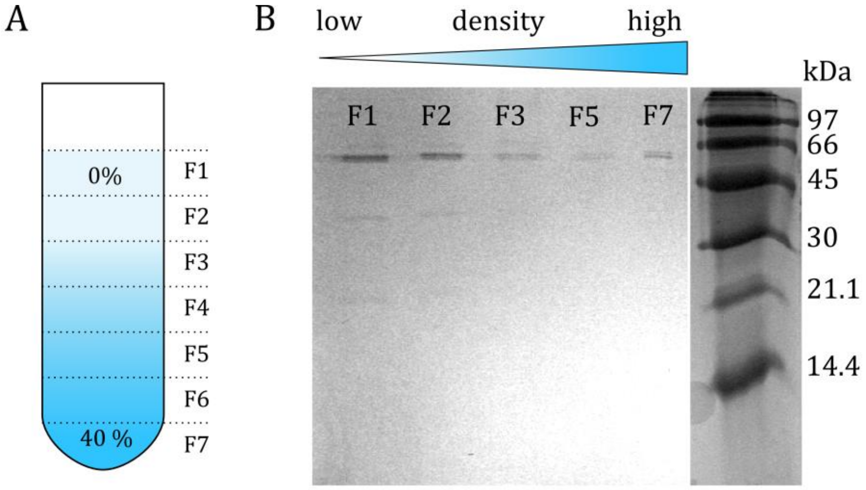

Figure 4.3. (A) The Nycodenz density gradient (0 % to 40 % (w/v)) was prepared in ATPase-buffer (0.5 mM MOPS, 100 mM KCl, 2 mM $MgCl_2$, pH 7.3) and divided into seven 20 µL fractions for SDS-PAGE analysis. (B) The SDS-PAGE gel from the reconstitution sample with a nominal p/l ratio of 1:40,000 shows the strongest protein band intensities for the fractions of low density, F1–F3, representing reconstituted TF_0F_1-ATPase into vesicles of DOPC/POPE/POPS/cholesterol (50:20:10:20). The gel lane corresponding to the fraction of highest density, F7, shows that some amount of protein was not reconstituted into liposomes.

Because of their aqueous lumen, proteoliposomes have a density similar to that of pure buffer, consequently, intact proteoliposomes floated on top of the gradient. Non-reconstituted protein had a significantly higher density than the buffer and therefore accumulated in the high-density bottom region of the gradient. For the analysis, the total volume of 140 µL per gradient was carefully pipetted from the centrifuge tube (in 20 µL units) and applied to an SDS-PAGE. The stained gels of all nominal protein/lipid ratios showed that the ATPase was present in the three upper fractions, representing successfully reconstituted protein, as well as non-reconstituted protein in the bottom fractions. For quantifying the amounts of protein in the specific fractions, a calibration curve with protein standards of 1.0 µg, 0.5 µg, 0.25 µg and 0.1 µg TF_0F_1-ATPase was created. With the feature *Analyze > Gel*, implemented in ImageJ, the protein band intensities were analyzed, yielding intensity profiles for each gel lane. To obtain specific intensity values, the plugin reads out the peak areas in the intensity profile.

Figure 4.4 shows the calibration curve resulting from the peak areas of the α- and β-subunit bands for the standards of 0.1 µg, 0.25 µg, 0.5 µg and 1.0 µg ATPase. With the linear fit of those data points, the areas of the intensity peaks in each gel lane were allocated to the amount of protein.

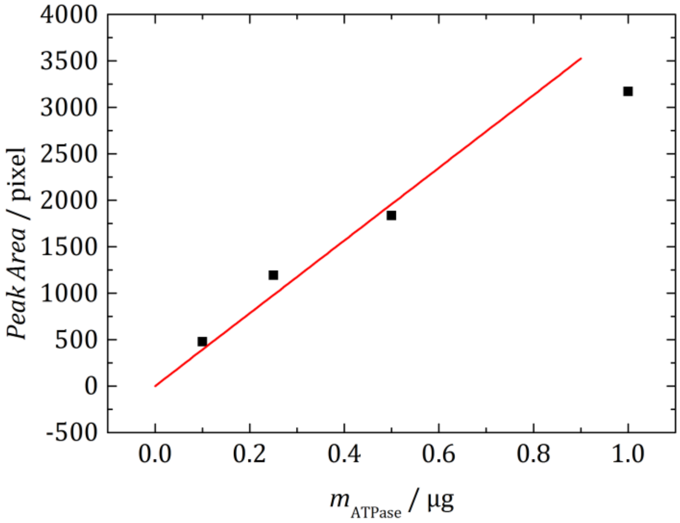

Figure 4.4. Calibration curve resulting from the total peak areas of the α- and β-subunit bands for the standards of 0.1 µg, 0.25 µg, 0.5 µg and 1.0 µg ATPase. A correlation of the peak areas obtained from the density gradient fractions with the calibration curve allowed ascribing the gel band intensities to a certain mass of protein.

For calculation of the reconstitution efficiency, the amount of lipids and cholesterol had to be determined. Therefore, phosphate tests of the reconstitution samples were carried out (Chapter 3.2.5). As the amount of cholesterol could not be determined by this test, it was assumed that the lost percentage of cholesterol during the reconstitution correlated to the loss of phospholipids. For the calculation of the final protein/lipid ratios, it was assumed that the ATPase present in the three upper fractions (F1–F3) was successfully reconstituted and that the determined amounts of lipids and cholesterol originated from liposomes only.

The results shown in Table 4-1 display the nominal protein/lipid ratio, the amount of ATPase located in fractions F1 to F3, the amount of lipids including cholesterol and the final lipid to protein ratios. A comparison between the protein/lipid ratios before and after the reconstitution procedure shows that for the nominal ratio of 1:40,000 the reconstitution efficiency was around 138 % (final p/l = 1:29,000). The nominal protein/lipid ratio of 1:20,000 changed to 1:21,000 for the final sample, and the nominal ratio of 1:8,000 decreased to 1:19,000, implying a 95 % and 42% reconstitution efficiency, respectively.

Table 4-1 Results for the ATPase reconstitution efficiency, obtained from a Nycodenz density centrifugation. With increasing nominal p/l of 1:40,000, 1:20,000 and 1:8,000 a saturation of protein amount occurred, resulting in final p/l of 1:29,000, 1:21,000 and 1:19,000.

Nominal protein/lipid	n_{ATPase} / mol	$n_{\text{lipid+chol}}$ / mol	final protein/lipid
1:40,000	$4.5 \cdot 10^{-13}$	$1.3 \cdot 10^{-8}$	1:29,000
1:20,000	$9.5 \cdot 10^{-13}$	$2.0 \cdot 10^{-8}$	1:21,000
1:8,000	$9.1 \cdot 10^{-13}$	$1.7 \cdot 10^{-8}$	1:19,000

Despite the decreased reconstitution efficiency for the latter ratios, the final protein/lipid ratio increased and seemed to saturate at approximately 1:20,000. Consequently, for all following reconstitutions a nominal protein/lipid ratio of 1:20,000 was used, providing a reconstitution efficiency of 71 % and being at the presumed saturation level of p/l ≈ 1:20,000. To be able to estimate the number of ATPase-proteins reconstituted into the vesicles, besides the final protein/lipid ratios, the size of the liposomes has to be known. To determine the size distribution of the proteoliposomes dynamic light scattering (DLS) experiments were performed. As shown in Figure 4.5, the intensity dependent size distribution of the proteoliposomes ranged from 35 nm to 450 nm, with an intensity-weighted average diameter of 95 nm.

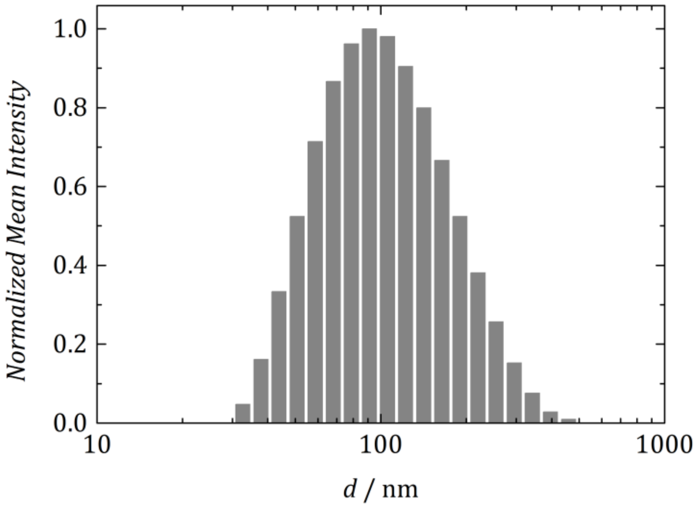

Figure 4.5. Intensity dependent size distribution of ATPase-liposomes (DOPC/POPE/POPS/cholesterol (50:20:10:20), nominal p/l = 1:20,000, ATPase-buffer: 0.5 mM MOPS, 100 mM KCl, 2 mM $MgCl_2$, pH 7.3) measured by dynamic light scattering. The ATPase-liposomes showed a diameter distribution of 35 nm to 450 nm, with an intensity-weighted mean diameter of 95 nm.

With knowledge of the vesicle size, the number of lipids per liposome was calculated, presuming a mean lipid area of 0.62 nm^2 and a cross sectional area of 20 nm^2 for the ATPase (see

Appendix 8.7).[122] As a result, three ATPase molecules would be contained in a 95 nm diameter vesicle with a final protein/lipid ratio of 1:29,000 and four ATPase molecules each, in vesicles with a final p/l of 1:21,000 and 1:19,000.[123]

4.3 Investigation of TF_0F_1-ATPase activity in liposomes with a membrane permeable fluorophore

The analysis of the density gradient centrifugation revealed that the TF_0F_1-ATPase was reconstituted into the liposomes and even allowed a quantification of the reconstitution efficiency (Chapter 4.2), but no information on the activity of the reconstituted protein was obtained. A wrong orientation, the ATP-hydrolyzing F_1-unit pointing into the vesicle, would for example result in inactive proteoliposomes. Therefore, an assay proving ATPase mediated vesicle acidification is essential. For observing protein mediated acidification of liposomes, fluorescent acridine dyes, such as 9-amino-6-chloro-2-methoxyacridine (ACMA), are commonly used.[72,124–127] For monitoring the activity of reconstituted TF_0F_1-ATPase, the ACMA-based acidification assay is a well-established method.[64,65,116,128]

ACMA is a weak base ($pK_a = 8.6$) and membrane permeable in its deprotonated form, but upon protonation, the fluorescence is quenched and the membrane permeability is reduced drastically.[72,126,129] These features allow conducting an activity assay with the proteoliposomes by adding ACMA in micromolar concentration (0.9 µM) to the bulk solution, where it is distributed in the bulk medium and vesicular lumina.

Upon addition of ATP (1.2 mM), the TF_0F_1-ATPase starts a net transport of protons into the liposomes, protonating the ACMA molecules that are quenched and entrapped in the lumina. As a result, deprotonated ACMA from the bulk solution diffuses into the lumina and the overall fluorescence intensity is reduced.[72] When the proton uncoupler carbonyl cyanide 3-chlorophenylhydrazone (CCCP, 0.4 µM) is added, the gradient collapses and the initial fluorescence intensity is restored. The addition of the potassium ionophore valinomycin (5 nM) before the addition of ATP ensures an equilibration of positive charge, as soon as protons are transported across the vesicle membrane (Figure 4.6). ACMA was excited with 410 nm and the fluorescence emission at 490 nm was detected.

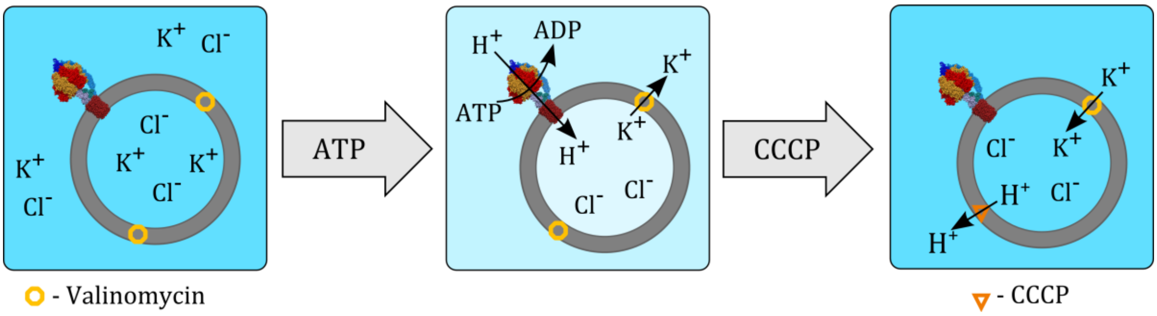

Figure 4.6. Scheme of the ACMA based ATPase activity assay. To the ATPase-buffer (0.5 mM MOPS, 100 mM KCl, 2 mM $MgCl_2$, pH 7.3), ACMA (0.9 µM), proteoliposomes ($c_{\text{phospholipid}} \approx 60$ µM) and the K^+-ionophore valinomycin (5 nM) are added. Addition of ATP (1.2 mM) results in ATPase-mediated proton pumping into the lumina and therewith a protonation and quenching of ACMA. Valinomycin guarantees a charge equilibration by enabling a K^+-efflux. CCCP (0.4 µm) addition leads to a collapse of the proton gradient, thus, the fluorescence intensity of ACMA restores.

Since temperature has a severe impact on enzyme activity, ACMA assays were conducted at different temperatures. Figure 4.7 shows fluorescence intensity courses of ACMA assays at 20 °C, 25 °C, 30 °C, 37 °C and 50 °C, that were normalized to the intensity I_0 immediately after ATP addition ($t = 0$ s). With increasing temperature, the fluorescence intensity decreases became significantly faster and the minimal fluorescence intensity reached got lower (Figure 4.7). At 20 °C (blue curve) the minimal fluorescence intensity of $I/I_0 = 0.3$ was reached after 700 s. A temperature increase of 5 °C (cyan curve) led to a significant acceleration of luminal acidification, as the minimal intensity of 0.2 was reached at approx. 480 s after ATP addition. Measurements at 30 °C (green curve), 37 °C (orange curve) and 40 °C (red curve) reached the intensity minima of 0.1 within 300 s, 160 s and 100 s, respectively. The course of the measurement at 50 °C (dark red curve) differs considerably from the others, not only that the minimal intensity of 0.14 was attained within about 30 s, but also the intensity started to increase linearly a few seconds after the minimum was reached. The measurement at 40 °C also showed a slight linear intensity increase after reaching the minimum intensity, but it was much weaker than in the measurement at 50 °C. The CCCP addition led to an instant recovery of fluorescence intensity in all measurements. Higher temperature would even increase the ATPase proton pumping rate but also the vesicle membrane, composed of DOPC/POPE/POPS/cholesterol (50:20:10:20), becomes increasingly leaky for protons, which would explain the fluorescence intensity increases observed in the measurements at 40 °C and 50 °C. Because of these results, all following TF$_0$F$_1$-ATPase activity measurements were performed at 37 °C, where the enzyme exhibited a high activity and the membrane showed no increased proton leakage.

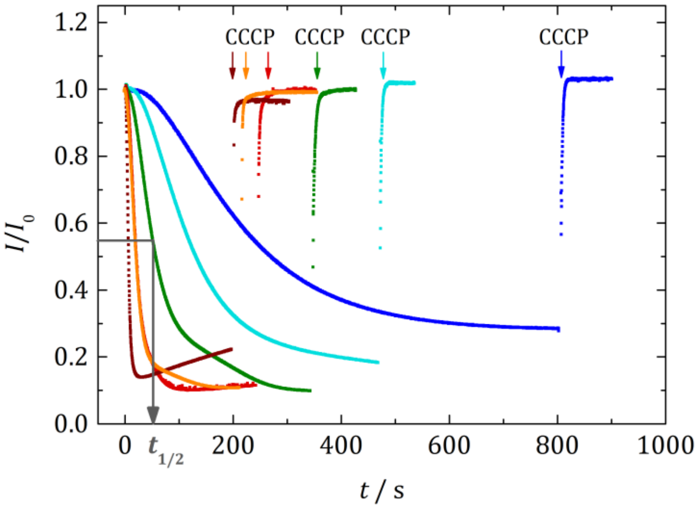

Figure 4.7. ACMA based activity measurements of ATPase-liposomes (DOPC/POPE/POPS/cholesterol (50:20:10:20), nominal p/l = 1:20,000). The assay was performed in ATPase-buffer (5 nM valinomycin, 0.5 mM MOPS, 100 mM KCl, 2 mM $MgCl_2$, pH 7.3) with 0.9 µM ACMA at 20 °C (blue), 25 °C (cyan), 30 °C (green), 37 °C (orange), 40 °C (red) and 50 °C (dark red). After ATP addition (1.2 mM) at $t = 0$, all samples showed significant quenching of fluorescence, while the intensity minima were attained faster with elevating temperatures. CCCP addition (0.4 µM) led to a collapse of the proton gradients, resulting in a restoration of fluorescence intensity to the initial value. At 50 °C (dark red), the minimal fluorescence intensity was reached most rapidly, but proton leakage through the membrane was increased, resulting in a significant linear intensity increase. A slightly increased proton leakage was also found at 40 °C, but not at lower temperatures. $\lambda_{ex/em}$ = 410/490 nm.

To obtain a value that describes the temperature dependence of the enzyme activity, the temperature coefficient Q_{10} was determined (Equation 4.1).[130]

$$\left(\frac{Rate_n}{Rate_{20}}\right) = Q_{10}^{\;(T_n-T_{20})/_{10}} \qquad 4.1$$

For this purpose, the time the fluorescence intensity took to decrease to half of its minimal value ($t_{½}$) was readout for each temperature (indicated by grey arrow for the measurement at 30 °C in Figure 4.7). The reciprocal value of $t_{½}$ corresponds to the fluorescence-quenching rate (referred to as $Rate_n$) and correlates to the protein's proton pumping rate. Subsequently, the temperature differences T_n–T_{20} were calculated by subtracting 20 °C (T_{20}) from each of the other temperatures (T_n). Furthermore, the ratios of the different quenching rates $Rate_n$/$Rate_{20}$ were calculated by dividing each of the rates ($Rate_n$) through the rate obtained from the measurement at 20 °C ($Rate_{20}$). The above-mentioned values are listed in Table 4-2. The values for $Rate_n/Rate_{20}$ are plotted against those for T_n–T_{20} in Figure 4.8. Fitting Equation 4.1 to the plotted values yielded a Q_{10}-value of 3.14. This result indicated that the enzyme activity is increased approx. 3-fold for a temperature elevation of 10 K.

Table 4-2 Parameters derived from the ACMA assay performed at different temperatures (cf. Figure 4.7, Chapter 4.3). T_n–T_{20} being the particular difference between the assay temperatures, $t/2$ the time it took until half of the fluorescence intensity minimum was reached and *Rate* its reciprocal values, which is the quenching rate. *Rate*$_n$/Rate$_{20}$ represents the ratio of the quenching rate for each temperature to the one at 20 °C.

T_n / °C	T_n–T_{20} / K	$t_{½}$ / s	*Rate* / s^{-1}	*Rate*$_n$/Rate$_{20}$
20	0	189	$5.29 \cdot 10^{-3}$	1.00
25	5	109	$9.24 \cdot 10^{-3}$	1.75
30	10	51.2	$1.95 \cdot 10^{-2}$	3.69
37	17	18.6	$5.28 \cdot 10^{-2}$	10.2
40	20	19.2	$5.21 \cdot 10^{-2}$	9.85
50	30	6.20	$1.61 \cdot 10^{-1}$	30.5

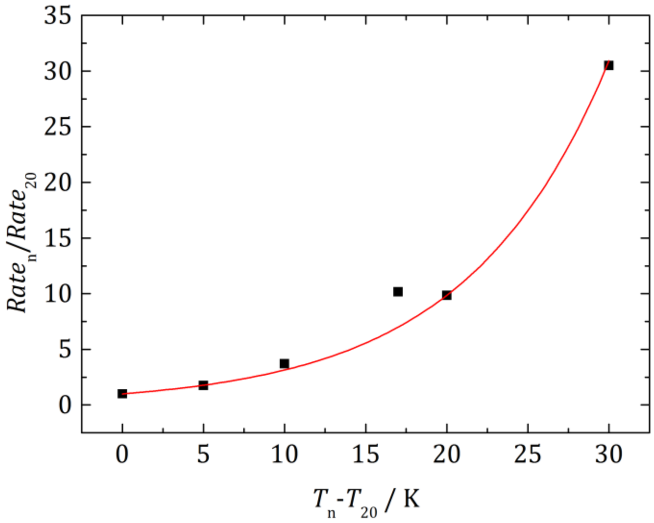

Figure 4.8. Temperature dependence of the TF$_O$F$_1$-ATPase proton pumping activity in DOPC/POPE/POPS/cholesterol (50:20:10:20) liposomes. Ratios of the different quenching rates *Rate*$_n$/*Rate*$_{20}$ were calculated by dividing each of the rates (*Rate*$_n$) through the rate obtained from the measurement at 20 °C (*Rate*$_{20}$) and plotted against the corresponding temperature differences T_n–T_{20}. Fitting Equation 4.1 to the data results in $Q_{10} = 3.14$, which indicates a 3-fold increase of the ATPase activity for each increase of temperature by 10 K.

4.4 Analysis of the TF_0F_1-ATPase activity with the lipid-coupled pH-sensor Oregon Green 488-DHPE

- Parts of this Chapter have been published: M. Schwamborn, J. Schumacher, J. Sibold, N. K. Teiwes, C. Steinem, Monitoring ATPase induced pH changes in single proteoliposomes with the lipid-coupled fluorophore Oregon Green 488, *Analyst* **2017**, *accepted,* DOI: 10.1039/C7AN00215G.

Usually, pH-value alterations in vesicles are detected with pH-sensitive fluorophores that are membrane permeable, like ACMA and acridine orange. These substances are added to the bulk solution of the sample and upon vesicular acidification, the dye molecules currently located in the vesicle are protonated, thereby become quenched and membrane impermeable. As a result, the equilibrium distribution is disturbed and more deprotonated dye molecules from the bulk solution diffuse into the acidified vesicles, were the dye accumulates. Additionally, deprotonated and thus hydrophobic ACMA molecules partition into the lipid membrane. This mechanism makes it quite difficult to quantify the vesicle acidification.[72,124,125,127]

By utilizing a lipid-coupled, pH-sensitive fluorophore that is anchored to the proteoliposome membrane, it is possible to determine the luminal pH-value of the sample and no effects from changes in partition equilibrium have to be taken into account.[131] First, all vesicles emit the fluorescence of the lipid-coupled pH-sensor, but when ATP is added and liposomes with functionally reconstituted TF_0F_1-ATPase are acidified, only the fluorophores present in their inner lipid monolayer contribute to the fluorescence intensity change of the whole sample. Therefore, a calibration curve that correlates the fluorescence intensities to pH-values allows determining the mean luminal pH-value of the proteoliposomes.

Fluorescein and Oregon Green 488 are the only commercially available fluorophores that are pH-sensitive and coupled to a lipid (1,2-dihexadecanoyl-*sn*-glycero-3-phosphoethanolamine, DHPE), with Oregon Green 488 having the greater photostability.[71,132] Here, for the first time, Oregon Green 488-DHPE (OG488-DHPE) has been applied to monitor the active acidification of proteoliposomes and to determine the resulting mean luminal pH-value.

In the following chapters, the fluorophore's emission behavior dependent on the pH-value will be described and the acidification of TF_0F_1-ATPase liposomes will be monitored by reading out the OG488-DHPE fluorescence intensity change.

4.4.1 Characterization of the pH-dependent Oregon Green 488-DHPE fluorescence

To ensure the suitability of OG488-DHPE as a fluorophore for detecting ATPase activity in liposomes, its fluorescence emission behavior dependent on the pH-value was analyzed. The literature known pK_a-value of free Oregon Green 488 in water is 4.7 ± 0.1, while the pK_a of OG488-DHPE in a pure DOPC or DOPG matrix is 6.3 ± 0.1 and 6.7 ± 0.1, respectively.[104] These values show a significant difference between free fluorophore and the lipid-coupled one, and that even a different lipid head group can alter the pK_a by 0.4 units. Therefore, the pK_a-value of OG488-DHPE was determined in the employed lipid environment of DOPC/POPE/POPS/cholesterol/OG488-DHPE (49:20:10:20:1).

Large unilamellar vesicles, with a diameter of 100 nm and the above-mentioned composition were prepared in ATPase-buffer (0.5 mM MOPS, 100 mM KCl, 2 mM $MgCl_2$) with pH-values of 4.3, 5.3, 6.3 and 7.3. The lipid concentration of each sample was quantified (Chapter 3.2.5) and kept constant in each experiment ($c_{\text{phospholipid}}$ = 64 µM). Subsequently, the fluorescence intensities of the samples were measured (λ_{ex} = 508 nm, λ_{em} = 510-650 nm). Figure 4.9 shows the emission spectra at different pH-values that were normalized to the maximal fluorescence intensity at $\lambda_{\text{em, max}}$ = 534 nm obtained from the measurement at pH 7.3. With increasing acidity, the fluorescence intensities are strongly reduced. For a pH-value of 6.3, the intensity decreased by 35 % (blue curve), for a pH-value of 5.3 by 84 % (green curve) and at pH-value of 4.3, no significant fluorescence emission was found (black curve).

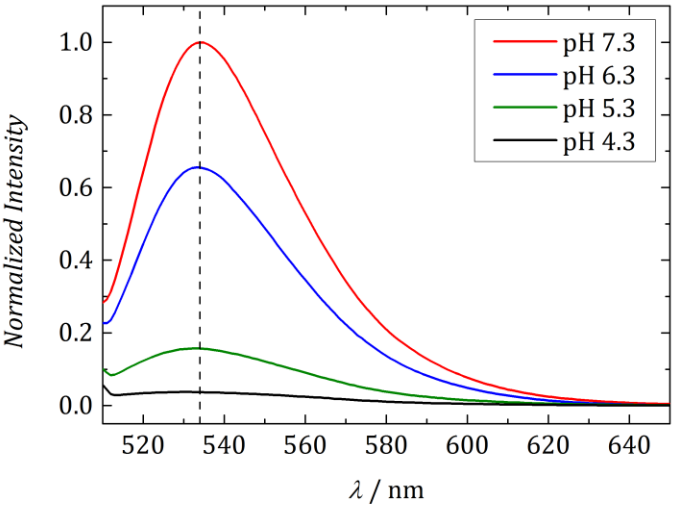

Figure 4.9. OG488-DHPE emission spectra of LUVs ($c_{\text{phospholipid}}$ = 64 µM) with a composition of DOPC/POPE/POPS/cholesterol/OG488-DHPE (49:20:10:20:1) at pH-values of 7.3 (red), 6.3 (blue), 5.3 (green) and 4.3 (black) (0.5 mM MOPS, 100 mM KCl, 2 mM $MgCl_2$). With decreasing pH-values, the maximal fluorescence emission ($\lambda_{\text{em, max}}$ = 534 nm, indicated by dashed line) was reduced by 35 % for a pH-value of 6.3 and by 84 % for a pH-value of 5.3. At a pH-value of 4.3, there was nearly no fluorescence emission. λ_{ex} = 508 nm.

To determine the pK_a-value from the data presented in Figure 4.9, the emission peak intensities were plotted against the corresponding pH-values (Figure 4.10). Equation 4.2 is a variant of the Henderson-Hasselbalch equation, describing the fluorescence intensity I of a fluorophore as a function of the pH-value, [105]

$$I = I_{\text{min}} + \frac{I_{\text{max}} - I_{\text{min}}}{1 + 10^{\text{p}K_{\text{a}} - \text{pH}}} \qquad 4.2$$

With I_{min} being the minimal, I_{max} the maximal pH-dependent fluorescence intensity and pK_a the pK_a-value of the fluorophore. Fitting Equation 4.2 to the data in Figure 4.10 yielded a pK_a-value of 6.1 for OG488-DHPE in a DOPC/POPE/POPS/cholesterol/OG488-DHPE (49:20:10:20:1) matrix. Besides the pK_a-value, the fit generated pH-dependent minimal and maximal fluorescence intensities of I_{min} = 2.8 a.u. and I_{max} = 530.3 a.u., respectively.[123] For comparison, the dashed grey line shows the simulated curve for the free fluorophore with a pK_a of 4.7.[104]

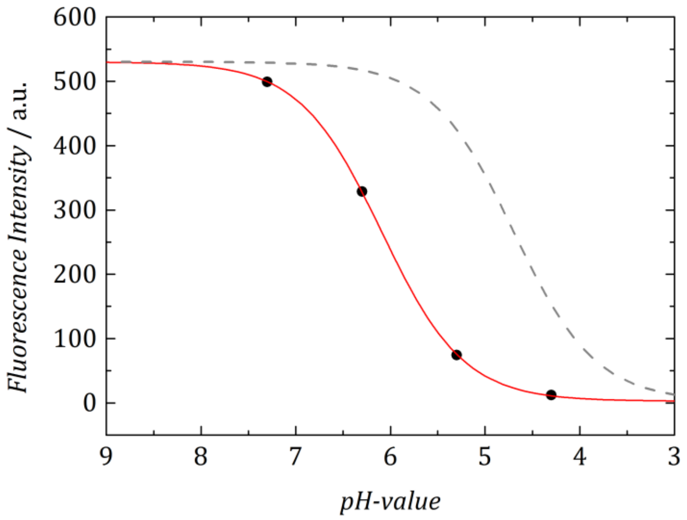

Figure 4.10. Fitting Equation 4.2 to the pH-dependent fluorescence intensities (black dots), yielded a p*K*a-value of 6.1 for OG488-DHPE in a DOPC/POPE/POPS/cholesterol/OG488-DHPE (49:20:10:20:1) matrix in ATPase-buffer (0.5 mM MOPS, 100 mM KCl, 2 mM $MgCl_2$). For I_{max} and I_{min} values of 530 a.u. and 2.80 a.u. were obtained. For comparison, the simulated curve for pK_a = 4.7 of the free Oregon Green is shown (grey dashed curve).

In an ATPase activity assay, only the inner lipid monolayer of acidified vesicles contributes to a decrease in the overall fluorescence signal, since the outer leaflet is buffered by the large bulk solution (buffer inside and outside the liposomes: 0.5 mM MOPS, 100 mM KCl, 2 mM $MgCl_2$). To investigate the overall fluorescence response of OG488-DHPE doped vesicles under these conditions, spectra of liposomes with luminal pH-values of 6.3, 5.3 and 4.3 were measured in a bulk solution of pH 7.3.

The emission peak intensities at $\lambda_{em, max}$ = 534 nm were normalized to the minimal fluorescence intensity obtained from the fit with Equation 4.2 (Figure 4.10) I_{min} = 2.80 a.u. and the intensity of 499 a.u. from the sample with a luminal and bulk pH-value of 7.3, representing the maximal fluorescence intensity attainable in the conducted experiments. The resulting data is presented in Figure 4.11. For a luminal pH-value of 6.3 a normalized intensity of 0.83 was found and for luminal pH-values of 5.3 and 4.3 the normalized intensities were both 0.61.[123]

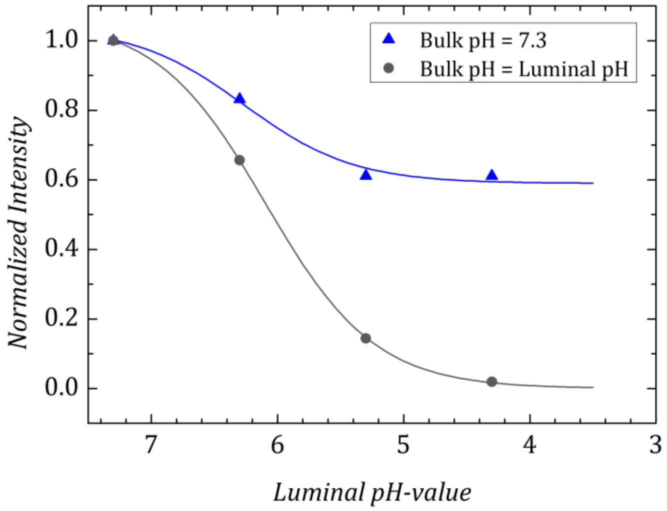

Figure 4.11. Normalized fluorescence intensities of vesicles DOPC/POPE/POPS/cholesterol/OG488-DHPE (49:20:10:20:1) with different luminal pH-values in a bulk solution of pH 7.3 (0.5 mM MOPS, 100 mM KCl, 2 mM $MgCl_2$) (blue triangles) and with identical luminal and bulk pH. The grey curve displays the function fitted to the intensities resulting from the measurements with identical luminal and bulk pH-values. The blue curve shows the function fitted to the intensities resulting from the measurements with differing luminal and a constant bulk pH-value of 7.3.

The grey curve is a result of fitting Equation 4.2 to the normalized intensities from the measurements with identical luminal and bulk pH-values ($pK_a = 6.09$, $I_{max} = 1.06$, $I_{min} = 0$), while the blue curve resulted from fitting Equation 4.2 to the intensities from the measurements with differing luminal and a constant bulk pH-value of 7.3 ($pK_a = 6.26$, $I_{max} = 1.04$, $I_{min} = 0.59$). These results show that the maximum possible fluorescence intensity decrease in an OG488-DHPE acidification assay would be approx. 40 % of the initial fluorescence. Such a decrease would only be obtained, if all liposomes experienced a luminal pH-reduction from pH 7.3 to approx. pH 4.5. In this case, the emission intensity from the fluorophores of the inner membrane leaflet is nearly completely quenched and one can assume that the measured intensity results only from the fluorophores anchored to the outer vesicle membrane. The vesicles for the calibration were made by extrusion through a polycarbonate membrane with 100 nm diameter pore size, yielding large unilamellar vesicles with diameters around 100 nm, which is a similar size as the TF_0F_1-ATPase-liposomes with an average diameter of 95 nm (Figure 4.5, Chapter 4.2).[133] Assuming a uniform distribution of OG488-DHPE, the fluorescence intensity emitted from the outer membrane leaflet corresponds to the outer membrane area fraction of the vesicle. Figure 4.12 shows the calculated outer membrane area fractions in dependence of the vesicle size and an assumed bilayer thickness of 4.5 nm.[134,135] For a 50 nm diameter vesicle the outer membrane surface represents about 60 % of the total membrane area, for a 100 nm diameter the value is decreased to 55 % and for a 200 nm diameter vesicle to 52 %.

The remaining 59 % fluorescence intensity are thus in good agreement with the 55 % of the outer membrane area fraction.

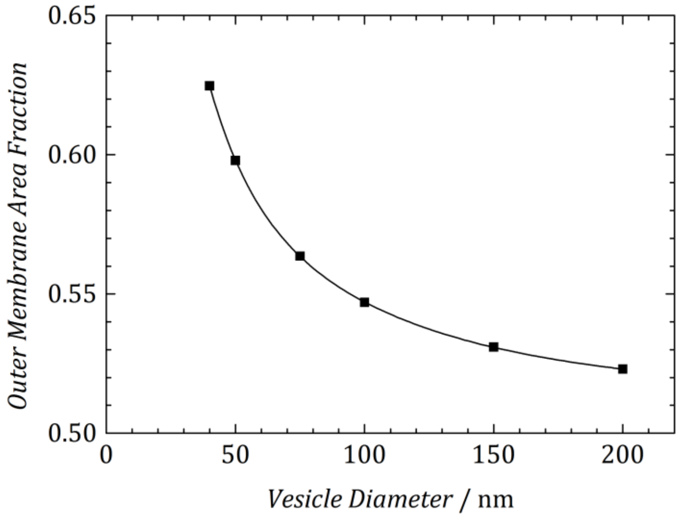

Figure 4.12. Calculated outer membrane area fraction as a function of vesicle diameter, assuming a bilayer thickness of 4.5 nm.[134,135] The relative amount of fluorescence intensity emitted from the OG488-DHPE of the outer vesicles membrane leaflet, correlates with the area fraction of the outer vesicle surface. For a 100 nm diameter vesicle the outer membrane area is approx. 55 % of the total area, which is in good agreement with minimum of 59 % remaining intensity in the calibration curve.

The correlation of the fluorescence intensities to pH-values will permit to determine a mean pH-value for the liposomes in the OG488-DHPE-based ATPase-activity bulk assay.

4.4.2 Results of the Oregon Green 488-DHPE based TF_0F_1-ATPase activity assay

For monitoring the TF_0F_1-ATPase activity in liposomes based on OG488-DHPE fluorescence emission, fluorimeter measurements, similar to the ACMA acidification assay (see Chapter 4.3), were conducted.

Figure 4.13 shows a scheme of the OG488-DHPE based ATPase activity assay. The proteoliposomes (DOPC/POPE/POPS/cholesterol/OG488-DHPE (49:20:10:20:1), $c_{\text{phospholipid}} \approx 60$ µM) are added to the ATPase-buffer (0.5 mM MOPS, 100 mM KCl, 2 mM $MgCl_2$, pH 7.3), containing the K^+-ionophore valinomycin (5 nM) to enable a charge equilibration for transported protons. ATP addition (1.2 mM, $t = 0$ s) causes the ATPase to pump protons, leading to a pH-value decrease in the lumina of proteoliposomes with active ATPase. Consequently, OG488 molecules anchored to the inner leaflet of the vesicle membrane are protonated and their fluorescence is quenched. Finally, the addition of CCCP (0.4 µM) leads to a collapse of the proton gradient, so that the fluorescence intensity is restored quickly.

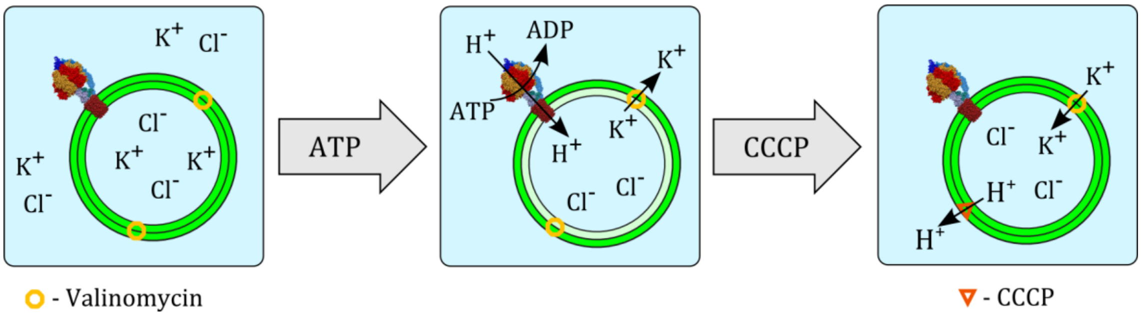

Figure 4.13. Scheme of the OG488-DHPE based ATPase activity assay. To the ATPase-buffer (0.5 mM MOPS, 100 mM KCl, 2 mM $MgCl_2$, pH 7.3), proteoliposomes ($c_{\text{phospholipid}} \approx 60$ µM) and the K^+-ionophore valinomycin (5 nM) are added. Addition of ATP (1.2 mM) results in ATPase-mediated proton pumping into the lumina and therewith a protonation and quenching of the OG488-DHPE molecules located on the inner membrane leaflet. CCCP (0.4 µM) addition leads to a collapse of the proton gradient and the OG488-DHPE fluorescence restores.

The measured fluorescence intensities were normalized to the intensity immediately after ATP addition and then converted into pH-values with Equation 4.3. The parameters were obtained from the fit in Figure 4.11 ($pK_a = 6.3$, $I_{max} = 1.04$ and $I_{min} = 0.59$).

$$\mathrm{pH} = \mathrm{p}K_\mathrm{a} + \log\frac{I - I_\mathrm{min}}{I_\mathrm{max} - I} \qquad 4.3$$

Figure 4.14 displays the result of a representative OG488-DHPE-based acidification assay. The black curve displays a measurement of non-inhibited ATPase, while the red curve represents a sample inhibited by sodium azide (1 mM). Sodium azide strongly reduces the ATP-hydrolysis activity by forming hydrogen bonds with Lysine-162 from the β-subunit and Arginine-373 from the α-subunit, preventing ADP from being released, thus hindering further ATP from binding and therewith proton translocation.[136]

After ATP addition ($t = 0$ s), the mean pH-values of the non-inhibited as well as of the azide-inhibited sample started to decrease. The sample with active ATPase activity experienced a mean luminal pH-value decrease by 0.45 units to a mean pH-value of approx. 6.85. For the inhibited enzyme, the mean pH-value decreased by only 0.1 unit to a mean luminal pH-value of 7.20, proving a significant enzyme inhibition. In both cases, CCCP addition led to an instant breakdown of the pH-gradient, however, in case off the azide-inhibited sample the luminal pH-value did not fully recover.

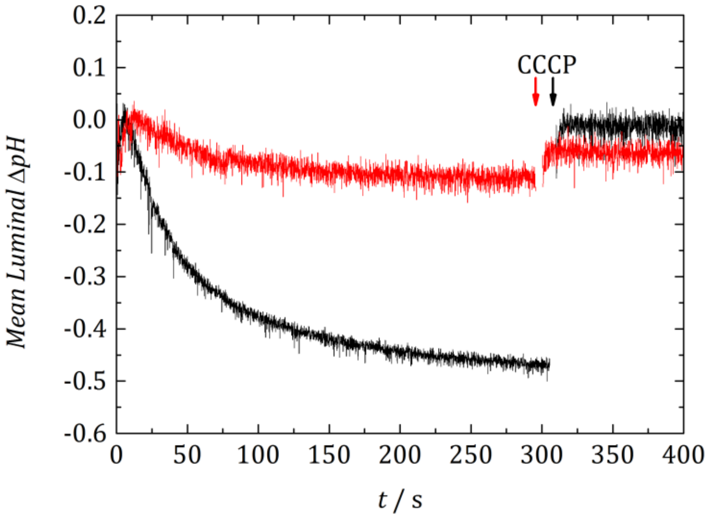

Figure 4.14. OG488-DHPE acidification assay for TF$_0$F$_1$-ATPase vesicles (DOPC/POPE/POPS/cholesterol/OG488-DHPE (49:20:10:20:1), nominal p/l = 1:20,000, $c_{\text{phospholipid}} \approx 60$ µM) in ATPase-buffer (5 nM valinomycin, 0.5 mM MOPS, 100 mM KCl, 2 mM MgCl$_2$, pH 7.3). ATP (1.2 µM) was added at $t = 0$ s. In case of the non-inhibited ATPase-liposomes (black curve) the mean pH-value decreased from pH 7.30 to 6.85 (ΔpH = 0.45) within 300 s. The activity of the NaN$_3$ (1 mM) inhibited ATPase-liposomes (red curve) was reduced significantly, as the mean pH-value only decreased from pH 7.3 to 7.2. CCCP addition (0.4 µM) caused a collapse of the proton gradient. $\lambda_{\text{ex/em}} = 508/534$ nm.

The distribution of ΔpH-values reached during the performed OG488-DHPE acidification assays ($n = 17$) is shown in Figure 4.15. The average of the mean luminal pH-values was 6.85 ± 0.07 (SD) or ΔpH = −0.45 ± 0.07 (SD), respectively; the strongest mean pH-value decrease observed was ΔpH = −0.80 to a mean pH-value of 6.50 and the weakest was ΔpH = −0.27 to a mean pH-value of 7.03.[123]

In this work, the TF$_0$F$_1$-ATPase activity has been monitored for the first time with a lipid-coupled fluorophore, the commercially available OG488-DHPE. Furthermore, it was possible to determine the mean luminal pH-value decreases of the proteoliposomes by correlating the fluorescence intensities to luminal pH-values. Thus, the OG488-DHPE based acidification assay is a powerful tool, not only to monitor the acidification activity, but also to quantify the mean luminal pH-values reached upon acidification.

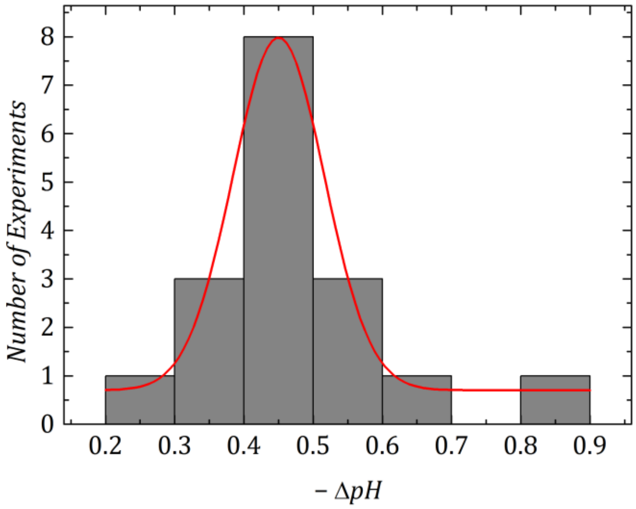

Figure 4.15. Distribution of mean luminal ΔpH-values obtained in the OG488-DHPE acidification assay (n = 17). The mean luminal ΔpH-values showed a Gaussian distribution with an average mean luminal ΔpH of −0.45 ± 0.07 (SD) or pH of 6.85 ± 0.07 (SD).

4.5 Combined fusion and acidification assay based on Oregon Green 488-DHPE

As described in Chapter 1.3.2, lipid bilayer fusion mediated by SNARE-proteins (soluble *N*-ethylmaleimide-sensitive-factor attachment receptor) could be a useful tool to reconstitute the TF_0F_1-ATPase into pore-spanning lipid-bilayers (PSLBs). To induce the fusion of two lipid membranes, synaptobrevin 1-116 (Sb1-116), anchored to the one membrane, and the ΔN49-complex, anchored to the other membrane, form a coiled-coil motif to overcome the energy needed for the bilayer fusion.[137,138] With the lipids of both membranes mixing, cargo membrane proteins should also be merged into the resulting fusion product.

To test the feasibility of the SNARE-mediated reconstitution, a combined fusion and acidification assay has been conceived. As shown in Figure 4.16, the first step consists of monitoring the dequenching of OG488-DHPE doped liposomes that contain the SNARE-protein Sb1-116 and fuse with non-fluorescent ATPase-ΔN49-liposomes. Besides the pH-sensitivity, which was charaterized in Chapter 4.4., OG488-DHPE experiences self-quenching when a certain amount is present in a lipid bilayer. This self-quenching effect is used to monitor fusion, since the mixing with non-fluorescent lipids leads to a dilution of the fluorophors, entailing a dequenching effect, i.e.an increase in fluorescence emission.[108] In the second step, the OG488-DHPE acidification assay is performed with the fusion products (cf. Chapter 4.4.2).

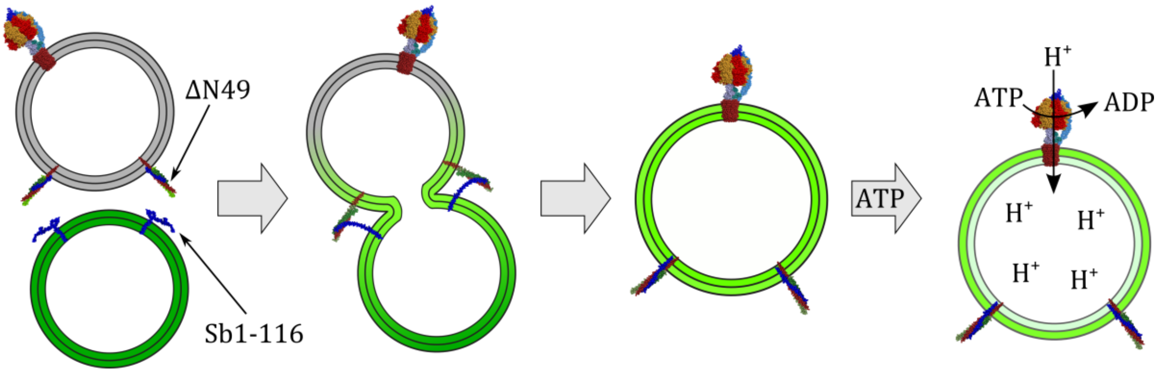

Figure 4.16. Scheme of the combined fusion and acidification assay based on the pH-sensitive, lipid-coupled fluorophore OG488-DHPE. First, the fusion process of ATPase-ΔN49-LUVs and Sb1-116-OG488-liposomes is monitored via OG488-DHPE dequenching. Succeeding, ATPase-mediated acidification of the fusion products is observed. It is important to note, that the activity of non-fused or hemi-fused ATPase-vesicles will not be detectable, as there is no contact with the pH-sensor OG488.

At this point, it is important to note that only ATPase-ΔN49-vesicles that successfully fused with OG488-DHPE doped Sb1-116-vesicles can contribute to a signal in the acidification assay.

4.5.1 Characterization of SNARE-mediated vesicle fusion

Generally vesicle fusion can be monitored by lipid mixing and/or content mixing assays.[139,140] The lipid mixing assays often monitor a Förster resonance energy transfer (FRET) between two lipid-coupled fluorophores. For example, one liposome population is doped with a lipid-coupled donor fluorophore and the other population with an acceptor fluorophore. Upon mixing of both an increasing FRET between the fluorophores occurs.[141] It is also possible to dope one liposome population with a donor and an acceptor fluorophore that perform a FRET. When the donor fluorophore is excited and its fluorescence emission intensity is measured, a dilution of the FRET-pairs through fusion with non-fluorescent liposomes leads to a reduced FRET-efficiency, thus increasing the donor fluorescence emission intensity.[140] Another method for monitoring lipid mixing is to use a high concentration of a lipid-coupled fluorophore in one liposome population so that a self-quenching effect occurs. Upon fusion with non-fluorescent liposomes, the fluorophore is diluted and the self-quenching is reduced. This method was applied by Pähler *et al.* to monitor and quantify peptide-induced vesicle fusion.[108]

In this work, the pH-sensitivity of OG488-DHPE has been used to monitor ATPase-mediated acidification (cf. Chapter 4.4.2) and its self-quenching will be characterized in the following, to allow a quantification of the lipid mixing efficiency resulting from SNARE-mediated fusion. It is necessary to assess the fusion efficiency, which corresponds to the lipid mixing efficiency, in order to ensure the generation of enough fusion products that can later contribute to the signal in the acidification assay (see scheme in Figure 4.16, Chapter 4.5).

For the quantification of fusion by means of OG488-dequenching, a calibration curve of the fluorescence emission intensity depending on the fluorophore concentration was created.[108] For this purpose, liposomes with defined amounts of OG488-DHPE in a DOPC/POPE/POPS/cholesterol matrix (50-x:20:10:20:x, x = 0.7 mol%, 1.4 mol%, 2.8 mol%, 4.1 mol%, 5.5 mol%, 6.9 mol% and 8.3 mol%) were prepared and their fluorescence emission F_{quench} was measured (see Figure 4.17 A, left ordinate). Subsequently, Triton X-100 (1 mM) was added to lyse the vesicles and to eliminate the self-quenching effect, yielding the maximum intensity F_{max} (see Figure 4.17 A, right ordinate). To obtain the calibration curve, the values for $F_{\mathrm{max}}/F_{\mathrm{quench}}$ were plotted against the OG488-DHPE-concentration and exponential equation could be fitted to the data (Figure 4.17 B).

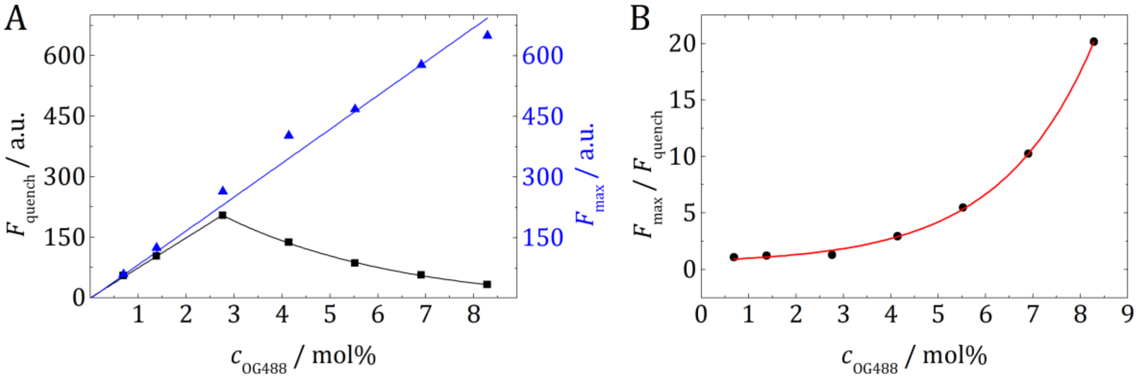

Figure 4.17. (A) Quenched fluorescence emission F_{quench} (left ordinate) and maximum fluorescence emission F_{max} (right ordinate) of vesicles (DOPC/POPE/POPS/cholesterol/OG488-DHPE (50-x:20:10:20:x) ($c_{\mathrm{phospholipid}} \approx 120$ µM) in ATPase-buffer (0.5 mM MOPS, 100 mM KCl, 2 mM $MgCl_2$, pH 7.3). Above $c_{\mathrm{OG488}} \approx 3$ mol%, the self-quenching effect strongly increased. The intensity F_{max} of lysed vesicles (Triton X-100, 1 mM) increased linearly with the c_{OG488}. (B) The calibration curve of $F_{\mathrm{max}}/F_{\mathrm{quench}}$ vs. c_{OG488} allows to ascertain c_{OG488} to a measured value of $F_{\mathrm{max}}/F_{\mathrm{quench}}$.

The experiments for the quantification of fusion were performed with vesicles containing Sb1-116 (nominal p/l = 1:500) and 5.5 mol% OG488-DHPE and an equimolar amount of ATPase-ΔN49-liposomes ($c_{\mathrm{phospholipid}} = 65$ µM, ATPase: nominal p/l = 1:20,000, ΔN49: nominal p/l = 1:500) at 37 °C (reconstitution methods see Chapter 0 and Chapter 3.2.2.2). Figure 4.18 A shows a representative dequenching curve. At $t = 0$ min both liposome populations were mixed and subsequently the fluorescence intensity started to increase. The intensity was normalized to its initial value I_0. After 50 min, the intensity did not seem to increase much further, indicating the end of the fusion process.

To determine the fusion efficiency, $F_{\text{max}}/F_{\text{quench}}$ was obtained at the very beginning of the fusion process, where hardly any lipid mixing could have taken place, and at the end of the process when the fusion did not proceed any further, indicated by a saturation of fluorescence intensity increase (Figure 4.18 A). To obtain $F_{\text{quench-start}}$, a spectrum was recorded immediately after mixing both liposome populations and the peak intensity $\lambda_{\text{em, max}}$ = 534 nm was readout. When the intensity increased no more, $F_{\text{quench-end}}$ was measured ($\lambda_{\text{em, max}}$ = 534 nm). Addition of Triton X-100 lysed the vesicles determining F_{max} ($\lambda_{\text{em, max}}$ = 534 nm). The spectra of $F_{\text{quench-start}}$, $F_{\text{quench-end}}$ and F_{max} are shown in Figure 4.18 B.

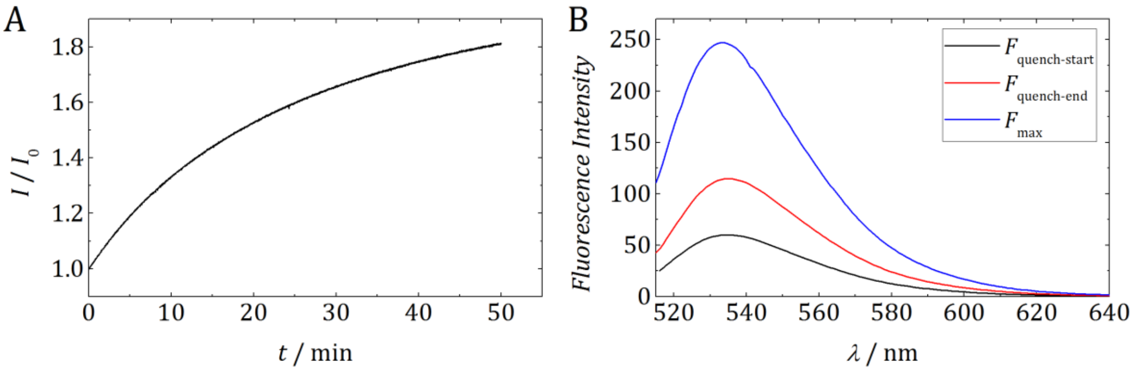

Figure 4.18. (A) Exemplary dequenching curve from fusion of ATPase-ΔN49- (DOPC/POPE/POPS/cholesterol (50:20:10:20), ATPase: nominal p/l = 1:20,000, ΔN49: nominal p/l =1:500) and Sb1-116-vesicles (DOPC/POPE/POPS/cholesterol/OG488-DHPE (44.5:20:10:20:5.5), nominal p/l =1:500) in ATPase-buffer (0.5 mM MOPS, 100 mM KCl, 2 mM $MgCl_2$, pH 7.3). Equal concentrations ($c_{\text{phospholipid}}$ = 65 μM) of both liposome populations were used. $\lambda_{\text{ex/em}}$ = 508/534 nm. (B) Fluorescence emission spectra of $F_{\text{quench-start}}$ (black), $F_{\text{quench-end}}$ (red) and F_{max} (blue). For calculation of $F_{\text{max}}/F_{\text{quench}}$, peak intensities were read out at 534 nm. λ_{ex} = 508 nm.

The calibration curve describing the fluorescence intensity depending on the fluorophore concentration (Figure 4.17 B) allowed to assign the determined values of $F_{\text{max}}/F_{\text{quench-start}}$ and $F_{\text{max}}/F_{\text{quench-end}}$ to the corresponding OG488-DHPE concentrations. The resulting ratio of $F_{\text{max}}/F_{\text{quench-start}}$ was 4.1 and corresponded to an effective content of 4.9 mol% OG488-DHPE at the beginning of the fusion process. The ratio of $F_{\text{max}}/F_{\text{quench-end}}$ resulted in a value of 2.1, corresponding to 3.3 mol% of OG488-DHPE in the fusion products. These values are marked with asterisks in Figure 4.19 A.

To quantify the lipid mixing efficiency χ_{fusion}, the concentration of 3.3 mol% OG488-DHPE obtained after the fusion process is compared to the theoretical value that would represent 100 % fusion efficiency. Ensuring the same concentration of the two fusing liposome populations, the initial OG488-DHPE concentration of 4.9 mol% would be halved to 2.45 mol% in case of complete fusion. With the knowledge of the OG488-DHPE concentrations assigned to 0 % and 100 % fusion efficiency, the concentration of 3.3 mol% in the fusion products could be allocated to 65 % fusion efficiency in this case (see Figure 4.19 B). From five experiments, an average lipid mixing efficiency of 59 ± 4 % (SD) was obtained.

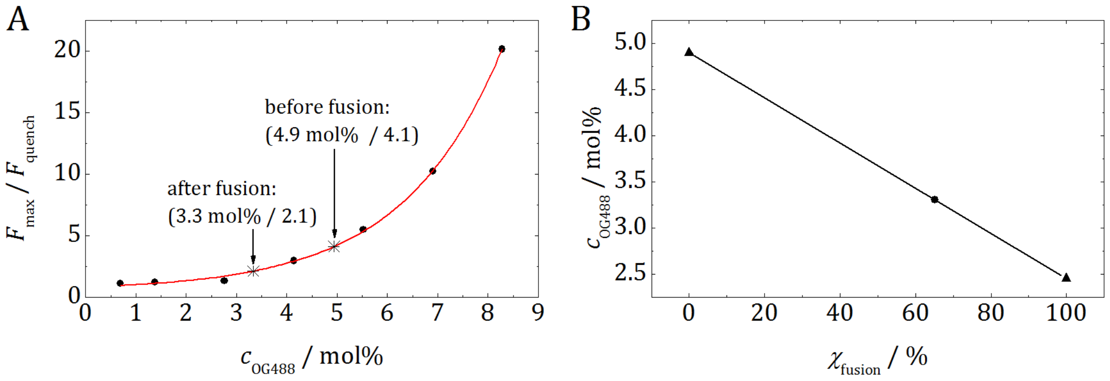

Figure 4.19. (A) With the calibration curve, values of F_{max}/F_{quench} before and after the fusion process are assigned to the corresponding OG488-DHPE concentrations (asterisks). (B) Dependence of the OG488-DHPE concentration on the lipid mixing efficiency χ_{fusion}. 3.3 mol% OG488-DHPE in the fusion products corresponds to a fusion efficiency of 65 % (circle).

With this method, the general percentage of fusion can be estimated, but it cannot be distinguished between full fusion and possible hemifusion states, where only the outer lipid leaflets fuse, while the inner monolayers are not mixed. Hernandez *et al.* discovered that approximately 25 % of the liposomes were found in a hemifusion state after 1 h fusion time, with exactly the same SNARE proteins as used in this work and a similar lipid composition (Hernandez *et al.*: PC:PE:PS:cholesterol (50:20:20:10), this work: PC:PE:PS:cholesterol (50:20:10:20)).[138]

4.5.2 Acidification assay after fusion

After characterizing the lipid mixing efficiency, the proton pumping activity of the TF_OF_1-ATPase in the fusion products was monitored by performing the OG488-DHPE acidification assay (cf. Chapter 4.4.2). Before starting the OG488-DHPE-based fusion- and succeeding acidification assay, the functional reconstitution of the ATPase was assured by means of an ACMA acidification assay (cf. Chapter 4.3). In Figure 4.20 an ACMA assay of ATPase-ΔN49-LUVs is shown. Upon ATP addition at $t = 0$ s the ACMA fluorescence intensity was significantly quenched and addition of CCCP led to a proton gradient collapse, i.e. fluorescence recovery.

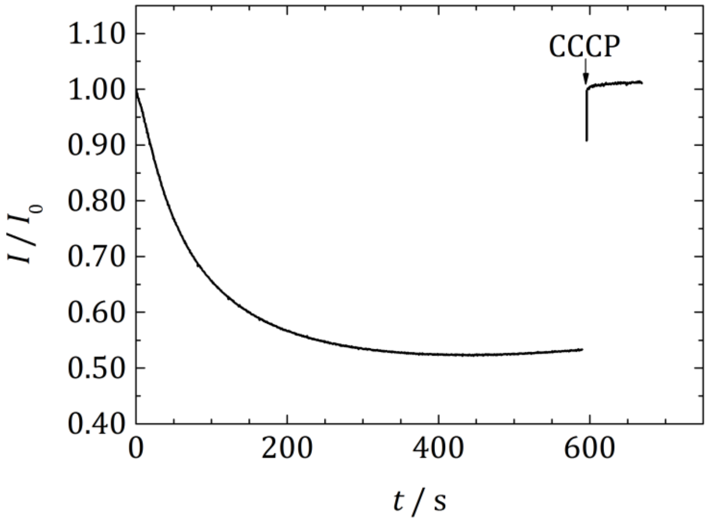

Figure 4.20. The functional ATPase reconstitution into the ATPase-ΔN49-LUVs (DOPC/POPE/POPS/cholesterol (50:20:10:20), ATPase p/l = 1:20,000, ΔN49 p/l = 1:500) was assured by means of an ACMA assay, before performing the combined fusion and acidification assay. Upon ATP addition (1.2 mM, t = 0 s), the ACMA (0.9 µM) fluorescence intensity decreased strongly and reached its minimal value after approx. 100 s. Addition of CCCP (0.4 µM) led to a collapse of the proton gradient, resulting in a recovery of the fluorescence intensity. Buffer: 5 nM valinomycin, 0.5 mM MOPS, 100 mM KCl, 2 mM $MgCl_2$, pH 7.3, $\lambda_{ex/em}$ = 410/490 nm.

With the functional reconstitution of the ATPase assured, the combined OG488-DHPE fusion and acidification assay was performed. The first step consisted of monitoring the fusion of colorless ATPase-ΔN49-liposomes with OG488-DHPE doped Sb1-116-LUVs. A fluorophore concentration of 2 mol% was chosen in order to obtain around 1 mol% OG488-DHPE in the fusion products, which was appropriate to monitor the ATPase mediated acidification (see Chapter 4.4.2). Both liposome populations were added in equimolar concentration ($c_{\text{phospholipid}}$ = 65 µM) to the cuvette and subsequently, the fluorescence intensity started to increase strongly due to a dequenching of the OG488-DHPE (Figure 4.21). After 10 min, the fluorescence intensity increase slowed down continuously, until saturation was reached after 40–50 min. This indicated that there was no more lipid mixing and the fusion process had ended.

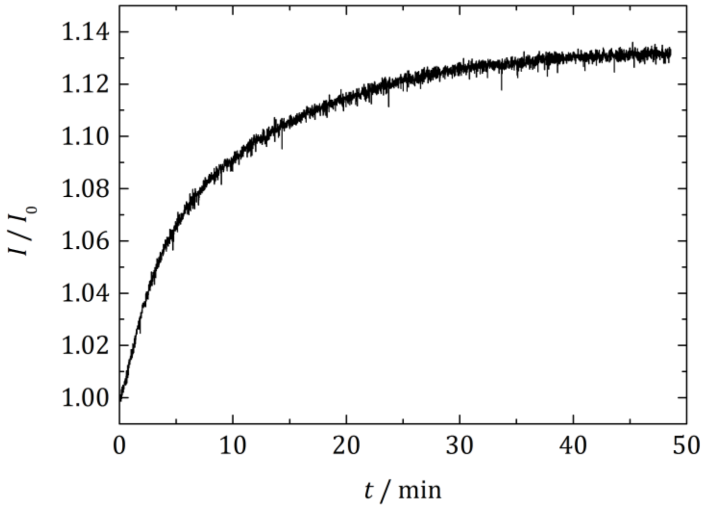

Figure 4.21. Exemplary dequenching curve from fusion of ΔN49-ATPase-LUVs (DOPC/POPE/POPS/cholesterol (50:20:10:20), ΔN49 p/l = 1:500, ATPase p/l = 1:20,000) and Sb1-116-LUVs (DOPC/POPE/POPS/cholesterol/OG488-DHPE (48:20:10:20:2), Sb1-116 p/l = 1:500). At t = 0 s, equimolar concentration ($c_{\text{phospholipid}}$ = 65 µM) of both vesicle populations were mixed. The intensity first increased fast, then slowed down and reached saturation after approx. 40 min, indicating the end of the fusion process. Buffer: 0.5 mM MOPS, 100 mM KCl, 2 mM $MgCl_2$, pH 7.3. $\lambda_{ex/em}$ = 508/534 nm.

Before starting the acidification assay of the fusion products, the potassium ionophore valinomycin was added to allow a charge equilibration upon proton influx into the liposomes driven by active ATPase. Figure 4.22 represents a typical time course of the mean pH-value, which was calculated from the OG488-fluorescence intensity as described in Chapter 4.4.2, after fusion of ΔN49-ATPase-LUVs with OG488-DHPE doped Sb1-116-LUVs. When ATP was added, no pH-decrease was observable over several minutes and addition of CCCP only leads to a slight drop in intensity or pH-value, respectively. Even though good ATPase activity was proven by means of ACMA assays and efficient fusion processes monitored by OG488-DHPE dequenching, a significant and reversible quenching of OG488-DHPE in fusion products due to ATPase activity could not be observed.

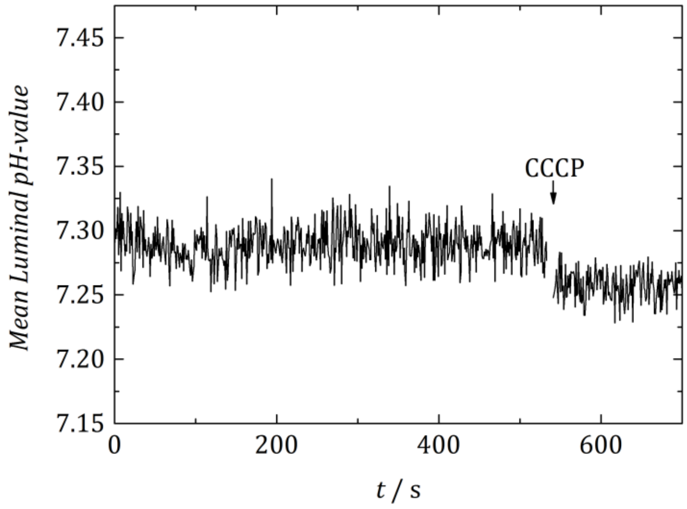

Figure 4.22. Course of the mean pH-value of the OG488-based acidification assay after fusion of ΔN49-ATPase-LUVs with OG488-DHPE doped Sb1-116-LUVs (2 mol% OG488). After ATP addition (1.2 mM, $t = 0$ s) no acidification was observable and CCCP addition (0.4 µM) only led to a minor pH-value or intensity decrease, respectively. Buffer: 5.0 nM valinomycin, 0.5 mM MOPS, 100 mM KCl, 2 mM $MgCl_2$, pH 7.3. $\lambda_{ex} = 508$ nm, $\lambda_{em} = 534$ nm.

By performing an ACMA assay after the fusion process, a total loss of ATPase activity during the fusion could be excluded. Figure 4.23 A shows an ACMA assays of ATPase-ΔN49-LUVs. With the functionality of the ATPase assured, ATPase-ΔN49-LUVs were fused with Sb1-116-LUVs (Figure 4.23 B). Subsequently, valinomycine (5 nM) and ATP (1.2 mM) were added to monitor ATPase-mediated acidification of the fusion product. As no OG488-DHPE fluorescence intensity decrease could be detected (Figure 4.23 C), ACMA (0.9 µM) was added and the measurement parameters were changed accordingly (OG488: $\lambda_{ex/em} = 508/534$ nm; ACMA: $\lambda_{ex/em} = 410/490$ nm). Figure 4.23 D shows the significant ACMA fluorescence intensity decrease, which was reversible upon CCCP addition (0.4 µM). This proved a maintaining of ATPase activity in the fusion mixture in general, but cannot give specific information about the ATPase activity in fusion products.

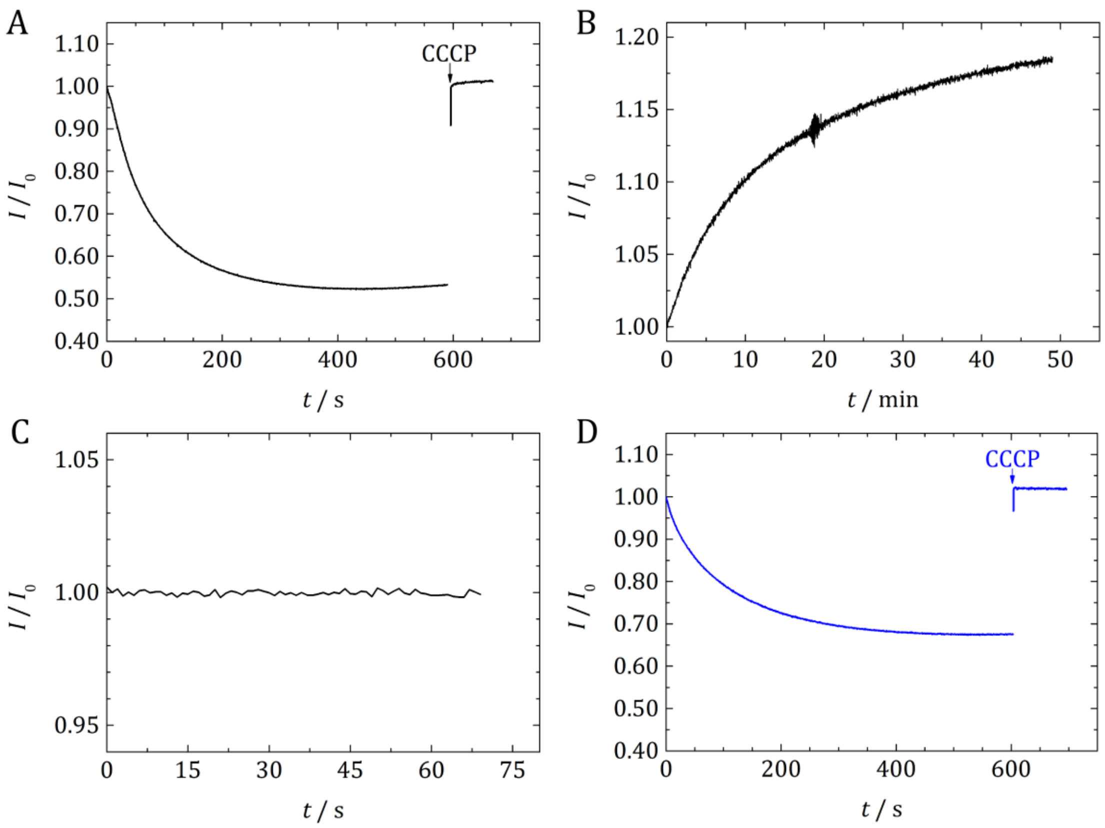

Figure 4.23. (A) Acidification of ATPase-ΔN49-LUVs (DOPC/POPE/POPS/cholesterol (50:20:10:20), ATPase nominal p/l = 1:20,000, ΔN49 nominal p/l = 1:20,000, $c_{\text{phospholipid}} \approx 64$ µM) monitored by means of an ACMA assay. ATP (1.2 mM) was added at $t = 0$ s, CCCP addition (0.4 µM) led to a collapse of the H^+-gradient. (B) Fusion of the ATPase-ΔN49-LUVs with Sb1-116-LUVs (DOPC/POPE/POPS/cholesterol/OG488-DHPE (48:20:10:20:2), Sb1-116 nominal p/l = 1:500). For both LUV populations: $c_{\text{phospholipid}} \approx 64$ µM. (C) No acidification was detectable after fusion with the OG488-DHPE assay. Addition of ATP (1.2 mM) at $t = 0$ s. (D) ACMA (0.9 µM) was added to check for ATPase activity in the former fusion mixture and a significant intensity decrease occurred. CCCP addition (0.4 µM) led to a collapse of the H^+-gradient. OG488: $\lambda_{\text{ex/em}}$ = 508/534 nm; ACMA: $\lambda_{\text{ex/em}}$ = 410/490 nm.

An explanation for this unexpected result would be a large heterogeneity in the distribution of the ΔN49-complex and the ATPase in the LUVs or that the SNARE-complex has a negative impact on the OG488-DHPE fluorescence emission.

A high heterogeneity in the ΔN49-ATPase-LUVs, in a way that a fraction of the vesicles contained primarily the ΔN49-compex and another fraction the ATPase, would result in ACMA assays showing a large proton pumping activity, while the ΔN49-compex containing liposomes would contribute to a positive result in the dequenching assay. In this case, the fusion products would contain hardly any ATPase, therefore, showing no detectable acidification of the fusion products. However, it was impossible to examine this consideration with a bulk experiment. To prove this hypothesis, experiments on the single vesicle level are required.

As OG488-DHPE and the SNARE-complex come in contact through the fusion, it should be tested whether the protein complex has an impact on the fluorescence characteristics of dye.

Therefore, OG488-DHPE acidification assays of ATPase-only and ATPase-ΔN49-vesicles were compared and the absorption and fluorescence emission of OG488-DHPE was characterized in presence of different amounts of ΔN49-complex.

For the acidification assays, ATPase (p/l = 1:20,000) and the ΔN49-complex (p/l = 1:500) were co-reconstituted into LUVs (DOPC/POPE/POPS/cholesterol/OG488-DHPE (49:20:10:20:1)) doped with 1 mol% OG488-DHPE and for comparison, the ATPase (p/l = 1:20,000) only was reconstituted into OG488 doped LUVs (DOPC/POPE/POPS/ cholesterol/OG488-DHPE (49:20:10:20:1)). The experiment was performed with the ΔN49-complex, because the water-soluble part of the ΔN49-complex resembles that of the full SNARE-complex very closely, as it contains a synaptobrevin fragment of amino acids 49–96, while in the SNARE-complex a full length synaptobrevin of the amino acids 1–116 is included. Hence, a possible effect of the ΔN49-complex or the full SNARE-complex on the OG488-DHPE fluorescence emission is expected to be very similar.

ACMA assays of both samples were performed, showing a slightly larger activity for the ΔN49-ATPase-LUVs than for the ATPase-LUVs (Figure 4.24 A). Having the ATPase activity ensured in both, the ATPase-ΔN49- and the ATPase-LUVs, the OG488-DHPE fluorescence response to the ATPase activity was monitored and converted into luminal pH-values.

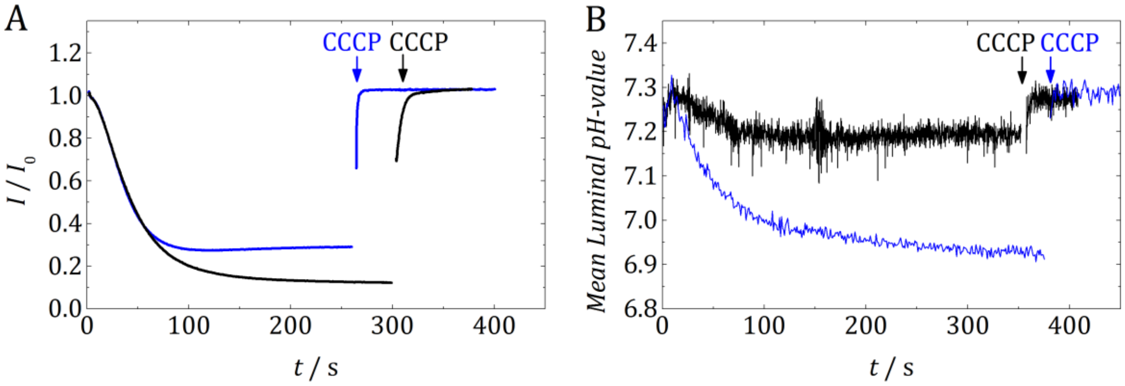

Figure 4.24. (A) Relative changes in fluorescence intensity of ACMA (0.9) upon luminal acidification ATPase-ΔN49-LUVs (black) and ATPase-LUVs (blue). ATP addition (1.2 µM, t = 0 s), induced fluorescence intensity decreases in both samples, indicating that the ATPase was functionally reconstituted. In case of the ATPase-ΔN49-LUVs (black), the decrease was even larger than for the ATPase-LUVs. Buffer: 0.9 µM ACMA, 5.0 nM valinomycin, 0.5 mM MOPS, 100 mM KCl, 2 mM $MgCl_2$, pH 7.3. $\lambda_{ex/em}$ = 410/490 nm. (B) Time-resolved mean luminal pH-value of OG488-DHPE fluorescence: ATP addition (1.2 µM, t = 0 s) lead to a pH-decrease in ATPase-ΔN49-LUVs (black) and ATPase-LUVs (blue). The ATPase-ΔN49-LUVs just decreased to a mean luminal pH-value of 7.2, while the ATPase-only sample reached a mean pH-value of 6.9. Buffer: 5 nM valinomycin, 0.5 mM MOPS, 100 mM KCl, 2 mM $MgCl_2$, pH 7.3. $\lambda_{ex/em}$ = 508/534 nm. Lipid composition: (DOPC/POPE/POPS/cholesterol/OG488-DHPE (50:20:10:20:1)), ATPase p/l =1:20,000, ΔN49 p/l = 1:500.

Surprisingly, the ATPase-ΔN49-liposomes showed only a very small pH-decrease from 7.3 to 7.2, while the ATPase-LUVs experienced a significantly stronger acidification, resulting in a final mean luminal pH-value of 6.9. However, it is unlikely that the result for ATPase-ΔN49-

LUVs displays the correct ATPase activity; otherwise, it could not have shown better activity in the ACMA assay than the ATPase-LUVs.

This result indicates that the ΔN49-complex might have an impact on the fluorescence emission characteristics of the OG488-DHPE. Therefore, absorption and fluorescence emission spectra of vesicles doped with 1 mol% OG488-DHPE and different amounts of ΔN49-complex were recorded. The ΔN49-complex was reconstituted into liposomes (DOPC/POPE/POPS/cholesterol/OG488-DHPE (50:20:10:20:1)) at protein/lipid ratios of 1:2000, 1:1000 and 1:500 and for comparison, a protein-free sample was prepared.

At first, absorption spectra were measured, which allowed to examine the absorption of the OG488-DHPE in the different samples, as well as the reconstitution efficiencies. For the latter, the peptide bond absorption peak at 220 nm was regarded. To correct the absorbance from contributions of the fluorophore and light scattering of the vesicles, the spectrum of the sample without protein was subtracted from the ones of the samples with reconstituted ΔN49-complex. The resulting spectra were normalized to the absorption peak (λ_{abs} = 220 nm) of the sample with the nominal p/l of 1:500 (Figure 4.25). The sample with a nominal p/l of 1:1000 exhibited 60 % of the absorbance of the sample with the highest amount of protein, and the sample with the nominal p/l of 1:2000 showed 33 % of normalized absorbance. For unaltered protein/lipid ratios after the reconstitution, normalized absorption intensities of 50 % and 25 % would have been expected, respectively, concluding that the nominal lipid/protein were only altered slightly.

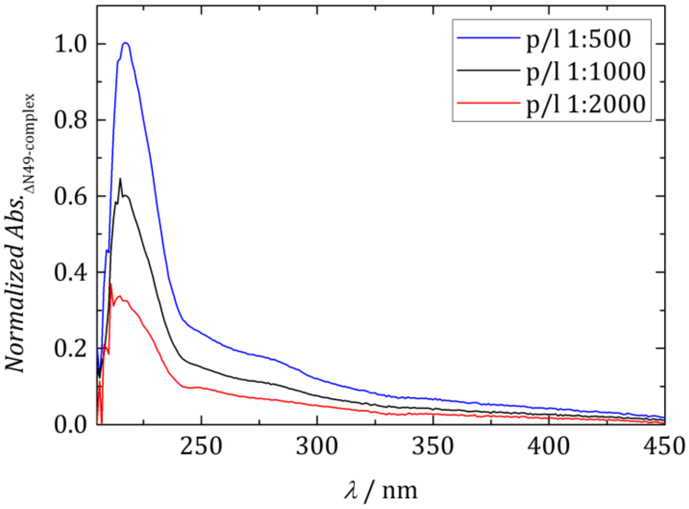

Figure 4.25. UV/Vis spectra of OG488-DHPE doped ΔN49-liposomes (DOPC/POPE/POPS/cholesterol/OG488-DHPE, 50:20:10:20:1). By subtracting a spectrum of protein-free LUVs, the shown spectra were corrected for light scattering and OG488-DHPE absorption in the range of 205-450 nm. The spectra were normalized to the absorption maximum at 220 nm, obtained for the sample with the nominal p/l of 1:500 (blue). The absorptions of the samples with nominal p/l of 1:1000 and 1:2000 were 60 % and 33 % of that for p/l 1:500, respectively.

Figure 4.26 depicts the normalized absorption and fluorescence emission spectra of OG488-DHPE doped liposomes or proteoliposomes, respectively. The equimolar samples show all a very similar absorption spectra, but the fluorescence emission intensities decreased with an increasing amount of ΔN49-complex to 92 % for a p/l of 1:2000, 85 % for a p/l of 1:1000 and 79 % for a p/l of 1:500. Because the absorption does not decrease in the same way as the fluorescence emission, but is nearly the same for the protein free sample and the all the protein/lipid ratio, a quenching effect of the ΔN49-complex on the OG488-DHPE can be presumed.

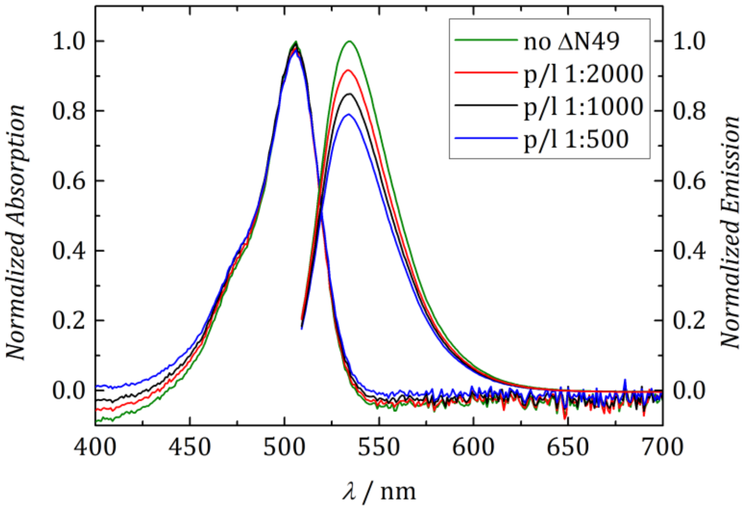

Figure 4.26. Normalized absorption and fluorescence emission spectra of liposomes (DOPC/POPE/POPS/cholesterol/OG488-DHPE (50:20:10:20:1)) with no ΔN49-complex (green curves) or nominal lipid/protein ratios of 1:500 (blue curves), 1:1000 (black curves) or 1:2000 (red curves). Each sample was measured at equimolar phospholipid concentration ($c_{\text{phospholipid}}$ = 64 µM). λ_{ex} = 508 nm.

The results from the examination of the ΔN49-complex influence on the OG488-DHPE fluorescence emission indicate an unfavorable effect, as the fluorescence emission seems to be quenched significantly. However, as 79 % of the fluorescence intensity from the sample with nominal p/l of 1:500 remained, compared to a protein-free sample, this effect cannot solely explain why acidification of the fusion products from OG488-Sb1-116-LUVs and ATPase-ΔN49-LUVs was not observed in any case. A combination of this unfavorable quenching effect with a possible heterogeneity of ATPase and ΔN49-complex distribution in the liposomes, however, could possibly result in unsuccessful acidification assays of the fusion products.

To examine possible heterogeneities in proteoliposomes, experiments on the level of single vesicle resolution are required. Therefore, the assays performed in bulk solution have to be adapted to a two-dimensional setup, allowing the observation of single proteoliposomes by means of fluorescence microscopy.

4.6 Microscopy-based 2D-single vesicle assay for observation of TF_0F_1-ATPase activity

- Parts of this Chapter are published as M. Schwamborn, J. Schumacher, J. Sibold, N. K. Teiwes, C. Steinem, Monitoring ATPase induced pH changes in single proteoliposomes with the lipid-coupled fluorophore Oregon Green 488, *Analyst* **2017**, *accepted,* DOI: 10.1039/C7AN00215G.

As the OG488-DHPE-based assay described in the preceding Chapter showed efficient fusion of OG488-DHPE doped Sb1-116-LUVs with ATPase-ΔN49-LUVs, and the latter exhibited a good activity in ACMA assays, the unsuccessful acidification assays of the fusion products were unexpected. In fact, a slight fluorescence quenching effect of the ΔN49-complex on the OG488-DHPE was found and consequently weaker signals for the acidification of the fusion products could be expected. However, ATPase activity in fusion products could not be detected in any case. Like considered in the previous chapter, a distinctive heterogeneity in the distribution of ATPase and ΔN49-complex in the liposomes could explain why no acidification was detectable in the fusion products. Therefore, an assay that allows to monitor the proton pumping activity of single TF_0F_1-ATPase-vesicles was established.

Experiments performed on single vesicle scale represent a powerful tool for the investigation of distinct processes such as fusion between single liposomes, transport of a substrate in to vesicles or for the analysis of lipid and protein distribution in vesicles. To enable an observation by means of fluorescence microscopic techniques, like confocal laser scanning microscopy (CLSM) or total internal reflection microscopy (TIRFM), vesicles have to be attached to a surface. Often, the avidin-biotin interaction is used for this purpose.[142–151]

4.6.1 Characterization of the vesicle immobilization

Initially, the success of the vesicle immobilization method was evaluated by attaching Texas Red DHPE doped liposomes (DOPC/POPE/POPS/cholesterol/Texas Red DHPE/biotin-cap-PE (49.5:20:10:20:0.1:0.4), approx. 100 nm diameter), encapsulating a pyranine solution (0.5 mM), to the functionalized substrate via the NeutrAvidin-biotin interaction (Figure 4.27). All particles showing a colocalization of the green fluorescence of pyranine (Figure 4.27 A) and Texas Red DHPE fluorescence (Figure 4.27 B) represent intact vesicles, while solely red fluorescing particles possibly resulted from ruptured vesicles or lipid aggregates. Figure 4.27 C represents the overlay of both channels, allowing to count all particles exhibiting a colocalization of Texas Red DHPE and pyranine fluorescence (Chapter 3.5.5). As a result, 357 vesicles were found on an area of 6056 µm^2, which corresponds to a vesicle density of 0.06 vesicles/µm^2. Besides single vesicles, a few large vesicle aggregates (<10) were found. However, it is important to note that most vesicles are smaller than the resolution limit of the microscope (intensity-weighted mean diameter: 95 nm, cf. Figure 4.5, Chapter 4.2), which is approx. 208 nm (expecting $\lambda = 500$ nm, 1.2 NA objective).[152] Consequently, aggregates of small liposomes may not be distinguishable as such. Figure 4.27 E shows the line profile of five particles, depicted in Figure 4.27 D. In four of the five particles, the fluorescence of the membrane-anchored red dye and the entrapped green dye are colocalized, indicating intact liposomes.

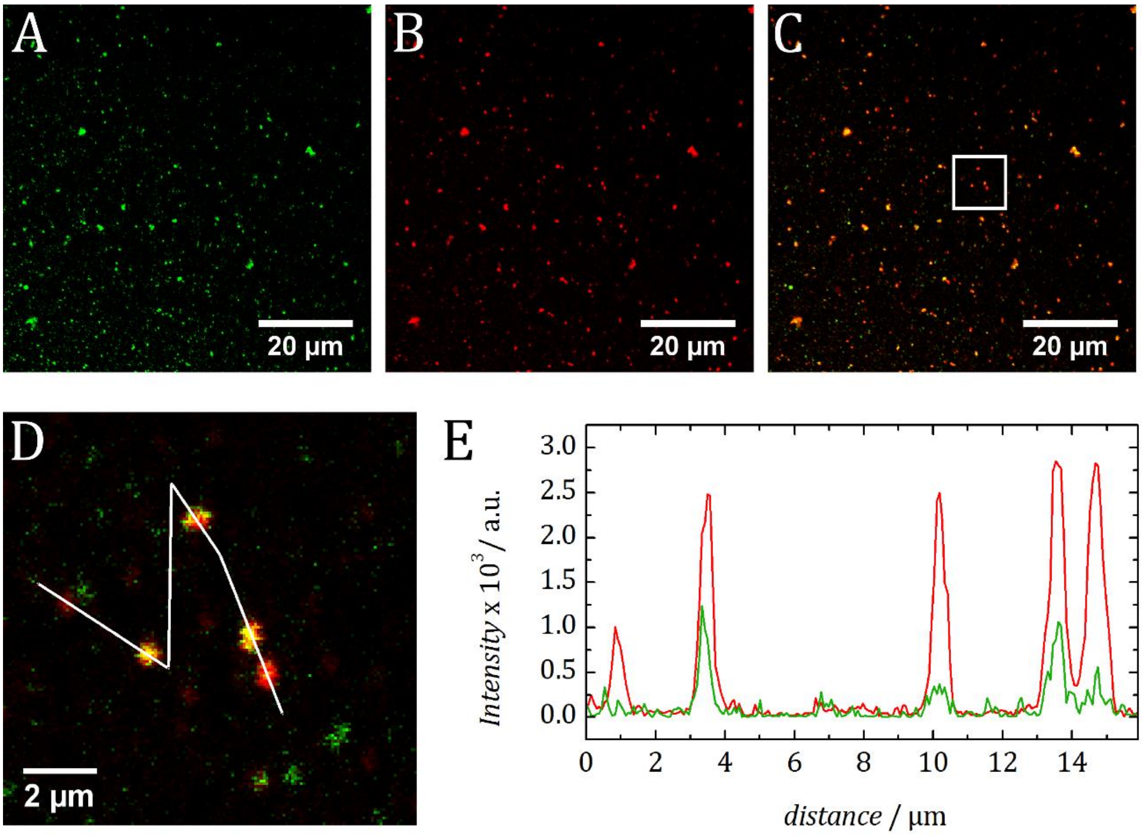

Figure 4.27. Representative images of vesicles DOPC/POPE/POPS/cholesterol/biotinyl-cap-PE/ Texas Red DHPE (49.5:20:10:20:0.4:0.1), filled with pyranine solution (0.5 mM), immobilized on a methoxy-PEG/Biotin-PEG (9:1) functionalized glass slide via NeutrAvidin-biotin interaction. The green channel shows the pyranine fluorescence (A), the red channel the fluorescence of the membrane-anchored dye Texas Red DHPE (B). The colocalization of both fluorophores (C) allowed to quantify intact, attached liposomes: a density of 0.06 vesicles/µm^2 was found. This density of liposomes is representative for all performed single vesicle assays.

4.6.2 Conduction and analysis of the single vesicles experiments

In this work, the liposomes were attached to glass slides by using the highly specific binding of NeutrAvidin to biotin.[153,154] The glass slides were functionalized with a mixture of biotin-

PEG/methoxy-PEG in a ratio of 1:9 (*n*/*n*) (see Chapter 3.5.3). Incubation with a NeutrAvidin solution (10 µg/mL ≙ 17 µM, 10 min) allowed a binding to the biotinylated PEGs. After removing non-bound NeutrAvidin by rinsing with ATPase-buffer (0.5 mM MOPS, 100 mM KCl, 2 mM $MgCl_2$, pH 7.3), vesicles doped with biotinyl-cap-PE ($c_{\text{phospholipid}} \approx 0.6$ µM) were allowed to bind, while non-bound vesicles were rinsed off with ATPase-buffer. Subsequently, the acidification assay was performed corresponding to the bulk assay described in Chapter 4.4.2, measuring the fluorescence intensities of single vesicles instead of the sample's overall fluorescence response. Figure 4.28 shows a scheme of the OG488-DHPE based single vesicle acidification assay.

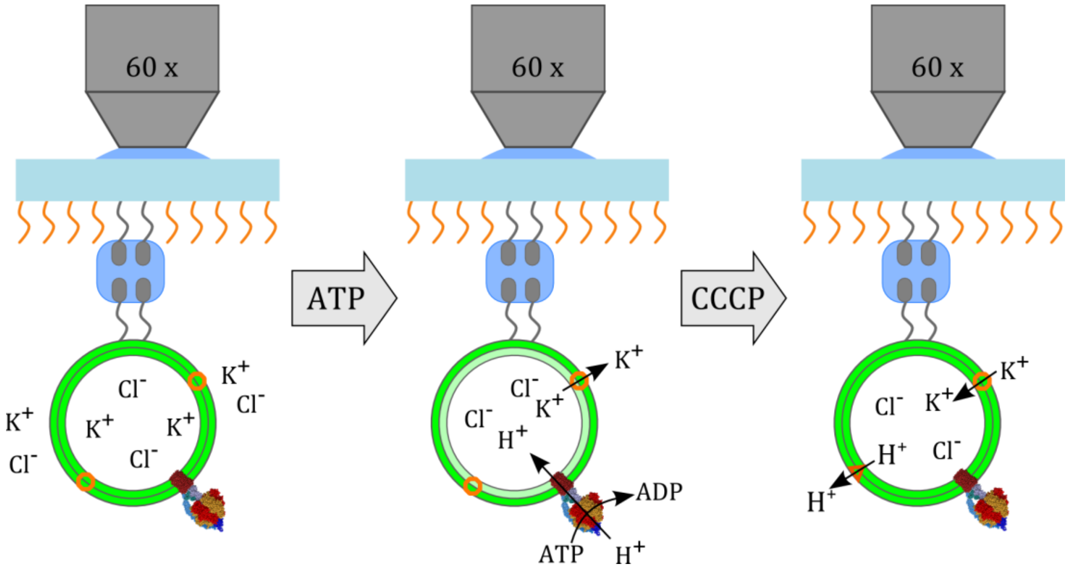

Figure 4.28. Scheme of ATPase-proteoliposomes (DOPC/POPE/POPS/cholesterol/OG488/biotin-cap-PE (48.6:20:10:20:1:0.4)) attached to a biotin-PEG/methoxy-PEG (1:9, *n*/*n*) functionalized glass slide. The NeutrAvidin tetramer (blue square) can bind to four biotin molecules (grey), thus it can bind to the biotin-PEG and to liposomes doped with a biotinylated lipid.[154] With the attached ATPase-vesicles, the OG488-DHPE acidification assay can be performed and monitored with a fluorescence microscope.

Upon addition of ATP, liposomes containing an active ATPase will show a decrease of fluorescence emission, as their lumen is acidified and the OG488-DHPE present in the inner membrane leaflet is protonated. Addition of the proton uncoupler CCCP leads to a collapse of the proton gradient, therefore restoring the fluorescence intensity.

The prerequisites for a successful single vesicle acidification assay were the instant addition of defined ATP and CCCP concentrations (1.2 mM and 0.4 mM, respectively) and a constant temperature of 37 °C (cf. Chapter 4.3). In bulk experiments, the cuvette could be heated and the sample was stirred, ensuring a fast and equal distribution of the added chemicals. To enable a conduction of the acidification assay under the above-mentioned conditions with a fluorescence microscope, a heatable flow chamber was developed by Johannes Schumacher.

Figure 4.29 A depicts the aluminum flow chamber and Figure 4.29 B shows the complete setup mounted to the microscope's heating stage, including the heated water immersion objective (Olympus UPlanSApo, 60 x, 1.2 NA).

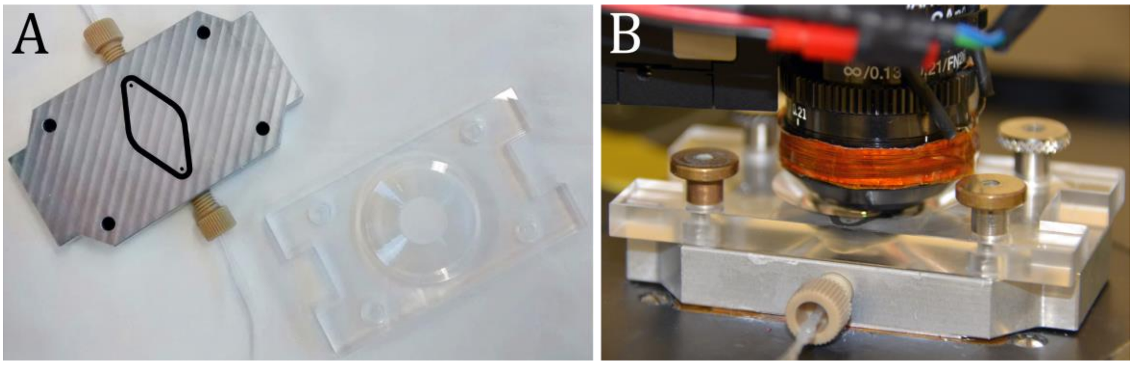

Figure 4.29. (A) Image of the unmounted heatable flow chamber. A biotin-PEG/methoxy-PEG (1:9) functionalized glass slide was placed onto the flow chamber's gasket. An acrylic glass lid was used to press the glass slide against the gasket, sealing the chamber. (B) Image of the flow chamber mounted to the microscope's heating stage. The water immersion objective (Olympus UPlanSApo, 60 x, 1.2 NA) was also heated with a custom build device. The tubing was connected to a peristaltic pump.

The desired solutions were pumped through the flow chamber with a peristaltic pump, that allowed to use a buffer reservoir to which ATP and CCCP could be added. When additions were made, the pump was turned off in order to avoid air bubbles getting into the tubing and the flow chamber. As a result, the pressure in the flow chamber was reduced leading to a minimal movement of the glass slide and the focus was lost until the pump was turned back on again.

All experiments were either performed with a confocal laser scanning microscope (CLSM) or a spinning disk confocal microscope (SDCM). Both allowed an installation of the heating stage and the objective. When using the CLSM, a total internal reflection illumination unit was utilized to illuminate the sample evenly with a defined laser power (0.5 % of 2 mW, 488 nm laser) (no total internal reflection was induced). The imaging was accomplished with an external CMOS camera (Andor, Zyla 5.5), employing a binning of 4x4 and a rolling shutter to obtain the optimal signal-to-noise ratio. As the focus often changed over the time of the measurement (approx. 10 min), time series of z-stacks were recorded with a spinning disk confocal microscope, equipped with an EM-CCD camera (Andor, iXon Ultra 897). A z-range of around 5 µm was selected with approximately 200 nm per slice. Laser intensity was adjusted to a value as low as possible to prevent the Oregon Green 488-DHPE from bleaching. The obtained image sequence was converted into a so-called hyperstack (image sequence with slices assigned time and z-position) with the ImageJ feature *Stack to Hyperstack*. Adding the images of each z-stack (ImageJ feature: *Sum Slices*) resulted in a two-dimensional time series with the accumulated intensities compensating for the z-drifts. In most measurements drifts in the xy-plane occurred, which were corrected with the ImageJ plug-in *Template Matching: Align Slices in Stack*.[113] To correct for the intensity counts resulting from the dark current of the cameras, a dark image was subtracted from each image prior to further image processing (ImageJ plug-in *Calculator plus*).

The corrected time series were finally analyzed with a custom Matlab script, written by Jeremias Sibold, locating the vesicles and assigning regions of interest (ROIs, 7 x 7 px) to each vesicle. After a background correction for each frame, ROI intensities of all time frames were read out, smoothed with a median filter and normalized to the intensity obtained immediately after ATP addition. These normalized intensities were converted into pH-values by Equation 4.3, Chapter 4.4.2. The equation parameters $I_{\mathrm{max}} = 1.04$, $I_{\mathrm{min}} = 0.59$ and $\mathrm{p}K_{\mathrm{a}} = 6.26$ were obtained from the fit (Equation 4.2) to the calibration data in Figure 4.11 (Chapter 4.4.1). It is important to note that the maximal intensity, which can be assigned to a luminal pH-value, is $I_{\mathrm{max}} = 1.04$. However, normalized fluorescence intensities from single vesicles could exceed a normalized intensity of 1.04, due to signal noise. An increase of the laser power in order to improve the signal-to-noise ratio was unfavorable, since a significant bleaching of the OG488-DHPE fluorescence occurred in this case.

4.6.3 Analysis of single vesicle acidification

The immobilization of Texas Red DHPE doped vesicles, filled with the water-soluble fluorophore pyranine, confirmed the suitability of the immobilization strategy based on the biotin-NeutrAvidin interaction.

OG488-DHPE doped ATPase-liposomes (DOPC/POPE/POPS/cholesterol/biotinyl-cap-PE/OG488-DHPE (48.6:20:10:20:0.4:1), p/l = 1:20,000) were immobilized and acidification assays were performed. Image acquisition was started and ATP (1.2 mM) was added to activate the ATPase, after 5 min the proton gradients were dissipated by addition of the proton uncoupling agent CCCP (0.4 µM). The image sequences were processed as described in Chapter 4.6.2. The intensity time courses were then screened manually for an intensity decrease of at least two times the standard deviation of the signal noise after ATP addition and a recovery of min. 50 % immediately after CCCP addition, clearly indicating ATPase mediated proton pumping.

Figure 4.30 A exemplarily shows the normalized intensity I/I_0, with I_0 being the intensity at ATP addition ($t = 0$ s), of an acidified vesicle (blue) and a non-acidified vesicle (black).

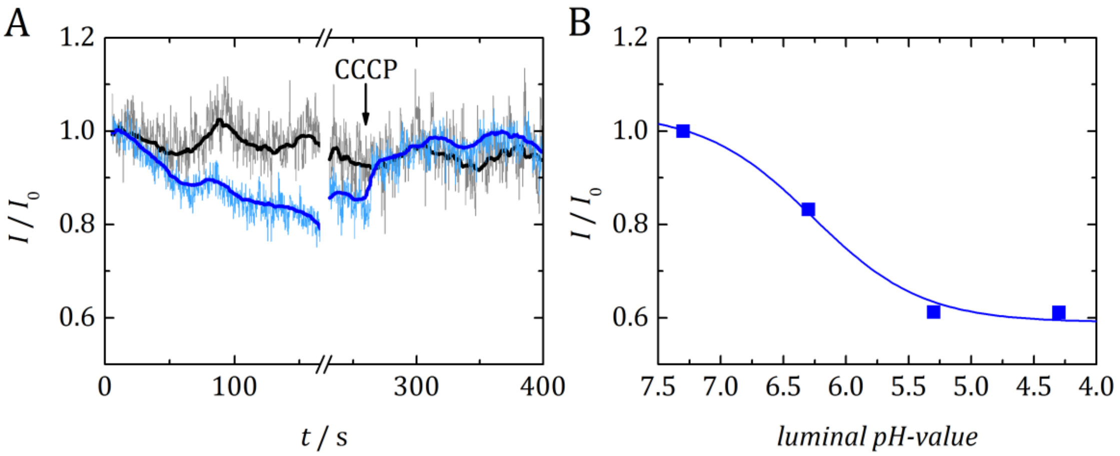

Figure 4.30. (A) Exemplary normalized intensity courses, original and smoothed (median filter), of an acidified (blue) and an inactive liposome (black) (DOPC/POPE/POPS/cholesterol/biotinyl-cap-PE/OG488-DHPE (48.6:20:10:20:0.4:1), p/l = 1:20,000, ATPase-buffer: 5 nM valinomycin, 0.5 mM MOPS, 100 mM KCl, 2 mM $MgCl_2$, pH 7.3). After ATP addition (1.2 mM, $t = 0$ s) the intensity of the active proteoliposome decreased about 15 %. CCCP addition (0.4 µM) resulted in a significant intensity restoration. The intensity of the inactive vesicle did neither show a relevant decrease nor a recovery after CCCP addition. The break in the *x*-axis from 165 s to 235 s resulted from stopping the peristaltic pump for CCCP addition. (B) Calibration curve obtained from vesicles with acidic lumina in a bulk solution of pH 7.3 for correlation of the normalized intensities to luminal pH-values (cf. Figure 4.11, Chapter 4.4.1).

Upon ATP addition ($t = 0$ s) the intensity of the acidified proteoliposome decreased approx. 15 %. After CCCP addition, the intensity was restored. The break in the *x*-axis from 165 s to 235 s resulted from losing the focal plane when the peristaltic pump was stopped for CCCP addition. With Equation 4.3 (Chapter 4.4) and the parameters obtained from fitting Equation 4.2 to the calibration data (Figure 4.30 B, cf. Figure 4.11, Chapter 4.4.1) the normalized intensities were converted into pH-values. However, in some intensity time courses the signal noise exceeded the maximal intensity assignable to a pH-value ($I_{max} = 1.04$, Figure 4.30 B). Figure 4.31 A shows the ΔpH time courses calculated from the two intensity courses shown in Figure 4.30 A. ATP addition (1.2 mM, $t = 0$ s) led to a decrease from pH 7.3 to pH 6.4 (ΔpH = −0.9) that could be dissipated by CCCP addition (0.4 µM).

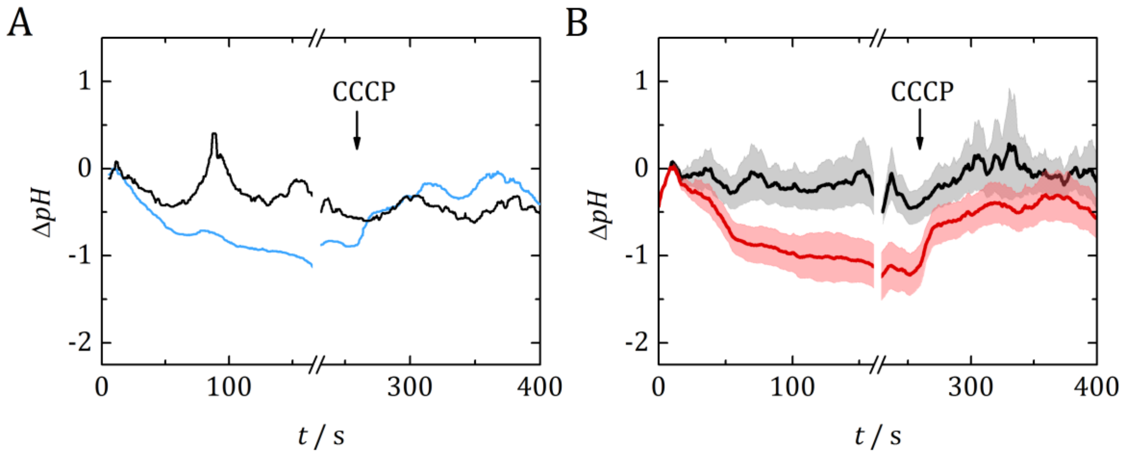

Figure 4.31. (A) ΔpH time courses calculated from the intensity courses shown in Figure 4.30 with Equation 4.3 (Chapter 4.4). After ATP addition (1.2 mM, $t = 0$ s) the acidified vesicle experienced a pH-decrease from pH 7.3 to approx. pH 6.4 (ΔpH = 0.9). Upon CCCP addition (0.4 µM) the pH-gradient was dissipated. The intensity fluctuations of the inactive vesicle correspond to pseudo-pH changes between ΔpH = +0.4 and ΔpH = −0.5. (B) Averaged ΔpH time courses of active (red) and inactive (black) vesicles obtained from one proteoliposome preparation. Shaded areas represent the standard error of the mean. The average pH-value of proteoliposomes with active ATPase decreased by ΔpH = −1.2 from pH 7.3 to pH 6.1 and recovered to pH = 6.8 after CCCP addition. The average pH-value of inactive vesicles did not change considerably. The break in the *x*-axis from 165 s to 235 s resulted from stopping the peristaltic pump for CCCP addition.

Fluctuations of the intensity of inactive vesicles correspond to pseudo-pH changes between ΔpH = +0.4 and ΔpH = −0.5. The averaged ΔpH time courses of active and inactive vesicles obtained from one proteoliposome preparation are shown in Figure 4.31 B. The active ATPase-liposomes experienced an average acidification of ΔpH = −1.2 ± 0.6 (SD) (pH 7.3 → 6.1), with a recovery to ΔpH = −0.6 (pH 6.1 → 6.8) upon CCCP addition (red time course). The inactive vesicles did not experience a considerable pH-change (black time course). The shaded areas represent the standard error of the mean of the active vesicle (red) and inactive vesicles (grey), respectively.

Altogether, three successful experiments were evaluated, leading to a statistic, shown in Figure 4.32. The intensities of 238 vesicles in total were analyzed and only 12 (5 %) of them were unambigiously acidified. The percentages of detected, acidified vesicles in the single experiments were 11.9 % (5 out of 42), 6.1 % (4 out of 66) and 3.1 % (4 out of 130). The strongest luminal acidifications found were ΔpH = −2.0, however, most vesicles were acidified by ΔpH = −0.5 to −1.0. An averaging of the intensity courses of all detected vesicles per experiment results in ΔpH of −0.55, −0.37 and −0.50 (average: ΔpH = −0.47).

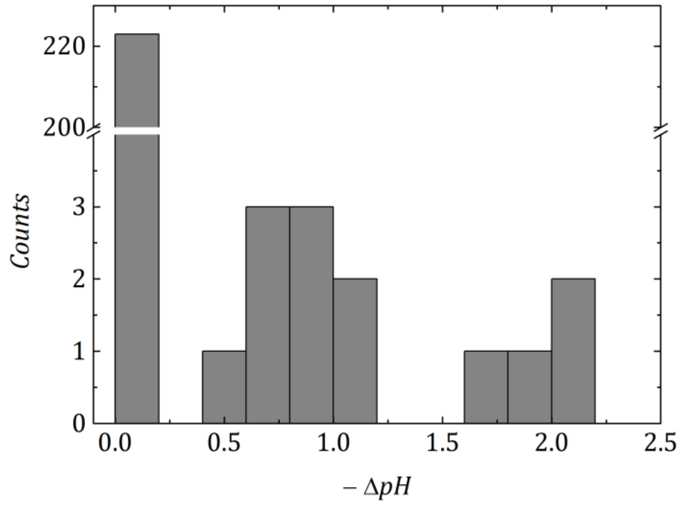

Figure 4.32. Overview of the total number of vesicles analyzed with respect to acidification. Overall, the OG488-DHPE fluorescence intensity courses of 238 vesicles were detected and converted into pH-values. For 12 (5 %) of them, an acidification of at least −0.5 pH-units was found. The averaged ΔpH of all detected vesicles is −0.47.

The OG488-DHPE based single vesicle assay revealed that active TF_0F_1-ATPase is only present in a fraction of the immobilized vesicles, a result that cannot be obtained with bulk experiments. Furthermore, the lipid-coupled pH-sensitive fluorophore OG488-DHPE proved suitable for monitoring active acidification of proteoliposomes not only in bulk solution but also on the single vesicle scale. For the latter, OG488-DHPE serves for identification of the attached liposomes and is a pH-sensor at the same time, obviating the need for any further fluorophore.[123]

5 DISCUSSION

To generate proton gradients across artificial lipid bilayers by active H^+-transport through the membrane, the recombinant TF_0F_1-ATPase was isolated from *E. coli* DK8 and reconstituted into large unilamellar vesicles. The reconstitution efficiency was investigated by means of a density gradient centrifugation and the protein's activity and its temperature dependence were ascertained by an assay based on the pH-sensitive, membrane permeable fluorophore 9-amino-6-chloro-2-methoxyacridine (ACMA). An acidification assay with the lipid-coupled fluorophore Oregon Green 488-DHPE (OG488-DHPE) was established, allowing the determination of the mean luminal pH-value of acidified ATPase-liposomes in bulk solution. Pore-spanning lipid bilayers (PSLBs) represent a sophisticated model membrane system, consisting of an array of cavities in a solid substrate that is sealed by a lipid membrane. Separating two aqueous compartments, PSLBs allow to monitor transport processes .[45] In several studies, PSLBs or the similar system of arrayed lipid membranes have been used for investigation of passive transport by α-hemolysin, aquaporin or gramicidin by means of fluorescence-based or electrophysiological measurements.[44,66,155–158] Furthermore, a nigericin mediated K^+/H^+-antiport across PSLBs has been studied by monitoring the fluorescence emission of a pH-sensitive dye entrapped inside the pores.[74] Investigation of active transport across PSLBs, such as proton pumping by TF_0F_1-ATPase, would be beneficial, as the array of membrane-spanned pores provides a high statistic and identical experimental conditions. To functionally insert the proton pump into this kind of model membrane, a reconstitution protocol maintaining physiological conditions, based on SNARE-mediated fusion was conceived (cf. Chapter 1.3.2).[75] The single pivotal steps of the protocol to be developed were analyzed quantitatively.

5.1 Purification of recombinant TF_0F_1-ATPase from *E. coli* DK8

E. coli is a well-characterized, easy-to-handle host for expression of recombinant proteins.[159] As part of a study investigating the inhibitory effect of the ε-subunit of *E. coli* F-type ATPase, Klionsky *et al.* created the *E. coli* strain DK8, which lacks all ATPase encoding genes.[160] This strain presents an ideal host for the pTR19-ASDS vector, which was created by Suzuki *et al.* in 2002 and carries the genetic information for the His-tagged F_0F_1-ATPase originating from thermophilic *Bacillus* PS3 (TF_0F_1-ATPase).[84] Since its introduction, the expression system has been widely used for isolation of the proton pump in order to investigate the ATPase's functionality itself or to actively build-up proton gradients in vesicles, e. g. for *in vitro* investigation of neurotransmitter uptake.[64,65,84,85,115–117,119,128,161] Hence, the recombinant TF_0F_1-ATPase represents a suitable proton pump for the generation of H^+-gradients across lipid membranes.

As described in Chapter 4.1, the TF_0F_1-ATPase was successfully purified, according to the protocol of Schenck *et al.*[85] Typically, approx. 1.5 mg were yielded from a 2 L culture, whereas in literature 10 mg were of protein were obtained.[85] As the same bacterial strain, medium and growth conditions, as well as same buffer compositions were used for protein purification, possible reasons for the lower yield might be due to less sufficient cell lysis and/or protein binding to the immobilized metal ion chromatography resin. However, the concentration and purity of the sample were well-suited for the following reconstitution into vesicles.

5.2 Detergent-mediated ATPase reconstitution into large unilamellar vesicles

- Parts of this Chapter have been published: M. Schwamborn, J. Schumacher, J. Sibold, N. K. Teiwes, C. Steinem, Monitoring ATPase induced pH changes in single proteoliposomes with the lipid-coupled fluorophore Oregon Green 488, *Analyst* **2017**, *accepted,* DOI: 10.1039/C7AN00215G.

In this work, the reconstitution efficiency was characterized for three different nominal protein/lipid ratios. The results indicated that at a protein/lipid ratio of approx. 1:20,000 a saturation occurs. For the intensity-weighted average proteoliposome diameter of 95 nm, this ratio corresponds to four ATPase-molecules per vesicle.

To extract a membrane protein from its native membrane environment it has to be solubilized by detergents. These amphiphilic molecules form a micelle around the hydrophobic region of the protein, mimicking the hydrophobic membrane core, thus retaining the protein's structure and functionality.[42,120] For the investigation of a protein's transport functionality from one into another compartment, reconstitution into a defined lipid bilayer is inevitable. Furthermore, the lipid environment can have an influence on the protein's structure and function.[162,163]

For the reconstitution of membrane proteins into liposomes several methods exist, and the most versatile ones rely on use of detergents.[42] In general, detergent-mediated reconstitution is the reverse process of the membrane protein solubilization: detergent micelles are enriched with lipids leading to the formation of so-called mixed micelles (stage I – mixed micelles) (Figure 5.1). When the detergent is incrementally depleted from the mixed micelles, detergent saturated vesicles start to form (stage II – coexistence of mixed micelles and detergent saturated liposomes). Below a critical lipid/detergent ratio, all mixed micelles are transformed into vesicles (stage III – liposomes only). After complete removal of the detergent, stable vesicles are obtained with the protein incorporated in the membrane. This process can be monitored e.g. by turbidimetry, light scattering measurements, isothermal titration calorimetry and dual-color fluorescence cross-correlation spectroscopy.[41,42,121,164–166]

The detergent-based solubilization process of vesicles is described by the so-called R-value, which expresses the effective detergent/lipid ratio in detergent containing liposomes or mixed micelles, respectively (Equation 5.1). The detergent concentration in the micelles or vesicles is described by the difference of the total detergent concentration $c_{\text{detergent}}$ and the aqueous monomeric concentration cmc (critical micelle concentration) relative to the total lipid c_{lipid}.[41,167]

$$R = \frac{c_{\text{detergent}} - cmc}{c_{\text{lipid}}} \tag{5.1}$$

The protein reconstitution may be started from stage I, the mixed micelles (co-micellization method, cf. Chapter 3.2.2.2) or from the detergent saturated liposomes (stage III) (direct method, cf. Chapter 0), where solubilized protein inserts into the destabilized liposomes.[42]

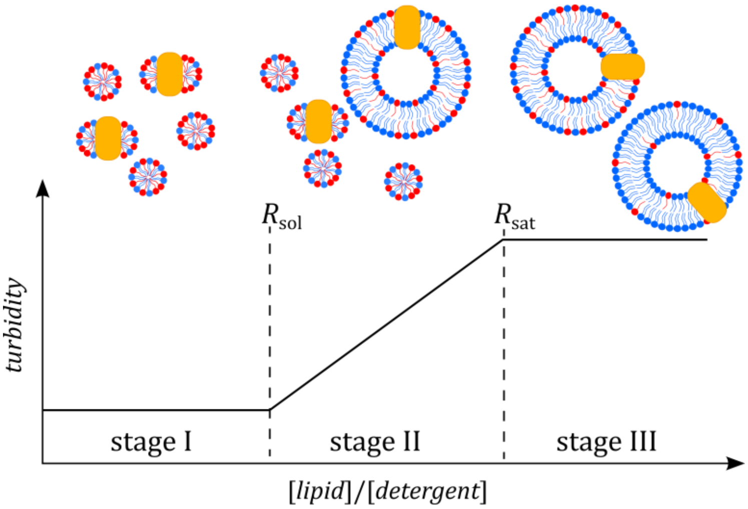

Figure 5.1. Scheme of the three solubilization stages in protein reconstitution. At low lipid (blue)/detergent (red) ratios, the proteins (yellow) are solubilized in mixed micelles (stage I). With increasing lipid concentration or detergent depletion, above the lipid/detergent ratio of R_{sol}, mixed micelles start transforming into detergent saturated vesicles (stage II) and finally, above the lipid/detergent ratio of R_{sat}, only proteoliposomes are present (stage III).[41]

The purified TF_0F_1-ATPase was reconstituted into DOPC/POPE/POPS/cholesterol (50:20:10:20) liposomes with the so-called direct method, where the protein is inserted into detergent destabilized liposomes (stage III) (Chapter 0). As described in literature, this method yields a highly unidirectional protein orientation, especially when detergents with a relatively high cmc, like *n*-octyl-*β*-D-glucoside (*n*OG, cmc = 20-25 mM[91]) are used in a concentration yielding predominantly the detergent saturated liposomes.[41,122] Rigaud *et al.* determined the *R*-values of *n*OG for detergent saturated vesicles to $R_{sat} = 1.3$ and for mixed micelles to $R_{sol} = 2.6$.[41] For the reconstitution of ATPase and co-reconstitution of the ΔN49-complex and ATPase in this work, the amount of detergent was adjusted to $R \approx 1$, avoiding the occurrence of mixed micelles that would occur above $R = 1.3$. Hence, a mostly unidirectional reconstitution of the proteins, with the water-soluble parts pointing outside of the vesicles, is expected. The unidirectional insertion into the detergent saturated liposome is especially favored in case of F-type ATPase, as it would be energetically unfavorable for the large hydrophilic F_1-part (diameter approx. 10 nm) to traverse the hydrophobic membrane core.[122] However, Jahnke *et al.* showed that the values of R_{sat} and R_{sol} obtained from a protein-free system were increased when they included the K^+-channel KcsA in the lipid-detergent mixture for reconstitution.[166] Thus, assuming that membrane proteins have nearly no influence on the lipid-detergent interaction, as they are much more diluted than lipids and detergent, has to be reconsidered.[164]

The finding of Jahnke *et al.* and the varying literature values of *n*OG's cmc indicate that the *R*-value can only be roughly estimated. Consequently, it is necessary to check if the membrane protein was successfully reconstituted into vesicles. A density gradient centrifugation allows separating non-reconstituted protein from intact proteoliposomes, as the latter have a lower density than non-reconstituted protein (cf. Chapter 4.2).[48,168] In this work, the reconstitution efficiency and the approximate number of TF_0F_1-ATPase molecules per vesicle have been quantified. As resumed in Table 5-1, the protein/lipid ratio (p/l) seemed to reach saturation at about 1:20,000, corresponding to four ATPase molecules per 95 nm diameter vesicle.[123] A saturation of the protein/lipid ratio was also reported by Parmar *et al.*, who used the gonococcal membrane protein I (Por) for reconstitution studies. At an initial p/l of 0.01:1 (w/w) the protein was completely incorporated into the vesicles, while starting with an initial p/l of 0.02:1 (w/w) (p/l ≈ 1:3000 (n/n)) 17 % of the protein was not reconstituted.[48] In a natural membrane the molar p/l is in the range of a few hundredths and generally several copies of a protein are present. However, in synaptic vesicles (diameter: 40-80 nm) only one copy of V-type ATPase, which is structurally very similar to F-type ATPase, was found.[90,164]

Table 5-1 Overview of nominally applied protein/lipid (p/l) ratios, the final p/l ratios in the proteoliposomes, the resulting reconstitution efficiencies and number of TF_0F_1-ATPase molecules per 95 nm diameter liposome.

Nominal p/l	Final p/l	Efficiency	N_{ATPase}/LUV
1:40,000	1:29,000	138 %	3
1:20,000	1:21,000	95 %	4
1:8,000	1:19,000	42 %	4

In most studies dealing with F-type ATPase reconstitution into liposomes, the reconstitution success was only characterized by conduction of ACMA-based acidification assays or alternatively, by monitoring the ATP synthesis activity of the proteoliposomes.[84,85,116,118,161] Only in the work of Soga *et al.*, the number of TF_0F_1-ATPase molecules per vesicle was calculated based on dynamic light scattering results. The proteoliposomes had an average diameter of 170 nm and based on a nominal protein/lipid ratio of approx. 1:40,000, seven ATPase molecules per liposome were expected. As the final protein/lipid ratio of the proteoliposomes was not determined, the calculated number might differ from the actual number of proteins per vesicle.[117]

In another publication by Iino *et al.*, the reconstitution efficiency of an F-type ATPase, reconstituted by means of detergent dilution and freeze-thawing, was stated to be “very high”. This was concluded from an SDS-PAGE analysis of a pellet and supernatant of the proteoliposome sample after centrifugation. Since the protein/lipid ratio was very low (1:200,000) and no protein was found in the supernatant, they assumed that the entire protein was incorporated into the liposomes. Based on the assumed liposome diameters of 100–200 nm, they expected that either no or only one protein had been reconstituted per liposome.[17]

Although the TF$_0$F1-ATPase has been often reconstituted into lipid vesicles, no systematic characterization of the reconstitution efficiency or quantification of ATPase molecules per vesicle can be found in literature.

5.3 Monitoring of the ATPase proton pumping activity with ACMA

Besides the quantification of ATPase molecules per vesicle, the protein functionality was proven. For correctly orientated TF$_0$F$_1$-ATPase, ATP hydrolysis provides the energy for active proton transport into the vesicle lumina. The luminal acidification can be easily detected by pH-sensitive fluorophores, changing their emission characteristics upon protonation inside the acidic vesicles.[126]

A well-established acidification assay to monitor the functionality of the reconstituted TF$_0$F$_1$-ATPase is based on the membrane permeable fluorophore ACMA.[64,65,72,84,116,128] As described in Chapter 4.3, this fluorophore is protonated in the acidified lumina, resulting in a fluorescence quenching and accumulation of the dye, as the protonated and therewith positively charged molecules have a significantly lower membrane permeability than the deprotonated ones.[72,169]

Since the activity of enzymes is highly dependent on temperature, the ATPase activity in proteoliposomes was assessed by means of an ACMA assay at different temperatures (Figure 4.7, Chapter 4.3). With increasing temperatures (20 °C to 50 °C), the minimum of ACMA fluorescence intensity was reached much faster, i.e. proton pumping was enhanced significantly. The maximum activity of the TF$_0$F$_1$-ATPase is reported to be obtained at 60 °C, which is reasonable for a protein naturally occurring in a thermophilic organism.[117] The temperature coefficient Q_{10} quantifies the temperature dependent activity increase (Equation 4.1 and Figure 4.8, Chapter 4.3).[130] The obtained Q_{10}-value of 3.14 indicated a 3-fold increase of proton pumping activity for a temperature elevation of 10 K. The only information about temperature dependent activity of the TF$_0$F$_1$-ATPase found in literature is from Soga and coworkers, who investigated the ATP synthesis activity between 10 °C and 30 °C. They found a Q_{10} temperature coefficient of 3–4 for the ATP synthesis activity, which matches the activity coefficient for ATP hydrolysis determined in this work.[117]

Apparently, not only the proton pumping rate changes with temperature, but also the reached minimum of ACMA fluorescence intensity seemed to decrease with increasing temperatures (see Figure 4.7, Chapter 4.3). Besides the ATPase activity this might result from the temperature influence on the ACMA fluorescence emission, since at higher temperatures the same fluorophore concentration exhibits less fluorescence intensity.[101]

All measurements up to a temperature of 40 °C reached a minimum and showed no significant fluorescence intensity increase until the protonophor CCCP was added. An exception from that was found at 50 °C. Here, the minimal fluorescence intensity was reached fastest, but then started increasing shortly after the minimum was attained, which results from an increased proton permeability of the membrane associated with increased temperature.[170] Thermophilic organisms adapt their membrane lipid composition in a way that the membrane permeability is not affected by the high temperatures.[67,171–173] Consequently, measurements at 37 °C ensured an enhanced ATPase activity compared to room temperature, and a membrane (DOPC/POPE/POPS/cholesterol (50:20:10:20)) tight enough to prevent massive proton leakage.

With the well-established ACMA acidification assay, the ATPase proton pumping activity was proven and the temperature dependence was characterized. At 37 °C the ATPase showed fast proton pumping and the vesicle membrane was not leaky for protons, while at higher temperature the vesicles showed significant proton leakage.

For proving proteoliposome acidification, the pH-sensitive membrane permeable dye ACMA is well-suited as its fluorescence intensity is significantly quenched upon vesicle acidification. At physiological pH ACMA occurs in neutral and monocationic form ($\mathrm{p}K_\mathrm{a} = 8.6$) and distributes in the vesicles after addition to the bulk solution.[72] A protonation-deprotonation equilibrium at the solution-membrane interface enables a partitioning of the neutral dye into the membrane. Upon acidification of the vesicles, the equilibrium is disturbed and a redistribution of dye molecules takes place, making it difficult to correlated fluorescence intensities to luminal pH-values.[72,125,127] The characterization of the optimal measurement conditions presents the basis for the development of a novel acidification assay that will allow to quantify the luminal pH of acidified proteoliposomes.

5.4 Quantitative Oregon Green 488-DHPE based acidification assay

- Parts of this Chapter have been published: M. Schwamborn, J. Schumacher, J. Sibold, N. K. Teiwes, C. Steinem, Monitoring ATPase induced pH changes in single proteoliposomes with the lipid-coupled fluorophore Oregon Green 488, *Analyst* **2017**, *accepted,* DOI: 10.1039/C7AN00215G.

Alternatives to ACMA for measurement of proteoliposome acidification are water soluble, membrane impermeable dyes like pyranine (8-hydroxypyrene-1,3,6-trisulfonic acid, HPTS) or SNARF (seminaphthorhodafluor) that have to be encapsulated in the proteoliposomes and do not redistribute upon acidification.[70] However, for detergent-based reconstitution methods the efficiency of dye entrapment is far from 100 % as the detergent-saturated vesicle membranes are permeable and the dye is depleted during the detergent removal.[174] Alternatively, the fluorophore concentration would have to be kept constant during the whole reconstitution procedure, which would require a large amount of fluorophore, e. g. in the dialysis buffer or in the buffer for gel filtration. A further step of gel filtration or dialysis would then be required to remove the external dye from the proteoliposomes.

When using a lipid-coupled pH-sensitive fluorophore, there are no redistribution or accumulation processes that complicate the fluorescence intensity-pH correlation and there is no extra afford for dye encapsulation, as the lipid-coupled fluorophore is mixed with the other lipids prior to liposome formation. The principle of measuring internal liposomal acidification with a lipid-coupled pH-sensitive fluorophore was first realized by Thelen *et al.* in 1984. They synthesized fluorescein-phosphatidylethanolamine (fluorescein-PE) and applied it for measuring the acidification by cytochrome *c* oxidase that had been reconstituted into fluorescein-PE containing liposomes. In Triton X-100 micelles, the pK_a of fluorescein-PE was determined to 7.2, while embedded in asolectin vesicles a $\mathrm{p}K_\mathrm{a} = 7.5$ was obtained for the fluorophore.[71] Similar measurements were performed with fluorescein-PE in 1985 by Azzi *et al.* in order to elucidate the proton transport mechanism by cytochrome *c* oxidase.[175] Moreover, surface pH-value changes due to protein binding of solid supported lipid bilayers have been monitored by the pH-sensitive fluorescence emission of *ortho*-Texas Red DHPE ($\mathrm{p}K_\mathrm{a} = 7.8$ in a DOPC/DPPC/cholesterol (1:1:1) matrix) and *ortho*-rhodamine B POPE ($\mathrm{p}K_\mathrm{a} = 6.2$ in a pure POPC membrane), which both experience an increase of fluorescence emission upon acidification.[176,177] OG488-DHPE is a commercially available and ready-to-use fluorophore, decreasing its fluorescence emission intensity upon acidification. Sandén *et al.* investigated the local protonation and deprotonation of membrane-anchored fluorescein and Oregon Green 488 (OG488). Within the scope of their work, the $\mathrm{p}K_\mathrm{a}$-values of free OG488 and

OG488 anchored to DOPG and DOPC membranes, at different ionic strength, were determined. The pK_a-value of the free fluorophore was with 4.7 significantly lower than the ones of the membrane-anchored fluorophore, with 6.7 for a DOPG membrane and 6.3 for a DOPC membrane (both with 0.15 M NaCl solution), respectively. From these variations, the authors concluded that the protonation/deprotonation behavior is determined by the confined environment of the membrane and not by the fluorophore's intrinsic pK_a-value.[104] In this work, the pK_a-value for OG488-DHPE anchored to a lipid membrane consistent of DOPC/POPE/POPS/cholesterol (50:20:10:20) in a solution of 0.5 mM MOPS, 100 mM KCl, 2 mM $MgCl_2$, pH 7.3, was determined to 6.1, which seems reasonable as it is similar to the literature-known values.[123] The pK_a-dependence of a membrane-anchored fluorophore was also reported by Kemmer *et al.*, who coupled the pHrodo Red succinimidyl ester to DOPE. They found a pK_a-value of 5.6 for the dye in a soybean lecithin membrane and a pK_a-value of 4.5 in a pure DOPC membrane.[131]

To compare the sensitivity of the fluorophores for a certain pH-range, their fluorescence emission intensities in dependence of the pH-value were calculated using their Equation 4.2, Chapter 4.4.1 and their specific pK_a-values. Figure 5.2 shows the resulting curves. The fluorescence response towards pH-changes is most sensitive in the linear range, where the slope is steepest. Thus, with fluorescein-PE, OG488-DHPE or pHrodo DOPE, pH-values in the ranges of pH 8.8-6.2, pH 7.4-4.8 (shaded area in Figure 5.2) or pH 6.9-4.3, can be measured, respectively. Consequently, for measuring pH-value decreases starting from around pH 7.3, like in this work, OG488-DHPE will be suited best.

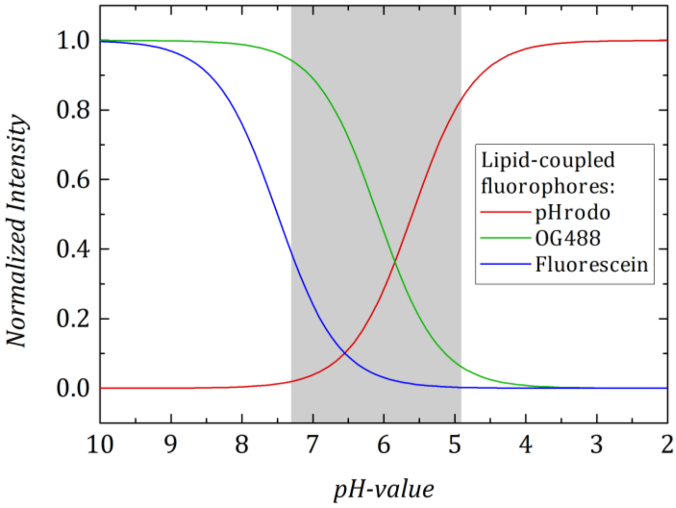

Figure 5.2. A comparison of the fluorescence intensity-pH correlation curves of pHrodo Red DOPE (red curve, pK_a = 5.6 in soybean lecithin membrane)[131], of fluorescein-PE (blue curve, pK_a = 7.5 in asolectin membrane) and OG488-DHPE (green line, pK_a = 6.1 in DOPC/POPE/POPS/cholesterol (50:20:10:20)) emphasizes the suitability of OG488-DHPE for pH-measurement up to approx. 2.5 units below pH 7.4 (grey area). Curves for pHrodo Red DOPE and fluorescein-PE were calculated according to Equation 4.2 (Chapter 4.4.1).

Table 5-2 gives a summary on the pK_a-values and pH detection ranges of different pH-sensitive lipid-coupled fluorophores. *Ortho*-rhodamine B POPE and pHrodo DOPE can be used for a similar pH-range like OG488-DHPE, but these fluorophores are not commercially available in the lipid conjugated form. A significant difference in their fluorescence response compared to OG488-DHPE is that their emission intensity does not decrease but increases upon acidification. A fluorescence intensity increase upon acidification is advantageous because it is an opposed process to possible photo bleaching. However, no significant photo bleaching occurred during the experiments performed with OG488-DHPE in this work. Fluorescein-PE and the *ortho*-isomer of Texas Red DHPE have pK_a > 7, thus being more appropriate for observing pH-value changes in the pH-range from neutral to slightly alkaline.

Table 5-2 Overview of the p*K*a-values and pH detection ranges of lipid-coupled fluorophores.

	pK_a	pH detection range	response upon acidification
ortho-Texas Red DHPE	7.8[176]	~ 9.1-6.5	intensity increase
fluorescein-PE	7.5[71]	~ 8.8-6.2	intensity decrease
ortho-rhodamine B POPE	6.2[177]	~ 7.5-4.9	intensity increase
OG488-DHPE	6.1	~ 7.4-4.8	intensity decrease
pHrodo DOPE	5.6[131]	~ 6.9-4.3	intensity increase

To convert the measured OG488-DHPE fluorescence intensity courses of the acidification assays into luminal pH-values, a calibration curve was prepared from vesicles with acidic lumina in a bulk solution of pH 7.3 (Figure 4.11, Chapter 4.4.1). With the calibration curve, the normalized fluorescence intensities of the OG488-DHPE based acidification assays were converted into pH-values (Equation 4.3, Chapter 4.4.2). From 17 performed measurements, an average mean luminal ΔpH of −0.45, from pH 7.3 to pH 6.85 ± 0.07 (SD), was obtained (Figure 4.15, Chapter 4.4.2).[123] Kemmer *et al.* monitored the acidification of P-type plasma membrane H^+-ATPase (AHA2, cf. Chapter 1.1, Figure 1.2) proteoliposomes with pHrodo Red DOPE. In their experiments the pH decreased from 6.78 to 6.16, corresponding to a ΔpH of −0.53 ± 0.16.[131] F-type ATPase induced proton gradients have been determined with membrane permeable dyes ACMA and acridine orange that were calibrated for the particular experiment. Rottenberg *et al.* used a mixture of ACMA and acridine orange to determine ATP-induced pH-changes of sub-mitochondrial particles from beef heart and inverted *E. coli* particles to −3.1 and −2.2, respectively.[124] D'Alessandro *et al.* reconstituted purified F_0F_1-ATPase from *E. coli* into liposomes and measured luminal acidifications from ΔpH = −2.9 to ΔpH = −3.7, depending on the experimental condition.[127] For comparison, the largest pH-difference found in a common eukaryotic cell is ΔpH = −2.5 between lysosomes (pH = 4.7) and the cytosol (pH = 7.2).[34]

In this work, OG488-DHPE has been used for the first time to monitor vesicle acidification and to quantify the mean luminal pH-value of TF_0F_1-ATPase-liposomes. Furthermore, lipid-coupled fluorophores allow performing lipid mixing assays that are primarily used to monitor fusion of lipid membranes. This offers the possibility to develop a new reconstitution approach for ATPase based on membrane fusion, which is discussed in the next chapter.

5.5 Combined fusion and acidification assay based on Oregon Green 488-DHPE

The model system of pore-spanning lipid bilayers (PSLBs) allows in principle the generation of proton gradients by active transport. It has been proven well-suited for the observation of the nigericin mediated K^+/H^+-antiport.[74] In this case, protein free pore-spanning lipid bilayers need to be prepared, which is an established procedure and ionophores like nigericin just have to be added to the bulk solution. However, the reconstitution of integral membrane proteins under physiological conditions into PSLBs is a key challenge and motivates for the development of a suitable reconstitution method. To guarantee successful proton transport, a specific orientation of the protein in the PSLBs is required and physiological conditions have to be guaranteed in order to maintain protein functionality. Schwenen *et al.* established the SNARE-mediated fusion of large unilamellar vesicles with pore-spanning lipid bilayers, giving rise to a reconstitution concept that meets the abovementioned criteria.[75]

Before attempting to insert the TF_0F_1-ATPase into PSLBs by means of SNARE-mediated fusion, the basic principle of the method, a transfer of ATPase-liposomes into another vesicle population, needed to be investigated. Therefore, a combined fusion and acidification assay, based on the lipid-coupled Oregon Green 488 fluorophore, was developed. In the first step, fusion was monitored by dequenching of OG488-DHPE and in the second step, the acidification assay was started by adding valinomycin and ATP. As the fluorophore was present in the vesicle population with Synaptobrevin 1-116 (Sb1-116), only successful fusion with ΔN49-ATPase liposomes could bring the OG488-DHPE in contact with the proton pump (cf. Chapter 4.5). Consequently, only the activity of the ATPase contained in fusion products was detectable. For both, the fusion and the acidification assay, only OG488-DHPE is needed, representing an easy system, where no phenomena like Förster resonance energy transfer (FRET) or cross talk, have to be taken into account between different fluorophores.

5.5.1 Fusion efficiency and acidification assay

Before the combined fusion and acidification assay was performed, the SNARE-mediated fusion efficiency, i.e. the lipid mixing efficiency, was determined by quantifying the dequenching of OG488-DHPE (Chapter 4.5.1). The same method was applied by Pähler *et al.* for the determination of the fusion efficiency of fusogenic peptides.[108]

A lipid mixing efficiency of 59 ± 4 % (SD) (n = 5) was found. However, the applied method does not allow to distinguish between full and hemifusion, where only the outer membrane leaflets fuse but the vesicle lumina do not merge since the inner leaflets do not fuse. Hernandez *et al*. performed inner leaflet mixing assays to distinguish between full- and hemifusion and found that 25 % of the overall lipid mixing originated from hemifusion. However, an absolute fusion efficiency was not assessed. Since the authors used the same SNARE-proteins (Sb1-116 and ΔN49-complex) in an identical protein/lipid ratio of 1:500 and a similar lipid composition (PC:PE:PS:cholesterol (50:20:20:10), this work: PC:PE:PS:cholesterol (50:20:10:20)), it can be assumed that the hemifusion percentage is similar.[138] A recent study on single vesicle fusion with a planar membrane by Kreutzberger and coworkers revealed that an increase in cholesterol concentration enhanced the amount of full fusion.[178] As the cholesterol concentration used in this work was 20 mol% it can be assumed that the percentage of hemifusion was slightly lower, than the 25 % ascertained by Hernandez *et al*. Nordlund and colleagues found a fusion efficiency of 70 % for proteoliposomes that contained reduced cytochrome *c* in the lumen of the one fusion partner, and cytochrome *c* oxidase in the membrane of the other fusion partner. As a result, only full fusion could bring the reduced cytochrome *c* in contact with the cytochrome *c* oxidase, which led to an oxidation of the cytochrome *c* and therewith resulted in a change of cytochrome *c* absorption spectra.[179] In contrast to this relatively high fusion efficiency, Schuette *et al*. found a lipid mixing efficiency of 22 %.[180] Schwenen *et al*. investigated SNARE-mediated fusion of LUVs with pore-spanning lipid bilayers and discovered that of all docked vesicles on rim parts 19 % hemifused and 32 % fully fused, whereas on the free-standing parts 21 % of vesicles docked performed hemi- and 26 % full fusion.[75]

The lipid mixing efficiency of 59 ± 4 % (SD), determined in this work, is in the range of the few literature known fusion efficiencies and it has to be assumed that up to 25 % of the lipid mixing efficiency may result from hemifusion, which would result in a minimum of 30 % full fusion. Since an average vesicle contains four TF_0F_1-ATPase molecules (Chapter 4.2), a minimum of 30 % full fusion should be sufficient to detect luminal acidification of fusion products by Oregon Green 488 quenching.

5.5.2 Influence of the ΔN49-complex on the OG488-DHPE fluorescence emission intensity

The lipid mixing efficiency of 59 ± 4 % (SD), suggests that a significant amount of ATPase molecules should be present in fusion products and hence have access to the pH-sensor OG488-DHPE. Surprisingly, an ATPase induced acidification of fused vesicles could not be observed in any case. Possible reasons could be an interaction of the OG488-DHPE dye with the

SNARE-fusion complex and/or heterogeneities in the protein distribution, like already mentioned in Chapter 4.5.2. To test on possible interactions of the SNARE-fusion complex with the dye, proteoliposomes with 1 mol% OG488-DHPE and different amounts of ΔN49-complex were prepared and their absorption and fluorescence emission spectra were measured. The ΔN49-complex should not differ much from the full SNARE-fusion complex in its possible interaction with the lipid-coupled fluorophore, since it has a synaptobrevin fragment of amino acids 49-96 instead of the full Sb1-116, therewith being identical in the membrane plane (Figure 5.3).[181] Astonishingly, the fluorescence emission intensity decreased with increasing protein/lipid ratio (−8% for p/l of 1:2000, −15% for p/l of 1:1000 and −21% for p/l of 1:500) (cf. Figure 4.26, Chapter 4.5.2) , whereas the absorption did not continuously reduce with ΔN49-complex concentration, which shows that there is a quenching effect of the protein on the dye. Studies about interactions between fluorophores and proteins or peptides are rare, although fluorophores are often coupled to them for studying conformational changes or protein-protein interactions. Chen *et al*. published a communication in 2010, dealing with the fluorescence quenching of Alexa Fluor dyes by amino acids. For Alexa Fluor 488, they found that tryptophan (Trp) and tyrosine (Tyr) exhibit a strong quenching effect, while histidine (His) and methionine (Met) were weaker quenchers. For Trp and His a combination of static and collisional quenching was found, while for Try and Met only collisional quenching occurred.

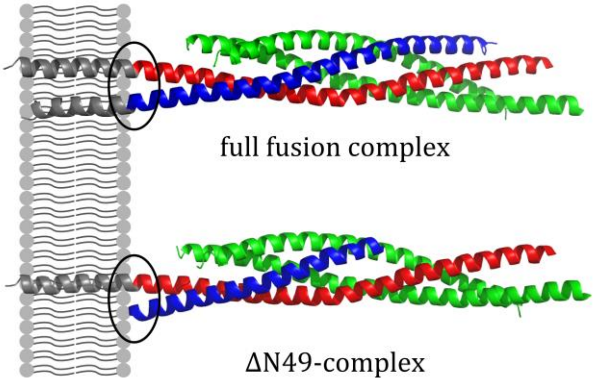

Figure 5.3. Scheme of the membrane embedded full fusion complex and the ΔN49-complex (PDB ID: 3hd7). Instead of full length Sb1-116, like in the full fusion complex, the ΔN49-complex harbors a truncated Sb49-96, which lacks the transmembrane domain and part of the *N*-terminus. On the membrane surface, both complexes are identical (black circles) and, therefore, should show the same interaction with the fluorophore OG488-DHPE.

The static quenching was postulated to result from stacking interactions between the amino acids and the fluorophore, whereas the collisional quenching was assigned to photo-induced electron transfer.[182] Since Alexa Fluor 488 and Oregon Green 488 have the same hydrocarbon scaffold and very similar fluorescence excitation and emission spectra (cf. Figure 5.4), it is likely for Oregon Green 488 to show a behavior similar to Alexa Fluor 488, regarding the quenching mechanisms described above.[132]

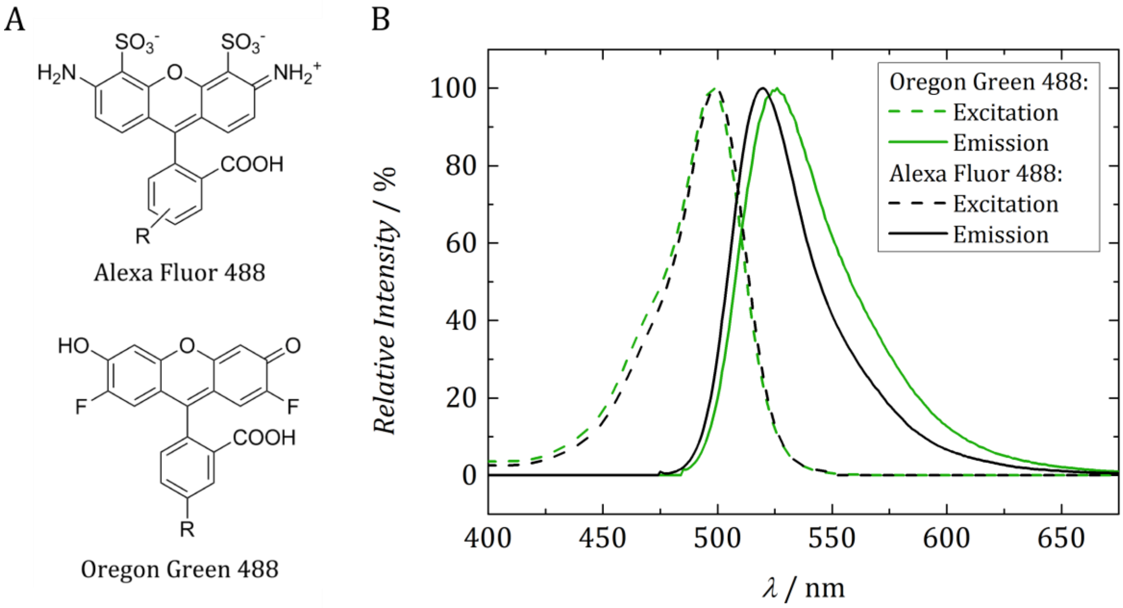

Figure 5.4. Alexa Fluor 488 and Oregon Green 488 share the same hydrocarbon scaffold (A) and have very similar excitation and emission spectra (B) (Alexa Fluor 488: black, Oregon Green 488: green).[183]

Locating the four quenching amino acids in the ΔN49-complex with PyMOL (DeLano Scientific LLC, 2006) revealed that Sb1-116 has a tyrosine (Tyr88) and two adjacent tryptophan residues (Trp89, Trp90) and Syntaxin has a tyrosine (Tyr257) that are all located close to the membrane surface, which is a common motif of membrane proteins. These amino acids are preferentially found at the lipid bilayer surface (c.f. Figure 5.5).[184] As the Oregon Green 488 is coupled to the amine function of DHPE's head group, the fluorescent moiety is located directly on the hydrophilic surface so that an interaction with Tyr88, Trp89 and Trp90 is conceivable. These fluorescence-quenching amino acids were also localized in the structure of the ATPase. Figure 5.5 B shows the cryo-electron microscopic structure of *E. coli* F_0F_1-ATPase (PDB ID: 5t4o).[24] The c_{10}-ring contains methionine residues (red) in close proximity to the membrane surface and the *a*-subunit also has some of the quenching amino acids that might be accessible for interaction with the fluorophore.

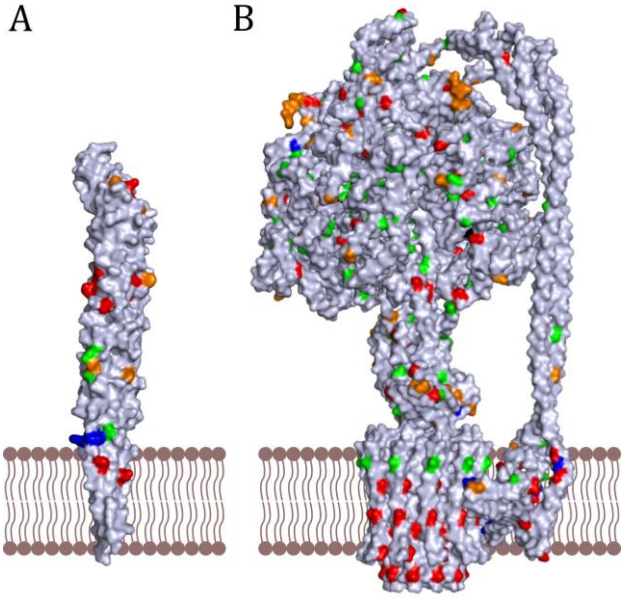

Figure 5.5. Crystal structure of the SNARE-fusion complex (PDB ID: 3hd7) (A) and cyro-electron microscopic structure of *E. coli* F_0F_1-ATPase (PDB ID: 5t4o) (B). The fluorescence-quenching amino acids tryptophan (blue), tyrosine (green), methionine (red) and histidine (orange) are highlighted. In case of the SNARE-complex two tryptophan residues and a threonine stick out after the transmembrane domain (TMD).

However, the number of ATPase molecules per vesicle (95 nm diameter) is only around four (p/l of 1:20,000), whereas about 70 SNAREs are present in such a liposome at a p/l of 1:500. Comparing these numbers to the approx. 800 OG488-DHPE molecules (≙ 1 mol%) suggests that a quenching effect by the ATPase molecules is negligible, while the amount of SNARE complexes accounts to nearly 10 % of the dye's amount, making a quenching of up to 20 % conceivable.

5.5.3 Possible protein heterogeneities in the liposomes

Although the OG488-DHPE fluorescence emission intensity seems to be quenched by the SNARE-fusion complex, about 80 % of fluorescence intensity remains, which should be enough for detection of ATPase activity, i.e. vesicle acidification. However, inhomogeneities in the distribution of the SNARE-proteins and the TF_0F_1-ATPase could explain why no OG488-DHPE quenching could be detected in the fusion products. If one assumes the presence of proteoliposome subpopulations, which may contain SNARE proteins but no ATPase and *vice versa*, it would be possible to observe lipid mixing via OG488-DHPE dequenching as well as ATPase activity by means of an neity of protein distribution in proteoliposomes, but in the last few years studies were published indicating that the extent of inhomogeneity in protein reconstitution into lipid vesicles might have been greatly underestimated.[151,185,186]

Chen *et al.* found that synaptobrevin, which was incorporated into preformed liposomes of a lipid composition similar to that of synaptic liposomes (PC:PE:PS:cholesterol (48:20:12:20)), resulted in a very heterogeneous sample with 10 % of the liposomes containing 90 % of the protein.[185] In this work, the ATPase and ΔN49-complex were reconstituted into preformed liposomes of similar composition (DOPC:POPE:POPS:cholesterol (49:20:10:20:1)). The co-micellization method, which was used for synaptobrevin reconstitution in this work, might also result in a heterogeneous protein distribution because the proteoliposomes emerge from a heterogeneous lipid-detergent-protein mixture when the detergent is depleted.[42,185] However, results obtained by Kyoung *et al.* contradict this finding, as they reconstituted SNARE-proteins into proteoliposomes that also resembled the synaptic vesicle lipid composition (PC:PE:PS:cholesterol:fluorophore; 44.5:20:12:20:3.5) by the co-micellization reconstitution method and state to have a homogeneous protein distribution in the liposomes.[144] Not only proteins seem to be unevenly distributed when reconstituted into liposomes, even among the lipid distribution significant inhomogeneities can occur.

Larsen *et al*. detected the fluorescence emission intensity of two different lipid-coupled fluorophores, Atto633 and fluorescein, in single vesicles and found a distinct heterogeneity in the distribution of both fluorophores. Depending on the lipid-anchor of the two fluorophores and the vesicle preparation method, the degree of inhomogeneity varied to a certain extent, but was pronounced in each case. Vesicles were also prepared by removal of the detergent *n*-octyl-*β*-D-glucoside (*n*OG) from mixed micelles by means of dialysis, which is often used for protein reconstitution and represents a slow process allowing the system to reach equilibrium. Nevertheless, these samples did also show significant compositional heterogeneities, from which the authors concluded that inhomogeneities in lipid composition do not result from kinetically trapped states during vesicle formation, but are a general phenomenon in liposome systems.[149]

To examine inhomogeneities in lipid- and protein distribution, single vesicle assays provide a well suited method. Mathiasen and colleagues analyzed compositional heterogeneities of single immobilized proteoliposomes for three different fluorescently labeled G-protein coupled receptors (GPCRs). For protein/lipid ratios of 1:1,000, between 9 % and 60 % of the liposomes did not contain any protein, depending on the protein and reconstitution method. Furthermore, for a range of nominal protein/lipid ratios (1:300,000–1:1,000) the amount of the empty fraction of vesicles was analyzed and the final protein/lipid ratio was determined. Other than expected, the measured final protein/lipid ratio did not correlate linearly with the nominal protein/lipid ratio, but remained constant in the low protein/lipid ratio range (approx. 1:300,000–1:50,000), while the fraction of empty liposomes decreased (from approx.

90 % to 70 %). For a case of thermodynamic equilibrium and no cooperative effects, a Poisson distribution of empty and filled liposomes would be expected, which was not found in any of the observed cases.[151]

Similar findings were obtained in 2016 in the work of Veshaguri *et al*. They reconstituted the P-type ATPase AHA2 (cf. Chapter 1.1, Figure 1.2) into liposomes (p/l 1:12,000) doped with a pH-sensitive lipid-coupled fluorophore (pHrodo Red DOPE) by adding *n*OG and protein to preformed vesicles (extrusion through a 0.2 µm size nucleopore polycarbonate membrane) and removing the detergent from the solubilized protein/lipid/detergent by gel filtration. Monitoring the proton pumping activity of the proteoliposomes attached to a surface, they discovered that 80 % (for AHA2 wt) and 84 % (for an AHA2 mutant) of the vesicles did not show any activity. The protein's orientation was determined to 80 ± 19 % pointing outwards with the ATP-hydrolyzing unit. Accordingly, the 80 % or 84 % of inactive vesicles cannot result from an unfavorable protein orientation, but mostly from compositional heterogeneities.[186] These findings agree with those from Mathiasen *et al*. and might also be true for the proteoliposomes prepared in this work.

In the studies of Mathiasen *et al.* and Veshaguri *et al.* only one specific protein was reconstituted at a time, while in this work the ΔN49-complex and the TF_0F_1-ATPase have been co-reconstituted. Thus, the probability of both proteins being reconstituted into the same liposome is low.

In literature, only little information is found about the co-reconstitution of membrane proteins. One of the first, who co-reconstituted two membrane proteins, bacteriorhodopsin and mitochondrial ATP-synthase (or F-type ATPase), were Racker and Stoeckenius in 1974. Bacteriorhodopsin is a light-driven proton pump and it was used to acidify the vesicular lumina so that ATP could be produced by the co-reconstituted ATP-synthase.[187] In the 1990's several groups followed the approach of Racker and Stoeckenius and reconstituted bacteriorhodopsin with ATP synthase from several organisms, in order to examine the light-driven ATP synthesis.[188–192] At that time, also the reconstitution methods were systematically investigated. [41,47,48,193] The only further published studies of ATP-synthase co-reconstitution with other proteins were from the group of von Ballmoos in recent years.[179,194,195] However, in those studies, which were all performed in bulk solution, the occurrence of inhomogeneities is not mentioned at all. In some cases ACMA assays were performed to prove the functional reconstitution of the F-type ATPase,[191,194] but in most cases only the ATP synthesis was monitored by means of luciferin-luciferase assays.[188,190,192] As this assay is highly sensitive (detection of picomol amounts of ATP), a very small fraction of proteoliposomes with successfully co-reconstituted proteins might produce enough ATP in the bulk solution to be detected.[196] This luciferin-luciferase assay was also performed in studies, where a co-reconstitution was achieved by vesicle fusion. The first assay of this kind was published by Nordlund *et al.* in 2014 and was based on SNARE-mediated fusion. In particular, F-type ATPase was co-reconstituted with SNAP-25 and syntaxin (corresponding to the ΔN49-complex) and *bo*$_3$ oxidase with synaptobrevin. With increasing fusion time, the ATP-synthesis rate increased and reached a saturation after approx. 50 min.[179] In 2016, two very similar studies (Biner *et al.* and Ishmukhametov *et al.*) were published that used oppositely charged liposomes to fuse two liposome populations, one carrying an ATP synthase and the other a *bo*$_3$ oxidase, which transports protons across the membrane by oxidizing quinone Q_1.[59,60] Biner *et al.* measured the ATP synthesis rate that leveled off after approx. 5 min of charge-mediated fusion,[59] while Ishmukhametov *et al.* found a linear increase of ATP concentration during 180 s fusion time.[60]

These studies prove that in principle the fusion-based reconstitution (SNARE-protein or charge mediated) should be possible and that it represents a versatile and valuable tool for the reconstitution of diverse membrane proteins into a variety of model membrane systems. It might be possible that the acidification of the fusion products in this work could not be detected due to a lower sensitivity of the OG488-DHPE based acidification assay, compared to the ATP determination with the luciferin-luciferase assay, or that the protein distribution exhibited a higher inhomogeneity than in the presented literature.

Like described in the studies of Mathiasen *et al.* and Veshaguri *et al.*, single vesicle assays are very well suited to investigate compositional inhomogeneities in proteoliposome samples that remain undetectable in bulk measurements.[151,186] Consequently, single vesicle experiments should reveal, if inhomogeneities in protein distribution are present in the liposome samples.

5.6 Single vesicle assay

- Parts of this Chapter have been published: M. Schwamborn, J. Schumacher, J. Sibold, N. K. Teiwes, C. Steinem, Monitoring ATPase induced pH changes in single proteoliposomes with the lipid-coupled fluorophore Oregon Green 488, *Analyst* **2017**, *accepted,* DOI: 10.1039/C7AN00215G.

Like discussed in Chapter 5.5.3, a heterogeneous distribution of TF_0F_1-ATPase and SNARE-proteins in the liposomes could explain the results of the combined fusion and acidification assay. To detect compositional inhomogeneities in liposome samples, single vesicle assays are performed, as they allow observing a large number of liposomes immobilized on a surface simultaneously.[149,151]

To examine the distribution of active TF_0F_1-ATPase, which was reconstituted into OG488-DHPE doped vesicles, a single vesicle assay was established. Previously, bulk assays with membrane permeable ACMA and lipid-coupled Oregon Green 488 have been performed for observation of TF_0F_1-ATPase activity. These assays show an averaged response of active and inactive proteoliposomes, thus making it impossible to assess the percentage of liposomes reaching specific pH-values. To elucidate the activities of single proteoliposomes, ATPase was reconstituted into OG488-DHPE and biotinyl-cap-PE doped vesicles (DOPC/POPE/POPS/cholesterol/OG488-DHPE/biotin-cap-PE (48.6:20:10:20:1:0.4)) that were subsequently immobilized on a NeutrAvidin-functionalized glass slide. As the glass slide was mounted to a custom-build, heatable flow chamber, the experiments could be performed at 37 °C, guaranteeing sufficient ATPase activity (cf. Chapter 4.3). Images series were taken with a confocal fluorescence microscope and analyzed as described in Chapter 4.6.2.

5.6.1 ATPase-liposome immobilization

A common strategy for immobilization of single vesicles on a surface is based on the biotin-avidin interaction. Avidin and similar proteins like streptavidin or NeutrAvidin exhibit a very high binding affinity for biotin and can act as a connector between biotinylated proteins, vesicles, etc. and biotinylated surfaces.[197,198]

In this work, vesicles doped with the biotinylated lipid (1,2-dihexadecanoyl-*sn*-glycero-3-phosphoethanolamine-*N*-(cap biotinyl)) were attached to a methoxy-polyethylene glycol (PEG)/biotin-PEG (9:1) functionalized glass slide via NeutrAvidin.

Other functionalization strategies based on silanization and PEGylation, rely on silanization with (3-aminopropyl)triethoxysilane (APTES), covering the surface with amino-groups that enable a coupling with PEGs having an amine reactive group, like the succinimidyl-moiety.[144–146] The use of 3-glycidyloxipropyltrimethoxysilane (GOPTS) instead of amino-functionalized silanes and the omission of solvents in the functionalization method of Piehler *et al.* should result in a high-density PEG layer, preventing unspecific adsorption.[112] Furthermore, a PEG-functionalized surface provides an entropic barrier against adhesion, thus preventing the deformation and increased leakiness of the immobilized vesicles.[199,200]

The suitability of the applied immobilization strategy was confirmed by attaching Texas Red DHPE doped large unilamellar vesicles (diameter approx. 100 nm) filled with the water soluble green fluorophore pyranine. A colocalization of red membrane-anchored and entrapped green fluorophore indicated the predominance of intact vesicles (see Figure 4.27, Chapter 4.6.1). The coverage of 0.06 vesicles/µm^2 ensured a clear separation between the single liposomes. Thus, the applied immobilization strategy is perfectly suited for conduction of single vesicle experiments on ATPase-mediated acidification.[123]

5.6.2 TF$_0$F$_1$-ATPase activity in attached liposomes

The key advantage of single vesicle assays is that they provide information about possible heterogeneities that are averaged and remain hidden in ensemble assays. In recent years, assays on the single vesicle scale have been applied for investigation of transport mechanisms for the neurotransmitters glutamate and γ-aminobutyric acid (GABA), the SNARE-mediated fusion of vesicles, of compositional heterogeneities concerning membrane protein and lipid distribution and for monitoring the proton-pumping activity of P-type ATPase *Arabidopsis thaliana* isoform 2 (AHA2, cf. Chapter 1.1, Figure 1.2).[144,149,150,186,201] Furthermore, single vesicle assays were used for investigation of dye-membrane interactions and curvature-selective binding of proteins to vesicle membranes.[202,203]

For analysis of the experiments, vesicles were automatically detected with a custom written Matlab script and the fluorescence intensities were read out for each frame of the time series. Then the fluorescence intensities of OG488-DHPE were normalized and converted to pH-values like described in Chapter 4.4.1 (cf. Chapter 4.6.2). In three experiments, a total of 12 from 238 detected vesicles experienced a distinct acidifcation, meaning that 95 % of the vesicles either showed no acidification at all or only to such extend that the OG488-DHPE intensity decrease was not clearly distinguishable from the signal noise. An averaging of all pH-value courses for the three single vesicle experiments resulted in ΔpH of −0.55, −0.37 and −0.50 (average: ΔpH = −0.47), which is in the same range as the average mean luminal ΔpH of −0.45 ± 0.07 (SD) obtained from the bulk OG488-DHPE acidification assays (cf. Figure 4.15, Chapter 4.4.2). However, the analysis of the single vesicles revealed that luminal ΔpH-values of up to −2 were measurable and that only 3.1 %–11.9 % ($n = 3$, average: 5 %) of the vesicles showed an acidification of $\Delta pH < -0.4$. The low percentage of acidified vesicles hints at a heterogeneous distribution of active ATPase. This was quite unexpected, as according to the determined reconstitution efficiency four ATPase molecules should be reconstituted into an average-sized vesicle (95 nm diameter) (see Chapter 4.2).[123]

In literature, the luminal pH-changes induced by the reconstituted P-type H^+-ATPase AHA2 were measured in bulk and on the single vesicle scale with the lipid-coupled pH-sensitive fluorophore pHrodo Red. In the bulk assays an average luminal pH-decrease of 0.53 ± 0.16 units was obtained.[131] Observation of immobilized AHA2-vesicles revealed that only 20 % (or 16 % for a mutant of AHA2) of the vesicles were acidified upon ATP-hydrolysis, resulting in an average $\Delta pH \approx -0.6$, which is in the same range as the value obtained from bulk measurements. Additionally, experiments with Alexa Fluor 647 labeled AHA2 revealed that about 38 % of protein containing vesicles were inactive. As mentioned in Chapter 5.5.3, protein orientation was determined to be 80 ± 19 % of proteins pointing outwards with their ATP-hydrolyzing part, thus a wrong protein orientation could be excluded as a main reason for non-acidified vesicles.[186] As discussed in detail in Chapter 5.5.3, Mathiasen *et al.* also found an inhomogeneous protein distribution with fractions of 10-60 % of empty vesicles when reconstituting different membrane proteins.[151]

So far, the activity of TF_0F_1-ATPase proteoliposomes has only been monitored in bulk experiments.[64,65,84,85,116,128] An assay for the observation of single TF_0F_1-ATPase vesicles was established in this work, and allowed a quantification of vesicular pH-decreases induced by ATPase induced proton pumping.[123] The results of the experiments performed in this work and in literature, revealed that significant heterogeneities can occur when reconstituting membrane proteins into vesicles. The commonly used bulk assays for detection of protein transport activity do not allow to uncover such phenomena, as only the response of the ensemble is monitored. This emphasizes the importance of single vesicle experiments for a realistic impression of proteoliposome activity.

In Chapter 5.5.3, inhomogeneities in protein distribution were discussed as a possible reason for undetectable acidification in fusion products. For the TF_0F_1-ATPase, evidence of an inhomogeneous distribution was found by means of the single vesicle assay. Concerning the homogenous distribution of SNARE-proteins in proteoliposomes, contradictory statements are found in literature. Chen *et al.* reported a severe heterogeneity for reconstituted Synaptobrevin, while Kyoung *et al.* found a homogeneous distribution.[144,185] If a SNARE-protein heterogeneity proved to be true for the experiments performed in this work (Chapter 4.5), it would possibly result in such few fusion products containing an active ATPase, that they were not detectable in the performed bulk assays. To successfully use the SNARE-mediated fusion as a universal reconstitution tool, an increased homogeneity of active ATPase has to be achieved and also for the SNAREs a homogenous distribution has to be ensured. For this purpose, the established single vesicle assay represents an indispensable tool.

6 CONCLUSION

Pore-spanning lipid bilayers (PSLBs) consist of a lipid membrane that seals an array of defined pores in a solid substrate, hence representing a potential model membrane system for the observation of membrane protein mediated active transport into or from the membrane-spanned pores. The preparation of PSLBs is accomplished by spreading electroformed giant unilamellar vesicles (GUVs) on a porous substrate, not allowing to permanently maintain physiological conditions, which is unfavorable for the functionality of most membrane proteins. However, small proteoliposomes fusing with preformed PSLBs could be envisaged as transporters for sensitive proteins, merging their cargo into preformed PSLBs under physiological conditions.

Therefore, this work aimed at investigating the potential of SNARE-protein mediated membrane fusion as a physiological reconstitution tool. In the first partof this work, the His$_{10}$-tagged TF$_0$F$_1$-ATPase, originating from a thermophilic *bacillus* PS3, was successfully isolated from *Escherichia coli*. Detergent-mediated protein reconstitution into preformed vesicles was quantified and indicated a saturation occurring at a protein/lipid ratio of 1:20,000, which corresponds to four proteins per average sized vesicle (d = 95 nm). TF$_0$F$_1$-ATPase induced vesicle acidification by addition of ATP was first characterized by monitoring the pH-sensitive fluorescence intensity of the membrane permeable fluorophore 9-amino-6-chloro-2-methoxyacridine (ACMA). To quantify the mean luminal acidification of TF$_0$F$_1$-ATPase-proteoliposomes, an assay based on the lipid-coupled fluorophore Oregon Green 488-DHPE (OG488-DHPE) was established. A calibration curve correlating the fluorescence intensity to different luminal pH-values allowed to determine the average luminal pH decrease of acidified ATPase-vesicles from pH 7.30 to pH 6.85 (ΔpH = −0.45).

After proving and quantifying the activity of ATPase reconstituted into small vesicles, the feasibility of SNARE-mediated fusion as a universal and physiological reconstitution tool was assessed. For this purpose, a combined fusion and acidification assay for small proteoliposomes was introduced. In the first stage of the assay, the fusion of OG488-DHPE-doped synaptobrevin-liposomes with ATPase-ΔN49-liposomes was monitored by a dequenching of OG488-DHPE, resulting from the fluorophore dilution by lipid mixing/fusion with the colorless proteoliposomes. The extent of dequenching could be correlated to a lipid mixing efficiency of 59 ± 4 %. The second stage of the combined assay consisted of an OG488-DHPE acidification assay of the fused vesicles. Most importantly, only successful fusion of ATPase-

ΔN49-liposomes and OG488-DHPE doped synaptobrevin-liposomes would bring the ATPase in contact with the pH-sensor OG488-DHPE, allowing only to detect ATPase mediated acidification in fused vesicles. Despite successful fusion in the first stage, acidification could not be detected in any case in the fused proteoliposomes. However, when ACMA assays were performed with the fused proteoliposomes, they showed ATPase-induced acidification, most likely resulting from non-fused liposomes. Consequently, a heterogeneous protein distribution was considered as a possible cause for this finding.

In the final step of this work, a single vesicle fluorescence microscopy assay was established to uncover possible heterogeneities in the distribution of reconstituted TF_0F_1-ATPase. For this purpose, the OG488-DHPE based bulk acidification assay was transferred to the single vesicle level by immobilizing the ATPase-liposomes via biotin-NeutrAvidin interaction on a surface. Reading out the fluorescence intensities of every immobilized vesicle, revealed that only 5 % of the vesicles showed a detectable acidification, ranging from luminal pH-values decreases of $\Delta pH = -0.5$ to -2. Averaging of the fluorescence intensities of all active and inactive single vesicles, resulted in $\Delta pH = -0.47$, which corresponds to the average mean luminal $\Delta pH = -0.45$ obtained from the bulk OG488-DHPE acidification assays. The low percentage of acidified ATPase-liposomes was surprising, as from the quantification of the ATPase reconstitution efficiency four proteins per average sized vesicle were expected.

If this distributional heterogeneity of active TF_0F_1-ATPase was also present in co-reconstituted ATPase-ΔN49-liposomes, it would result in a very small, most likely undetectable, population of fused vesicles with active ATPase, presumably explaining the non-detectable acidification of fused proteoliposomes in the second stage of the combined fusion and acidification assay.

To realize the idea of SNARE-mediated fusion as a physiological reconstitution tool for membrane proteins, the homogeneous and functional reconstitution of ATPase into proteoliposomes has to be improved. For this purpose, the established single vesicle assay is an indispensable tool, which will also be applicable for investigation of distributional heterogeneities of other reconstituted transport proteins. Once a homogeneous distribution of ATPase and SNARE-proteins will be achieved, the combined fusion and acidification assay should allow the detection of ATPase-mediated acidification in the fused proteoliposomes. Accomplishing this task will then allow to reconstitute the TF_0F_1-ATPase under physiological conditions into PSLBs by fusing small ATPase-SNARE-liposomes with a SNARE-protein containing PSLBs.

7 BIBLIOGRAPHY

[1] P. L. Luisi, P. Walde, T. Oberholzer, Lipid vesicles as possible intermediates in the origin of life, *Curr. Opin. Colloid Interface Sci.* **1999**, *4*, 33–39.

[2] P.-A. Monnard, D. W. Deamer, Membrane self-assembly processes: steps toward the first cellular life, *Anat. Rec.* **2002**, *268*, 196–207.

[3] D. M. Engelman, Membranes are more mosaic than fluid, *Nature* **2005**, *438*, 578–580.

[4] K. Simons, M. J. Gerl, Revitalizing membrane rafts: new tools and insights, *Nat. Rev. Mol. Cell Biol.* **2010**, *11*, 688–699.

[5] J. B. de la Serna, G. J. Schutz, C. Eggeling, M. Cebecauer, There is no simple model of the plasma membrane organization, *Front. Cell. Dev. Biol.* **2016**, *4*, 106.

[6] M. Wu, J. Gu, R. Guo, Y. Huang, M. Yang, Structure of mammalian respiratory supercomplex I1III2IV1, *Cell* **2016**, *167*, 1598-1609.

[7] J. S. Sousa, D. J. Mills, J. Vonck, W. Kühlbrandt, Functional asymmetry and electron flow in the bovine respirasome, *eLife* **2016**, *5*.

[8] J. A. Letts, K. Fiedorczuk, L. A. Sazanov, The architecture of respiratory supercomplexes, *Nature* **2016**, *537*, 644–648.

[9] J. Gu, M. Wu, R. Guo, K. Yan, J. Lei, N. Gao, M. Yang, The architecture of the mammalian respirasome, *Nature* **2016**, *537*, 639–643.

[10] J. K. Lanyi, Bacteriorhodopsin, *Annu. Rev. Physiol.* **2004**, *66*, 665–688.

[11] M. J. Buch-Pedersen, B. P. Pedersen, B. Veierskov, P. Nissen, M. G. Palmgren, Protons and how they are transported by proton pumps, *Pflugers Arch. - Eur. J. Physiol.* **2009**, *457*, 573–579.

[12] M. Bublitz, J. P. Morth, P. Nissen, P-type ATPases at a glance, *J. Cell Sci.* **2011**, *124*, 2515–2519.

[13] M. G. Palmgren, P. Nissen, P-type ATPases, *Annu. Rev. Biophys.* **2011**, *40*, 243–266.

[14] K. W. Beyenbach, H. Wieczorek, The V-type H^+ ATPase: Molecular structure and function, physiological roles and regulation, *J. Exp. Biol.* **2006**, *209*, 577–589.

[15] J. Zhao, S. Benlekbir, J. L. Rubinstein, Electron cryomicroscopy observation of rotational states in a eukaryotic V-ATPase, *Nature* **2015**, *521*, 241–245.

[16] M. Yoshida, E. Muneyuki, T. Hisabori, ATP synthase – a marvellous rotary engine of the cell, *Nat. Rev. Mol. Cell Biol.* **2001**, *2*, 669–677.

[17] R. Iino, R. Hasegawa, K. V. Tabata, H. Noji, Mechanism of inhibition by *C*-terminal α-helices of the subunit of *Escherichia coli* F_0F_1-ATP synthase, *J. Biol. Chem.* **2009**, *284*, 17457–17464.

[18] B. A. Feniouk, M. Yoshida, Regulatory mechanisms of proton-translocating F_0F_1-ATP synthase, *Results. Probl. Cell Differ.* **2008**, *45*, 279–308.

[19] D. Okuno, R. Iino, H. Noji, Rotation and structure of F_0F_1-ATP synthase, *J. Biochem.* **2011**, *149*, 655–664.

[20] R. Iino, H. Noji, Operation mechanism of F_0F_1-adenosine triphosphate synthase revealed by its structure and dynamics, *IUBMB Life* **2013**, *65*, 238–246.

[21] H. Noji, R. Yasuda, M. Yoshida, K. Kinosita Jr, Direct observation of the rotation of F_1-ATPase, *Nature* **1997**, *386*, 299–302.

[22] R. Yasuda, H. Noji, M. Yoshida, K. Kinosita Jr, H. Itoh, Resolution of distinct rotational substeps by submillisecond kinetic analysis of F_1-ATPase, *Nature* **2001**, *410*, 898–904.

[23] Y. Rondelez, G. Tresset, T. Nakashima, Y. Kato-Yamada, H. Fujita, S. Takeuchi, H. Noji, Highly coupled ATP synthesis by F_1-ATPase single molecules, *Nature* **2005**, *433*, 773–777.

[24] M. Sobti, C. Smits, A. S. Wong, R. Ishmukhametov, D. Stock, S. Sandin, A. G. Stewart, Cryo-EM structures of the autoinhibited *E. coli* ATP synthase in three rotational states, *eLife* **2016**, *5*.

[25] S. Nesci, F. Trombetti, V. Ventrella, A. Pagliarani, The *c*-ring of the F_1F_0-ATP synthase: Facts and perspectives, *J. Membr. Biol.* **2016**, *249*, 11–21.

[26] P. Mitchell, Coupling of phosphorylation to electron and hydrogen transfer by a chemi-osmotic type of Mechanism, *Nature* **1961**, *191*, 144–148.

[27] D. Voet, J. G. Voet, C. W. Pratt, *Principles of biochemistry*, Wiley, Hoboken, New Jersey, **2008**.

[28] V. P. Skulachev, A. V. Bogachev, F. O. Kasparinsky, *Principles of Bioenergetics*, Springer, Berlin Heidelberg, **2013**.

[29] E. R. Kashket, The proton motive force in bacteria: a critical assessment of methods, *Annu. Rev. Microbiol.* **1985**, *39*, 219–242.

[30] T. J. Montville, M. E. C. Bruno, Evidence that dissipation of proton motive force is a common mechanism of action for bacteriocins and other antimicrobial proteins, *Int. J. Food Microbiol.* **1994**, *24*, 53–74.

[31] J. M. Berg, J. L. Tymoczko, L. Stryer, *Stryer Biochemie*, Spektrum, Heidelberg, **2012**.

[32] W. Junge, N. Nelson, ATP synthase, *Annu. Rev. Biochem.* **2015**, *84*, 631–657.

[33] S. Steigmiller, P. Turina, P. Gräber, The thermodynamic H^+/ATP ratios of the H^+-ATPsynthases from chloroplasts and *Escherichia coli*, *Proc. Natl. Acad. Sci. USA* **2008**, *105*, 3745–3750.

[34] J. R. Casey, S. Grinstein, J. Orlowski, Sensors and regulators of intracellular pH, *Nat. Rev. Mol. Cell Biol.* **2009**, *11*, 50–61.

[35] A. D. Vinogradov, Steady-state and pre-steady-state kinetics of the mitochondrial F_1F_O ATPase: is ATP synthase a reversible molecular machine?, *J. Exp. Biol.* **2000**, *203*, 41–49.

[36] N. Demaurex, pH Homeostasis of cellular organelles, *News Physiol Sci.* **2002**, *17*, 1–5.

[37] J. A. Mindell, Lysosomal acidification mechanisms, *Annu. Rev. Physiol.* **2012**, *74*, 69–86.

[38] G. Sachs, J. M. Shin, C. Briving, B. Wallmark, S. Hersey, The pharmacology of the gastric acid pump: The H^+,K^+ ATPase, *Annu. Rev. Pharmacol. Toxicol.* **1995**, *35*, 277–305.

[39] E. P. Spugnini, P. Sonveaux, C. Stock, M. Perez-Sayans, A. de Milito, S. Avnet, A. G. Garcia, S. Harguindey, S. Fais, Proton channels and exchangers in cancer, *Biochim. Biophys. Acta* **2015**, *1848*, 2715–2726.

[40] Y.-H. M. Chan, S. G. Boxer, Model membrane systems and their applications, *Curr. Opin. Chem. Biol.* **2007**, *11*, 581–587.

[41] J.-L. Rigaud, B. Pitard, D. Lévy, Reconstitution of membrane proteins into liposomes: application to energy-transducing membrane proteins, *Biochim. Biophys. Acta* **1995**, *1231*, 223–246.

[42] J.-L. Rigaud, D. Lévy, Reconstitution of membrane proteins into liposomes, *Meth. Enzymol.* **2003**, *372*, 65–86.

[43] M. Urban, A. Kleefen, N. Mukherjee, P. Seelheim, B. Windschiegl, M. Vor der Bruggen, A. Kocer, R. Tampe, Highly parallel transport recordings on a membrane-on-nanopore chip at single molecule resolution, *Nano Lett.* **2014**, *14*, 1674–1680.

[44] H. Wang, T.-S. Chung, Y. W. Tong, K. Jeyaseelan, A. Armugam, Z. Chen, M. Hong, W. Meier, Highly permeable and selective pore-spanning biomimetic membrane embedded with aquaporin Z, *Small* **2012**, *8*, 1185-90, 1125.

[45] I. Mey, C. Steinem, A. Janshoff, Biomimetic functionalization of porous substrates: towards model systems for cellular membranes, *J. Mater. Chem.* **2012**, *22*, 19348.

[46] G. D. Eytan, Use of liposomes for reconstitution of biological functions, *Biochim. Biophys. Acta* **1982**, *694*, 185–202.

[47] D. Lévy, A. Bluzat, M. Seigneuret, J.-L. Rigaud, A systematic study of liposome and proteoliposome reconstitution involving Bio-Bead-mediated Triton X-100 removal, *Biochim. Biophys. Acta* **1990**, *1025*, 179–190.

[48] M. M. Parmar, K. Edwards, T. D. Madden, Incorporation of bacterial membrane proteins into liposomes: factors influencing protein reconstitution, *Biochim. Biophys. Acta* **1999**, *1421*, 77–90.

[49] W. J. de Grip, J. van Oostrum, P. H. Bovee-Geurts, Selective detergent-extraction from mixed detergent/lipid/protein micelles, using cyclodextrin inclusion compounds: a novel generic approach for the preparation of proteoliposomes, *Biochem. J.* **1998**, *330*, 667–674.

[50] M. Dezi, A. Di Cicco, P. Bassereau, D. Lévy, Detergent-mediated incorporation of transmembrane proteins in giant unilamellar vesicles with controlled physiological contents, *Proc. Natl. Acad. Sci. USA* **2013**, *110*, 7276–7281.

[51] M. I. Angelova, D. S. Dimitrov, Liposome electroformation, *Faraday Discuss. Chem. Soc.* **1986**, *81*, 303.

[52] M. Kocun, T. D. Lazzara, C. Steinem, A. Janshoff, Preparation of solvent-free, pore-spanning lipid bilayers: modeling the low tension of plasma membranes, *Langmuir* **2011**, *27*, 7672–7680.

[53] P. Girard, J. Pecreaux, G. Lenoir, P. Falson, J.-L. Rigaud, P. Bassereau, A new method for the reconstitution of membrane proteins into giant unilamellar vesicles, *Biophys. J.* **2004**, *87*, 419–429.

[54] K. Bacia, C. G. Schuette, N. Kahya, R. Jahn, P. Schwille, SNAREs prefer liquid-disordered over "raft" (liquid-ordered) domains when reconstituted into giant unilamellar vesicles, *J. Biol. Chem.* **2004**, *279*, 37951–37955.

[55] M. Kreir, C. Farre, M. Beckler, M. George, N. Fertig, Rapid screening of membrane protein activity: electrophysiological analysis of OmpF reconstituted in proteoliposomes, *Lab Chip* **2008**, *8*, 587–595.

[56] A. R. Battle, E. Petrov, P. Pal, B. Martinac, Rapid and improved reconstitution of bacterial mechanosensitive ion channel proteins MscS and MscL into liposomes using a modified sucrose method, *FEBS Lett.* **2009**, *583*, 407–412.

[57] C. Carnarius, M. Kreir, M. Krick, C. Methfessel, V. Moehrle, O. Valerius, A. Bruggemann, C. Steinem, N. Fertig, Green fluorescent protein changes the conductance of connexin 43 (Cx43) hemichannels reconstituted in planar lipid bilayers, *J. Biol. Chem.* **2012**, *287*, 2877–2886.

[58] N. Kahya, E.-I. Pécheur, W. P. de Boeij, D. A. Wiersma, D. Hoekstra, Reconstitution of membrane proteins into giant unilamellar vesicles via peptide-induced fusion, *Biophys. J.* **2001**, *81*, 1464–1474.

[59] O. Biner, T. Schick, Y. Muller, C. von Ballmoos, Delivery of membrane proteins into small and giant unilamellar vesicles by charge-mediated fusion, *FEBS Lett.* **2016**, *590*, 2051–2062.

[60] R. R. Ishmukhametov, A. N. Russell, R. M. Berry, A modular platform for one-step assembly of multi-component membrane systems by fusion of charged proteoliposomes, *Nat. Commun.* **2016**, *7*, 13025.

[61] D. Tareste, J. Shen, T. J. Melia, J. E. Rothman, SNAREpin/Munc18 promotes adhesion and fusion of large vesicles to giant membranes, *Proc. Natl. Acad. Sci. USA* **2008**, *105*, 2380–2385.

[62] L. V. Chernomordik, M. M. Kozlov, Mechanics of membrane fusion, *Nat. Struct. Mol. Biol.* **2008**, *15*, 675–683.

[63] C. Etzold, G. Deckers-Hebestreit, K. Altendorf, Turnover number of *Escherichia coli* F_0F_1 ATP synthase for ATP synthesis in membrane vesicles, *Eur. J. Biochem.* **1997**, *243*, 336–343.

[64] T. Suzuki, T. Murakami, R. Iino, J. Suzuki, S. Ono, Y. Shirakihara, M. Yoshida, F_0F_1-ATPase/synthase is geared to the synthesis mode by conformational rearrangement of ε-subunit in response to proton motive force and ADP/ATP balance, *J. Biol. Chem.* **2003**, *278*, 46840–46846.

[65] N. Mitome, Thermophilic ATP synthase has a decamer *c*-ring: Indication of noninteger 10:3 H^+/ATP ratio and permissive elastic coupling, *Proc. Natl. Acad. Sci. USA* **2004**, *101*, 12159–12164.

[66] N. Soga, R. Watanabe, H. Noji, Attolitre-sized lipid bilayer chamber array for rapid detection of single transporters, *Sci. Rep.* **2015**, *5*, 11025.

[67] T. H. Haines, Do sterols reduce proton and sodium leaks through lipid bilayers?, *Prog. Lipid Res.* **2001**, *40*, 299–324.

[68] S. Paula, A. G. Volkov, A. N. van Hoek, T. H. Haines, D. W. Deamer, Permeation of protons, potassium ions, and small polar molecules through phospholipid bilayers as a function of membrane thickness, *Biophys. J.* **1996**, *70*, 339–348.

[69] S. Aimon, J. Manzi, D. Schmidt, J. A. Poveda Larrosa, P. Bassereau, G. E. S. Toombes, Functional reconstitution of a voltage-gated potassium channel in giant unilamellar vesicles, *PLoS One* **2011**, *6*, e25529.

[70] N. R. Clement, J. M. Gould, Pyranine (8-hydroxy-1,3,6-pyrenetrisulfonate) as a probe of internal aqueous hydrogen ion concentration in phospholipid vesicles, *Biochemistry* **1981**, *20*, 1534–1538.

[71] M. Thelen, G. Petrone, P. S. O'Shea, A. Azzi, The use of fluorescein-dipalmitoylphosphatidylethanolamine for measuring pH-changes in the internal compartment of phospholipid vesicles, *Biochim. Biophys. Acta* **1984**, *766*, 161–168.

[72] R. Casadio, Measurements of transmembrane pH differences of low extents in bacterial chromatophores, *Eur. Biophys. J.* **1991**, *19*.

[73] A. L. Christensen, C. Lohr, S. M. Christensen, D. Stamou, Single vesicle biochips for ultra-miniaturized nanoscale fluidics and single molecule bioscience, *Lab. Chip* **2013**, *13*, 3613–3625.

[74] D. Frese, S. Steltenkamp, S. Schmitz, C. Steinem, In situ generation of electrochemical gradients across pore-spanning membranes, *RSC Adv.* **2013**, *3*, 15752.

[75] L. L. G. Schwenen, R. Hubrich, D. Milovanovic, B. Geil, J. Yang, A. Kros, R. Jahn, C. Steinem, Resolving single membrane fusion events on planar pore-spanning membranes, *Sci. Rep.* **2015**, *5*, 12006.

[76] M. Fuhrmans, M. Muller, Mechanisms of vesicle spreading on surfaces: Coarse-grained simulations, *Langmuir* **2013**, *29*, 4335–4349.

[77] G. E. Lyman, J. P. DeVincenzo, Determination of picogram amounts of ATP using the luciferin-luciferase enzyme system, *Anal. Biochem.* **1967**, *21*, 435–443.

[78] R. Watanabe, N. Soga, D. Fujita, K. V. Tabata, L. Yamauchi, S. Hyeon Kim, D. Asanuma, M. Kamiya, Y. Urano, H. Suga, H. Noji, Arrayed lipid bilayer chambers allow single-molecule analysis of membrane transporter activity, *Nat. Commun.* **2014**, *5*, 4519.

[79] S. Turkyilmaz, W.-H. Chen, H. Mitomo, S. L. Regen, Loosening and reorganization of fluid phospholipid bilayers by chloroform, *J. Am. Chem. Soc.* **2009**, *131*, 5068–5069.

[80] R. Reigada, F. Sagues, Chloroform alters interleaflet coupling in lipid bilayers: an entropic mechanism, *J. R. Soc. Interface* **2015**, *12*.

[81] R. Fettiplace, D. M. Andrews, D. A. Haydon, The thickness, composition and structure of some lipid bilayers and natural membranes, *J. Membr. Biol.* **1971**, *5*, 277–296.

[82] I. Mey, M. Stephan, E. K. Schmitt, M. M. Muller, M. Ben Amar, C. Steinem, A. Janshoff, Local membrane mechanics of pore-spanning bilayers, *J. Am. Chem. Soc.* **2009**, *131*, 7031–7039.

[83] G. Cevc, H. Richardsen, Lipid vesicles and membrane fusion, *Adv. Drug Deliv. Rev.* **1999**, *38*, 207–232.

[84] T. Suzuki, H. Ueno, N. Mitome, J. Suzuki, M. Yoshida, F_0 of ATP synthase is a rotary proton channel. Obligatory coupling of proton translocation with rotation of *c*-subunit ring, *J. Biol. Chem.* **2002**, *277*, 13281–13285.

[85] S. Schenck, S. M. Wojcik, N. Brose, S. Takamori, A chloride conductance in VGLUT1 underlies maximal glutamate loading into synaptic vesicles, *Nat. Neurosci.* **2009**, *12*, 156–162.

[86] P. K. Smith, R. I. Krohn, G. T. Hermanson, A. K. Mallia, F. H. Gartner, M. D. Provenzano, E. K. Fujimoto, N. M. Goeke, B. J. Olson, D. C. Klenk, Measurement of protein using bicinchoninic acid, *Anal. Biochem.* **1985**, *150*, 76–85.

[87] K. J. Wiechelman, R. D. Braun, J. D. Fitzpatrick, Investigation of the bicinchoninic acid protein assay: identification of the groups responsible for color formation, *Anal. Biochem.* **1988**, *175*, 231–237.

[88] U. K. Laemmli, Cleavage of structural proteins during the assembly of the head of bacteriophage T4, *Nature* **1970**, *227*, 680–685.

[89] A.-M. Lawrence, H. U. S. Besir, Staining of proteins in gels with Coomassie G-250 without organic solvent and acetic acid, *J. Vis. Exp.* **2009**.

[90] S. Takamori, M. Holt, K. Stenius, E. A. Lemke, M. Gronborg, D. Riedel, H. Urlaub, S. Schenck, B. Brugger, P. Ringler, S. A. Muller, B. Rammner, F. Grater, J. S. Hub, B. L. de Groot et al., Molecular anatomy of a trafficking organelle, *Cell* **2006**, *127*, 831–846.

[91] D. Linke, Detergents: an overview, *Meth. Enzymol.* **2009**, *463*, 603–617.

[92] N. A. Clark, J. H. Lunacek, G. B. Benedek, A study of brownian motion using light scattering, *Am. J. Phys.* **1970**, *38*, 575–585.

[93] F. R. Hallett, J. Watton, P. Krygsman, Vesicle sizing, *Biophys. J.* **1991**, *59*, 357–362.

[94] A. J. Jin, D. Huster, K. Gawrisch, R. Nossal, Light scattering characterization of extruded lipid vesicles, *Eur. Biophys. J.* **1999**, *28*, 187–199.

[95] D. Rickwood, T. Ford, J. Graham, Nycodenz: A new nonionic iodinated gradient medium, *Anal. Biochem.* **1982**, *123*, 23–31.

[96] G. Rouser, S. Fleischer, A. Yamamoto, Two dimensional thin layer chromatographic separation of polar lipids and determination of phospholipids by phosphorus analysis of spots, *Lipids* **1970**, *5*, 494–496.

[97] J. R. Lakowicz, *Principles of Fluorescence Spectroscopy*, Springer, New York, **2006**.

[98] P. J. Walla, *Modern Biophysical Chemistry*. *Detection and Analysis of Biomolecules*, Wiley-VCH, Weinheim, Germany, **2014**.

[99] J. W. Lichtman, J.-A. Conchello, Fluorescence microscopy, *Nat. Methods* **2005**, *2*, 910–919.

[100] A. Marty, M. Bourdeaux, M. Dell'Amico, P. Viallet, 9-amino-2-methoxy-6-chloroacridine monocation fluorescence analysis by phase-modulation fluorometry, *Eur. Biophys. J.* **1986**, *13*.

[101] J. S. Sun, M. Rougee, M. Delarue, T. Montenay-Garestier, C. Helene, Solvent relaxation around excited 2-methoxy-6-chloro-9-aminoacridine in aqueous solvents, *J. Phys. Chem.* **1990**, *94*, 968–977.

[102] A. Orte, L. Crovetto, E. M. Talavera, N. Boens, J. M. Alvarez-Pez, Absorption and emission study of 2',7'-difluorofluorescein and its excited-state buffer-mediated proton exchange reactions, *J. Phys. Chem. A* **2005**, *109*, 734–747.

[103] A. Orte, E. M. Talavera, A. L. Macanita, J. C. Orte, J. M. Alvarez-Pez, Three-state 2',7'-difluorofluorescein excited-state proton transfer reactions in moderately acidic and very acidic media, *J. Phys. Chem. A* **2005**, *109*, 8705–8718.

[104] T. Sanden, L. Salomonsson, P. Brzezinski, J. Widengren, Surface-coupled proton exchange of a membrane-bound proton acceptor, *Proc. Natl. Acad. Sci. USA* **2010**, *107*, 4129–4134.

[105] Y. Avnir, Y. Barenholz, pH determination by pyranine: medium-related artifacts and their correction, *Anal. Biochem.* **2005**, *347*, 34–41.

[106] R. I. MacDonald, Characteristics of self-quenching of the fluorescence of lipid-conjugated rhodamine in membranes, *J. Biol. Chem.* **1990**, *265*, 13533–13539.

[107] R. S. Brown, J. D. Brennan, U. J. Krull, Self-quenching of nitrobenzoxadiazole labeled phospholipids in lipid membranes, *J. Chem. Phys.* **1994**, *100*, 6019.

[108] G. Pähler, *PhD Thesis*, Georg-August-University, Göttingen, **2012**.

[109] D. J. Stephens, V. J. Allan, Light microscopy techniques for live cell imaging, *Science* **2003**, *300*, 82–86.

[110] J.-A. Conchello, J. W. Lichtman, Optical sectioning microscopy, *Nat. Methods* **2005**, *2*, 920–931.

[111] D. K. Toomre, M. F. Langhorst, M. W. Davidson, Introduction to spinning disk microscopy, can be found under http://zeiss-campus.magnet.fsu.edu/articles/spinningdisk/introduction.html, 2017/02/15.

[112] J. Piehler, A. Brecht, R. Valiokas, B. Liedberg, G. Gauglitz, A high-density poly(ethylene glycol) polymer brush for immobilization on glass-type surfaces, *Biosens. Bioelectron.* **2000**, *15*, 473–481.

[113] Q. Tseng, I. Wang, E. Duchemin-Pelletier, A. Azioune, N. Carpi, J. Gao, O. Filhol, M. Piel, M. Thery, M. Balland, A new micropatterning method of soft substrates reveals that different tumorigenic signals can promote or reduce cell contraction levels, *Lab. Chip* **2011**, *11*, 2231–2240.

[114] W. Junge, H. Sielaff, S. Engelbrecht, Torque generation and elastic power transmission in the rotary F_0F_1-ATPase, *Nature* **2009**, *459*, 364–370.

[115] H. Ueno, T. Suzuki, K. Kinosita Jr, M. Yoshida, ATP-driven stepwise rotation of F_0F_1-ATP synthase, *Proc. Natl. Acad. Sci. USA* **2005**, *102*, 1333–1338.

[116] T. Suzuki, C. Wakabayashi, K. Tanaka, B. A. Feniouk, M. Yoshida, Modulation of nucleotide specificity of thermophilic F_0F_1-ATP Synthase by ε-subunit, *J. Biol. Chem.* **2011**, *286*, 16807–16813.

[117] N. Soga, K. Kinosita Jr, M. Yoshida, T. Suzuki, Efficient ATP synthesis by thermophilic *Bacillus* F_0F_1-ATP synthase, *FEBS J.* **2011**, *278*, 2647–2654.

[118] J. Preobraschenski, *PhD Thesis*, Georg-August-Universität, Göttingen, **2012**.

[119] J. Preobraschenski, J.-F. Zander, T. Suzuki, G. Ahnert-Hilger, R. Jahn, Vesicular glutamate transporters use flexible anion and cation binding sites for efficient accumulation of neurotransmitter, *Neuron* **2014**, *84*, 1287–1301.

[120] M. Le Maire, P. Champeil, J. V. Møller, Interaction of membrane proteins and lipids with solubilizing detergents, *Biochim. Biophys. Acta* **2000**, *1508*, 86–111.

[121] A. M. Seddon, P. Curnow, P. J. Booth, Membrane proteins, lipids and detergents: not just a soap opera, *Biochim. Biophys. Acta* **2004**, *1666*, 105–117.

[122] M. Tutus, F. F. Rossetti, E. Schneck, G. Fragneto, F. Förster, R. Richter, T. Nawroth, M. Tanaka, Orientation-selective incorporation of transmembrane F_0F_1 ATP synthase complex from *Micrococcus luteus* in polymer-supported membranes, *Macromol. Biosci.* **2008**, *8*, 1034–1043.

[123] M. Schwamborn, J. Schumacher, J. Sibold, N. K. Teiwes, C. Steinem, Monitoring ATPase induced pH changes in single proteoliposomes with the lipid-coupled fluorophore Oregon Green 488, *Analyst* **2017**.

[124] H. Rottenberg, R. Moreno-Sanchez, The proton pumping activity of H^+-ATPases: an improved fluorescence assay, *Biochim. Biophys. Acta* **1993**, *1183*, 161–170.

[125] V. Fregni, R. Casadio, Kinetic characterization of the ATP-dependent proton pump in bacterial photosynthetic membranes: a study with the fluorescent probe 9-amino-6-chloro-2-methoxyacridine, *Biochim. Biophys. Acta* **1993**, *1143*, 215–222.

[126] J. Han, K. Burgess, Fluorescent indicators for intracellular pH, *Chem. Rev.* **2010**, *110*, 2709–2728.

[127] M. D'Alessandro, P. Turina, B. A. Melandri, Quantitative evaluation of the intrinsic uncoupling modulated by ADP and Pi in the reconstituted ATP synthase of Escherichia coli, *Biochim. Biophys. Acta* **2011**, *1807*, 130–143.

[128] N. Mitome, S. Ono, H. Sato, T. Suzuki, N. Sone, M. Yoshida, Essential arginine residue of the F_0-*a* subunit in F_0F_1-ATP synthase has a role to prevent the proton shortcut without *c*-ring rotation in the F_0 proton channel, *Biochem. J.* **2010**, *430*, 171–177.

[129] P. Fan, T. Haerd, D. R. Kearns, Origin of the complex fluorescence emission of 9-amino-6-chloro-2-methoxyacridine. 1. Experiment, *J. Phys. Chem.* **1989**, *93*, 6615–6622.

[130] T. Kätterer, M. Reichstein, O. Andrén, A. Lomander, Temperature dependence of organic matter decomposition: a critical review using literature data analyzed with different models, *Biol. Fertil. Soils* **1998**, *27*, 258–262.

[131] G. C. Kemmer, S. A. Bogh, M. Urban, M. G. Palmgren, T. Vosch, J. Schiller, T. Gunther Pomorski, Lipid-conjugated fluorescent pH sensors for monitoring pH changes in reconstituted membrane systems, *Analyst* **2015**, *140*, 6313–6320.

[132] M. T. Z. Spence, I. D. Johnson, *The molecular probes handbook. A guide to fluorescent probes and labeling technologies*, Life Technologies Corporation, Carlsbad, California, **2010**.

[133] S. Kölchens, V. Ramaswami, J. Birgenheier, L. Nett, D. F. O'Brien, Quasi-elastic light scattering determination of the size distribution of extruded vesicles, *Chem. Phys. Lipids* **1993**, *65*, 1–10.

[134] J. Gallova, D. Uhrikova, A. Islamov, A. Kuklin, P. Balgavy, Effect of cholesterol on the bilayer thickness in unilamellar extruded DLPC and DOPC liposomes: SANS contrast variation study, *Gen. Physiol. Biophys.* **2004**, *23*, 113–128.

[135] M. Alwarawrah, J. Dai, J. Huang, A molecular view of the cholesterol condensing effect in DOPC lipid bilayers, *J. Phys. Chem. B* **2010**, *114*, 7516–7523.

[136] M. W. Bowler, M. G. Montgomery, A. G. W. Leslie, J. E. Walker, How azide inhibits ATP hydrolysis by the F-ATPases, *Proc. Natl. Acad. Sci. USA* **2006**, *103*, 8646–8649.

[137] R. Jahn, D. Fasshauer, Molecular machines governing exocytosis of synaptic vesicles, *Nature* **2012**, *490*, 201–207.

[138] J. M. Hernandez, A. Stein, E. Behrmann, D. Riedel, A. Cypionka, Z. Farsi, P. J. Walla, S. Raunser, R. Jahn, Membrane fusion intermediates via directional and full assembly of the SNARE complex, *Science* **2012**, *336*, 1581–1584.

[139] S. Kreye, J. Malsam, T. H. Sollner, In vitro assays to measure SNARE-mediated vesicle fusion, *Methods Mol. Biol.* **2008**, *440*, 37–50.

[140] J. Chang, S.-A. Kim, X. Lu, Z. Su, S. K. Kim, Y.-K. Shin, Fusion step-specific influence of cholesterol on SNARE-mediated membrane fusion, *Biophys. J.* **2009**, *96*, 1839–1846.

[141] G. van den Bogaart, M. G. Holt, G. Bunt, D. Riedel, F. S. Wouters, R. Jahn, One SNARE complex is sufficient for membrane fusion, *Nat. Struct. Mol. Biol.* **2010**, *17*, 358–364.

[142] T.-Y. Yoon, B. Okumus, F. Zhang, Y.-K. Shin, T. Ha, Multiple intermediates in SNARE-induced membrane fusion, *Proc. Natl. Acad. Sci. USA* **2006**, *103*, 19731–19736.

[143] J. Diao, Z. Su, Y. Ishitsuka, B. Lu, K. S. Lee, Y. Lai, Y.-K. Shin, T. Ha, A single-vesicle content mixing assay for SNARE-mediated membrane fusion, *Nat. Commun.* **2010**, *1*, 54.

[144] M. Kyoung, A. Srivastava, Y. Zhang, J. Diao, M. Vrljic, P. Grob, E. Nogales, S. Chu, A. T. Brunger, In vitro system capable of differentiating fast Ca^{2+}-triggered content mixing from lipid exchange for mechanistic studies of neurotransmitter release, *Proc. Natl. Acad. Sci. USA* **2011**, *108*, E304-13.

[145] J. Diao, Y. Ishitsuka, H. Lee, C. Joo, Z. Su, S. Syed, Y.-K. Shin, T.-Y. Yoon, T. Ha, A single vesicle-vesicle fusion assay for in vitro studies of SNAREs and accessory proteins, *Nat. Protoc.* **2012**, *7*, 921–934.

[146] M. Kyoung, Y. Zhang, J. Diao, S. Chu, A. T. Brunger, Studying calcium-triggered vesicle fusion in a single vesicle-vesicle content and lipid-mixing system, *Nat. Protoc.* **2013**, *8*, 1–16.

[147] J. Diao, D. J. Cipriano, M. Zhao, Y. Zhang, S. Shah, M. S. Padolina, R. A. Pfuetzner, A. T. Brunger, Complexin-1 enhances the on-rate of vesicle docking via simultaneous SNARE and membrane interactions, *J. Am. Chem. Soc.* **2013**, *135*, 15274–15277.

[148] H. Sasaki, R. Kawano, T. Osaki, K. Kamiya, S. Takeuchi, Single-vesicle estimation of ATP-binding cassette transporters in microfluidic channels, *Lab. Chip* **2012**, *12*, 702–704.

[149] J. Larsen, N. S. Hatzakis, D. Stamou, Observation of inhomogeneity in the lipid composition of individual nanoscale liposomes, *J. Am. Chem. Soc.* **2011**, *133*, 10685–10687.

[150] Z. Farsi, J. Preobraschenski, G. van den Bogaart, D. Riedel, R. Jahn, A. Woehler, Single-vesicle imaging reveals different transport mechanisms between glutamatergic and GABAergic vesicles, *Science* **2016**, *351*, 981–984.

[151] S. Mathiasen, S. M. Christensen, J. J. Fung, S. G. F. Rasmussen, J. F. Fay, S. K. Jorgensen, S. Veshaguri, D. L. Farrens, M. Kiskowski, B. Kobilka, D. Stamou, Nanoscale high-content analysis using compositional heterogeneities of single proteoliposomes, *Nat. Methods* **2014**, *11*, 931–934.

[152] C. Cremer, Lichtmikroskopie unterhalb des Abbe-Limits. Lokalisationsmikroskopie, *Phys. Unserer Zeit* **2011**, *42*, 21–29.

[153] Y. Hiller, J. M. Gershoni, E. A. Bayer, M. Wilchek, Biotin binding to avidin. Oligosaccharide side chain not required for ligand association, *Biochem. J.* **1987**, *248*, 167–171.

[154] T. T. Nguyen, K. L. Sly, J. C. Conboy, Comparison of the energetics of avidin, streptavidin, NeutrAvidin, and anti-biotin antibody binding to biotinylated lipid bilayer examined by second-harmonic generation, *Anal. Chem.* **2012**, *84*, 201–208.

[155] P. V. Ganesan, S. G. Boxer, A membrane interferometer, *Proc. Natl. Acad. Sci. USA* **2009**, *106*, 5627–5632.

[156] J. S. Hansen, M. Perry, J. Vogel, J. S. Groth, T. Vissing, M. S. Larsen, O. Geschke, J. Emneus, H. Bohr, C. H. Nielsen, Large scale biomimetic membrane arrays, *Anal. Bioanal. Chem.* **2009**, *395*, 719–727.

[157] B. Le Pioufle, H. Suzuki, K. V. Tabata, H. Noji, S. Takeuchi, Lipid bilayer microarray for parallel recording of transmembrane ion currents, *Anal. Chem.* **2008**, *80*, 328–332.

[158] A. Kleefen, D. Pedone, C. Grunwald, R. Wei, M. Firnkes, G. Abstreiter, U. Rant, R. Tampe, Multiplexed parallel single transport recordings on nanopore arrays, *Nano Lett.* **2010**, *10*, 5080–5087.

[159] F. Baneyx, Recombinant protein expression in *Escherichia coli*, *Curr. Opin. Biotechnol.* **1999**, *10*, 411–421.

[160] D. J. Klionsky, W. S. Brusilow, R. D. Simoni, *In vivo* evidence for the role of the ε subunit as an inhibitor of the proton-translocating ATPase of *Escherichia coli*, *J. Bacteriol.* **1984**, *160*, 1055–1060.

[161] N. Soga, K. Kinosita Jr, M. Yoshida, T. Suzuki, Kinetic equivalence of transmembrane pH and electrical potential differences in ATP synthesis, *J. Biol. Chem.* **2012**, *287*, 9633–9639.

[162] S. Fiedler, J. Broecker, S. Keller, Protein folding in membranes, *Cell. Mol. Life Sci.* **2010**, *67*, 1779–1798.

[163] L. Wang, L. Tonggu, Membrane protein reconstitution for functional and structural studies, *Sci. China. Life Sci.* **2015**, *58*, 66–74.

[164] M. Ollivon, S. Lesieur, C. Grabielle-Madelmont, M. Paternostre, Vesicle reconstitution from lipid–detergent mixed micelles, *Biochim. Biophys. Acta* **2000**, *1508*, 34–50.

[165] P. Simeonov, S. Werner, C. Haupt, M. Tanabe, K. Bacia, Membrane protein reconstitution into liposomes guided by dual-color fluorescence cross-correlation spectroscopy, *Biophys. Chem.* **2013**, *184*, 37–43.

[166] N. Jahnke, O. O. Krylova, T. Hoomann, C. Vargas, S. Fiedler, P. Pohl, S. Keller, Real-time monitoring of membrane-protein reconstitution by isothermal titration calorimetry, *Anal. Chem.* **2014**, *86*, 920–927.

[167] M. Nič, J. Jirát, B. Košata, A. Jenkins, A. McNaught (Eds.) *IUPAC. Compendium of Chemical Terminology, 2nd ed. (the "Gold Book")*, Blackwell Scientific Publications, Oxford, **1997**.

[168] D. Lévy, A. Gulik, A. Bluzat, J.-L. Rigaud, Reconstitution of the sarcoplasmic reticulum Ca^{2+}-ATPase: mechanisms of membrane protein insertion into liposomes during reconstitution procedures involving the use of detergents, *Biochim. Biophys. Acta* **1992**, *1107*, 283–298.

[169] M. G. Palmgren, Acridine orange as a probe for measuring pH gradients across membranes: mechanism and limitations, *Anal. Biochem.* **1991**, *192*, 316–321.

[170] M. Rossignol, P. Thomas, C. Grignon, M. Rossignol, P. Thomas, C. Grignon, Proton permeability of liposomes from natural phospholipid mixtures, *Biochim. Biophys. Acta* **1982**, *684*, 195–199.

[171] H. H. Daron, Fatty acid composition of lipid extracts of a thermophilic *Bacillus* species, *J. Bacteriol.* **1970**, *101*, 145–151.

[172] Y. Koga, Thermal adaptation of the archaeal and bacterial lipid membranes, *Archaea* **2012**, *2012*, 789652.

[173] J. L. van de Vossenberg, A. J. M. Driessen, W. N. Konings, The essence of being extremophilic: the role of the unique archaeal membrane lipids, *Extremophiles* **1998**, *2*, 163–170.

[174] T. Leiding, K. Gorecki, T. Kjellman, S. A. Vinogradov, C. Hagerhall, S. P. Arskold, Precise detection of pH inside large unilamellar vesicles using membrane-impermeable dendritic porphyrin-based nanoprobes, *Anal. Biochem.* **2009**, *388*, 296–305.

[175] A. Azzi, M. Muller, P. O'Shea, M. Thelen, Molecular properties of reconstituted cytochrome c oxidase: new evidence supports vectorial proton translocation, *J. Inorg. Biochem.* **1985**, *23*, 341–347.

[176] H. Jung, A. D. Robison, P. S. Cremer, Detecting protein-ligand binding on supported bilayers by local pH modulation, *J. Am. Chem. Soc.* **2009**, *131*, 1006–1014.

[177] A. D. Robison, D. Huang, H. Jung, P. S. Cremer, Fluorescence modulation sensing of positively and negatively charged proteins on lipid bilayers, *Biointerphases* **2013**, *8*, 1.

[178] A. J. B. Kreutzberger, V. Kiessling, L. K. Tamm, High cholesterol obviates a prolonged hemifusion intermediate in fast SNARE-mediated membrane fusion, *Biophys. J.* **2015**, *109*, 319–329.

[179] G. Nordlund, P. Brzezinski, C. von Ballmoos, SNARE-fusion mediated insertion of membrane proteins into native and artificial membranes, *Nat. Commun.* **2014**, *5*, 4303.

[180] C. G. Schuette, K. Hatsuzawa, M. Margittai, A. Stein, D. Riedel, P. Kuster, M. Konig, C. Seidel, R. Jahn, Determinants of liposome fusion mediated by synaptic SNARE proteins, *Proc. Natl. Acad. Sci. USA* **2004**, *101*, 2858–2863.

[181] A. V. Pobbati, A. Stein, D. Fasshauer, N- to C-terminal SNARE complex assembly promotes rapid membrane fusion, *Science* **2006**, *313*, 673–676.

[182] H. Chen, S. S. Ahsan, M. B. Santiago-Berrios, H. D. Abruna, W. W. Webb, Mechanisms of quenching of Alexa fluorophores by natural amino acids, *J. Am. Chem. Soc.* **2010**, *132*, 7244–7245.

[183] ThermoFisher Scientific, Fluorescence SpectraViewer, can be found under https://www.thermofisher.com/de/de/home/life-science/cell-analysis/labeling-chemistry/fluorescence-spectraviewer.html, 2016/12/12.

[184] M. Schiffer, C.-H. Chang, F. J. Stevens, The function of tryptophan residues in membrane proteins, *Protein Eng. Des. Sel.* **1992**, *5*, 213–214.

[185] X. Chen, D. Arac, T.-M. Wang, C. J. Gilpin, J. Zimmerberg, J. Rizo, SNARE-mediated lipid mixing depends on the physical state of the vesicles, *Biophys. J.* **2006**, *90*, 2062–2074.

[186] S. Veshaguri, S. M. Christensen, G. C. Kemmer, G. Ghale, M. P. Møller, C. Lohr, A. L. Christensen, B. H. Justesen, I. L. Jørgensen, J. Schiller, N. S. Hatzakis, M. Grabe, T. G. Pomorski, D. Stamou, Direct observation of proton pumping by a eukaryotic P-type ATPase, *Science* **2016**, *351*, 1469–1473.

[187] E. Racker, W. Stoeckenius, Reconstitution of purple membrane vesicles catalyzing light-driven proton uptake and adenosine triphosphate formation, *J. Biol. Chem.* **1974**, *249*, 662–663.

[188] H.-J. Freisleben, K. Zwicker, P. Jezek, G. John, A. Bettin-Bogutzki, K. Ring, T. Nawroth, Reconstitution of bacteriorhodopsin and ATP synthase from *Micrococcus*

luteus into liposomes of the purified main tetraether lipid from *Thermoplasma acidophilum*: proton conductance and light-driven ATP synthesis, *Chem. Phys. Lipids* **1995**, *78*, 137–147.

[189] S. Matuschka, K. Zwicker, T. Nawroth, G. Zimmer, ATP synthesis by purified ATP-synthase from beef heart mitochondria after coreconstitution with bacteriorhodopsin, *Arch. Biochem. Biophys.* **1995**, *322*, 135–142.

[190] P. Richard, B. Pitard, J.-L. Rigaud, ATP synthesis by the F_0F_1-ATPase from the thermophilic *Bacillus* PS3 co-reconstituted with bacteriorhodopsin into liposomes, *J. Biol. Chem.* **1995**, *270*, 21571–21578.

[191] A. Wach, N. A. Dencher, P. Gräber, Co-reconstitution of plasma membrane H^+-ATPase from yeast and bacteriorhodopsin into liposomes. ATP hydrolysis as a function of external and internal pH, *Eur. J. Biochem.* **1993**, *214*, 563–568.

[192] B. Deisinger, T. Nawroth, K. Zwicker, S. Matuschka, G. John, G. Zimmer, H.-J. Freisleben, Purification of ATP synthase from beef heart mitochondria (F_0F_1) and co-reconstitution with monomeric bacteriorhodopsin into liposomes capable of light-driven ATP synthesis, *Eur. J. Biochem.* **1993**, *218*, 377–383.

[193] A. W. Scotto, D. Zakim, Reconstitution of membrane proteins. Spontaneous incorporation of integral membrane proteins into preformed bilayers of pure phospholipid, *J. Biol. Chem.* **1988**, *263*, 18500–18506.

[194] C. von Ballmoos, O. Biner, T. Nilsson, P. Brzezinski, Mimicking respiratory phosphorylation using purified enzymes, *Biochim. Biophys. Acta* **2016**, *1857*, 321–331.

[195] T. Nilsson, C. R. Lundin, G. Nordlund, P. Adelroth, C. von Ballmoos, P. Brzezinski, Lipid-mediated protein-protein interactions modulate respiration-driven ATP synthesis, *Sci. Rep.* **2016**, *6*, 24113.

[196] G. A. Kimmich, J. Randles, J. S. Brand, Assay of picomole amounts of ATP, ADP, and AMP using the luciferase enzyme system, *Anal. Biochem.* **1975**, *69*, 187–206.

[197] S. M. Christensen, D. Stamou, Surface-based lipid vesicle reactor systemsFabrication and applications, *Soft Matter* **2007**, *3*, 828.

[198] S. M. Christensen, D. Stamou, Sensing-applications of surface-based single vesicle arrays, *Sensors* **2010**, *10*, 11352–11368.

[199] P. M. Bendix, M. S. Pedersen, D. Stamou, Quantification of nano-scale intermembrane contact areas by using fluorescence resonance energy transfer, *Proc. Natl. Acad. Sci. USA* **2009**, *106*, 12341–12346.

[200] D. Stamou, C. Duschl, E. Delamarche, H. Vogel, Self-assembled microarrays of attoliter molecular vessels, *Angew. Chem. Int. Ed. Engl.* **2003**, *42*, 5580–5583.

[201] J. Diao, P. Grob, D. J. Cipriano, M. Kyoung, Y. Zhang, S. Shah, A. Nguyen, M. S. Padolina, A. Srivastava, M. Vrljic, A. Shah, E. Nogales, S. Chu, A. T. Brunger, Synaptic proteins promote calcium-triggered fast transition from point contact to full fusion, *eLife* **2012**, *1*, e00109.

[202] N. Ehrlich, A. L. Christensen, D. Stamou, Fluorescence anisotropy based single liposome assay to measure molecule-membrane interactions, *Anal. Chem.* **2011**, *83*, 8169–8176.

[203] N. S. Hatzakis, V. K. Bhatia, J. Larsen, K. L. Madsen, P.-Y. Bolinger, A. H. Kunding, J. Castillo, U. Gether, P. Hedegard, D. Stamou, How curved membranes recruit amphipathic helices and protein anchoring motifs, *Nat. Chem. Biol.* **2009**, *5*, 835–841.

[204] CHARMM-GUI Membrane Builder, can be found under http://www.charmm-gui.org/?doc=input/membrane_only&step=1, 2017/04/25.

8 APPENDIX

8.1 List of Figures

Figure 1.1. Overview of proton pumping proteins. 2

Figure 1.2. Schematic overview of antiport by P-type ATPases. 3

Figure 1.3. Structural comparison of different ATPase families. 4

Figure 1.4. (**A**) Structure of *E. coli* ATP synthase obtained from cryo-electron microscopy. (**B**) Scheme of the binding change mechanism of ATP hydrolysis. 6

Figure 1.5. Hydrolysis of adenosine triphosphate. 8

Figure 1.6. The orientation of membrane proteins (blue triangles) retained upon fusion of a small proteoliposomes with GUVs. 12

Figure 1.7. Spreading of a GUV on a porous substrate results in formation of a membrane patch, sealing the pores. 13

Figure 1.8. Scheme of protein orientation in a GUV and the resulting orientation in PSLBs.. 14

Figure 1.9. Depending on the orientation of F_0F_1-ATPase in the pore-spanning lipid bilayer, an acidification or ATP synthesis inside the pores would be achievable. 15

Figure 1.10. Preparation scheme of arrayed lipid bilayer chambers (ALBICs) in a microfluidic device. 16

Figure 3.1. Reaction scheme of the bicinchoninic acid (BCA) assay. 21

Figure 3.2. (**A**) Potential curves for molecules in the electronic ground state S_0 and the electronically excited S1 state. (**B**) The transitions into different vibrational states reflect in the absorption and emission spectra. 31

Figure 3.3. (**A**) Structures of 9-amino-6-chloro-2-methoxyacridine. (**B**) Excitation and emission spectrum of ACMA. 32

Figure 3.4. (**A**) In the physiological pH range the di-anionic Oregon Green 488 is predominant. (**B**) Excitation and emission spectra of Oregon Green 488-DHPE. 33

Figure 3.5. Typical setup of a fluorescence spectrometer. 34

Figure 3.6. Schemes of (**A**) a widefield fluorescence microscope, (**B**) a confocal laser scanning microscope, (**C**) a spinning disk confocal microscope. 37

Figure 3.7. Scheme of the heatable measuring setup. 39

Figure 3.8. Scheme of image series processing with ImageJ. 40

Figure 4.1. Elution profile of TF_0F_1-ATPase. 44

Figure 4.2. SDS-PAGE gel showing the bands of the eight single units of the TF_0F_1-ATPase. 45

Figure 4.3. (**A**) Scheme of Nycodenz density gradient. (**B**) SDS-PAGE gel for analysis of the density gradient centrifugation. 46

Figure 4.4. Calibration curve for quantification of reconstituted ATPase. 47

Figure 4.5. Intensity dependent size distribution of ATPase-liposomes. 48

Figure 4.6. Scheme of the ACMA based ATPase activity assay 50

Figure 4.7. ACMA based activity measurements of ATPase-liposomes. 51

Figure 4.8. Temperature dependence of the TF_0F_1-ATPase proton pumping activity. 52

Figure 4.9. OG488-DHPE emission spectra of LUVs at pH-values of 7.3, 6.3, 5.3 and 4.3. 55

Figure 4.10. pK_a determination of OG488-DHPE. 56

Figure 4.11. OG488-DHPE fluorescence intensity–pH-value calibration curve. 57

Figure 4.12. Calculated outer membrane area fraction as a function of vesicle diameter. 58

Figure 4.13. Scheme of the OG488-DHPE based ATPase activity assay. 59

Figure 4.14. OG488-DHPE acidification assay for TF_0F_1-ATPase vesicles. 60

Figure 4.15. Distribution of mean luminal ΔpH-values obtained in the OG488-DHPE acidification assay. 61

Figure 4.16. Scheme of the combined fusion and acidification assay based on the pH-sensitive, lipid-coupled fluorophore OG488-DHPE. 62

Figure 4.17. (**A**) Quenched and maximum fluorescence emission OG488-DHPE doped vesicles. (**B**) The calibration curve of $F_{\mathrm{max}}/F_{\mathrm{quench}}$ vs. c_{OG488} allows to ascertain c_{OG488} to a measured value of $F_{\mathrm{max}}/F_{\mathrm{quench}}$. 63

Figure 4.18. (**A**) Exemplary dequenching curve from vesicle fusion. (**B**) Fluorescence emission spectra of $F_{\text{quench-start}}$, $F_{\text{quench-end}}$ and F_{max}. 64

Figure 4.19. Quantification of vesicle fusion. 65

Figure 4.20. The functional ATPase reconstitution into the ATPase-ΔN49-LUVs was assured by means of an ACMA assay, before performing the combined fusion and acidification assay. 66

Figure 4.21. Exemplary dequenching curve from fusion of ΔN49-ATPase-LUVs and Sb1-116-LUVs. 67

Figure 4.22. Course of the mean pH-value of the OG488-based acidification assay after fusion of ΔN49-ATPase-LUVs with OG488-DHPE doped Sb1-116-LUVs. 68

Figure 4.23. (**A**) Acidification of ATPase-ΔN49-LUVs. (**B**) Fusion of the ATPase-ΔN49-LUVs with Sb1-116-LUVs. (**C**) No acidification was detectable after fusion with the OG488-DHPE assay. (**D**) ACMA was added to check for ATPase activity in the former fusion mixture and a significant intensity decrease occurred. 69

Figure 4.24. (**A**) Relative changes in fluorescence intensity of ACMA (0.9) upon luminal acidification ATPase-ΔN49-LUVs (black) and ATPase-LUVs (blue). (**B**) Time-resolved mean luminal pH-value of OG488-DHPE fluorescence. 70

Figure 4.25. UV/Vis spectra of OG488-DHPE doped ΔN49-liposomes. 72

Figure 4.26. Normalized absorption and fluorescence emission spectra of liposomes with no ΔN49-complex or nominal lipid/protein ratios of 1:500, 1:1000 or 1:2000. 73

Figure 4.27. Representative images of Texas Red DHPE-doped vesicles, filled with pyranine solution, immobilized on a methoxy-PEG/Biotin-PEG functionalized glass slide via NeutrAvidin-biotin interaction. 75

Figure 4.28. Scheme of ATPase-proteoliposomes attached to a biotin-PEG/methoxy-PEG functionalized glass slide. 76

Figure 4.29. (**A**) Image of the unmounted heatable flow chamber. (**B**) Image of the flow chamber mounted to the microscope's heating stage. 77

Figure 4.30. (**A**) Exemplary normalized intensity courses, original and smoothed, of an acidified and an inactive liposome. (B) Calibration curve obtained from vesicles with acidic lumina in a bulk solution of pH 7.3 for correlation of the normalized intensities to luminal pH-values. 79

Figure 4.31. (**A**) ΔpH time courses calculated from the intensity courses shown in Figure 4.30. (**B**) Averaged ΔpH time courses of active and inactive vesicles obtained from one proteoliposome preparation. 80

Figure 4.32. Overview of the total number of vesicles analyzed with respect to acidification. 81

Figure 5.1. Scheme of the three solubilization stages in protein reconstitution. 86

Figure 5.2. A comparison of the fluorescence intensity-pH correlation curves of pHrodo Red DOPE, of fluorescein-PE and OG488-DHPE. 92

Figure 5.3. Scheme of the membrane embedded full fusion complex and the ΔN49-complex. 96

Figure 5.4. Alexa Fluor 488 and Oregon Green 488 share the same hydrocarbon scaffold (**A**) and have very similar excitation and emission spectra (**B**). 97

Figure 5.5. Crystal structure of the SNARE-fusion complex (PDB ID: 3hd7) (**A**) and cyro-electron microscopic structure of *E. coli* F_0F_1-ATPase (PDB ID: 5t4o) (**B**). 98

8.2 Symbols

$[H^+]$	concentration of protons
c	concentration
F	Faraday constant
F_{max}	maximum fluorescence intensity after vesicle lysis
F_{quench}	fluorescence intensity of self-quenched fluorophore
I_{max}	maximal Intensity
I_{min}	minimal Intensity
I_0	initial intensity
m	mass

n	amount of substance
N	number of particles
$P_{\mathrm{H^+}}$	permeability coefficient for protons
$\mathrm{p}K_\mathrm{a}$	negative decadic logarithm of acid dissociation constant
Q_{10}	temperature coefficient of enzyme activity
R	effective detergent-lipid ratio in detergent containing liposomes or mixed micelles
R	universal gas constant
S_0	electronic singlet ground state
t	time
T	temperature
V	volume
(w/v)	concentration in weight/volume percent
$\Delta\bar{\mu}_{\mathrm{H^+}}$	electrochemical potential
$\Delta\psi$	electric potential
ΔG	Gibbs free energy
Δp	proton motive force
λ_{abs}	absorption wavelength
$\lambda_{\mathrm{em/ex}}$	emission/excitation wavelength
v'' or v'	vibrational state of electronic ground state or first excited electronic state
χ_{fusion}	lipid mixing efficiency

8.3 Abbreviations

ACMA	9-amino-6-chloro-2-methoxyacridine

ADP	Adenosine diphosphate
APS	ammonium peroxosulfate
APTES	(3-aminopropyl)triethoxysilane
ATP	Adenosine triphosphate
ATPase	adenosine triphosphatase
*β*CD	heptakis(2,6-di-*O*-methyl)-*β*-cyclodextrin
BCA	bicinchoninic acid
BSA	bovine serum albumin
CCCP	carbonyl cyanide 3-chlorphenylhydrazone
CHAPS	3-[(3-Cholamidopropyl)dimethylammonio]-1-propanesulfonate
Chol	cholesterol
CLSM	confocal laser scanning microscope / microscopy
cmc	critical micelle concentration
CV	column volume
DDM	*n*-dodecyl-*β*-D-maltoside
DHPE	1,2-dihexadecanoyl-*sn*-glycero-3-phosphoethanolamine
DLS	dynamic light scattering
DMSO	dimethyl sulfoxide
ΔN49-complex	Syntaxin-1A, SNAP25 and synaptobrevin 49-96
DOPC	1,2-dioleoyl-*sn*-glycero-3-phosphocholine
DOPG	1,2-dioleoyl-*sn*-glycero-3-phosphoglycerol
DPPC	1,2-dipalmitoyl-*sn*-glycero-3-phosphocholine
DTT	dithiothreitol
E. Coli	*Escherichia coli*
EDTA	ethylenediaminetetraacetic acid
FRET	Förster resonance energy transfer
GOPTS	3-glycidyloxipropyltrimethoxysilane
GPCRs	G protein-coupled receptors
GUV	giant unilamellar vesicle

HEPES	4-(2-hydroxyethyl)-1-piperazineethanesulfonic acid
His	histidine
HPTS	8-hydroxypyrene-1,3,6-trisulfonic acid, pyranine
IMAC	immobilized metal ion affinity chromatography
IPTG	isopropyl *β*-D-1-thiogalactopyranoside
LUV	large unilamellar vesicle
Met	methionine
MOPS	3-(*N*-morpholino)propanesulfonic acid
NA	numerical aperture
*n*OG	*n*-octyl-*β*-D-glucoside
OD_{600}	optical density at 600 nm
OG488	Oregon Green 488
p/l	protein/lipid ratio
PC	phosphatidylcholine
PE	phosphatidylethanolamine
PEG	polyethylenglycol
P_i	inorganic phosphate
PMF	proton motive force
POPC	1-palmitoyl-2-oleoyl-*sn*-glycero-3-phosphocholine
POPE	1-palmitoyl-2-oleoyl-*sn*-glycero-3-phosphoethanolamine
POPS	1-palmitoyl-2-oleoyl-*sn*-glycero-3-phospho-L-serine
PS	phosphatidylserine
PSLBs	pore-spanning lipid bilayers
ROI	region of interest
rpm	revolutions per minute
Sb 1-116	synaptobrevin 1-116 (also: VAMP-2, vesicle-associated membrane protein-2)
SD	standard deviation
SDCM	spinning disk confocal microscope / microscopy
SDS-PAGE	sodium dodecyl sulfate polyacrylamide gel electrophoresis

SNARE	soluble NSF attachment protein receptor
SNARF	seminaphthorhodafluor
TB	terrific broth
TEMED	*N*,*N*,*N*',*N*'-tetramethylethylendiamine
TIRFM	total internal reflection microscope / microscopy
Tris	tris(hydroxymethyl)aminomethane
Trp	tryptophan
Tyr	tyrosine

8.4 Chemicals and consumables

Aceton	Carl Roth GmbH, Karlsruhe, GER
ACMA	Sigma Aldrich, Taufkirchen, GER
Acrylamide/bisacrylamide (29:1, 30 %)	Carl Roth GmbH, Karlsruhe, GER
α-Methoxy-ω-amino PEG (2,000 Da)	Rapp Polymere GmbH, Tübingen, GER
Ampicillin	Carl Roth GmbH, Karlsruhe, GER
APS	Sigma Aldrich, Taufkirchen, GER
ATP sodium salt	Sigma Aldrich, Taufkirchen, GER
α-amino-ω-biotin-PEG (3,000 Da)	Rapp Polymere GmbH, Tübingen, GER
Bio-Beads SM-2 Resin	Bio-Rad Laboratories GmbH, München, GER
BSA, protease free	Carl Roth GmbH, Karlsruhe, GER
Cap-biotin-DOPE	Avanti Polar Lipids, Alabaster, USA
CCCP	Fluka Chemie GmbH, Seelze, GER
Chloroform	VWR, Darmstadt, GER
Cholesterol	Sigma-Aldrich, Taufkirchen, GER

Complete-mini, EDTA-free	Roche, Mannheim, GER
Coomassie Brillian Blue G250	Fluka Chemie GmbH, Seelze, GER
DDM	Carl Roth GmbH, Karlsruhe, GER
DMSO	Carl Roth GmbH, Karlsruhe, GER
DNase I	Applichem, Darmstadt, GER
DOPC	Avanti Polar Lipids, Alabaster, USA
DTT	Sigma Aldrich, Taufkirchen, GER
Ethanol, p.a.	VWR International, Darmstadt, GER
Glycerol, 87%	Merck, Darmstadt, GER
GOPTS	Sigma Aldrich, Taufkirchen, GER
HEPES	Carl Roth GmbH, Karlsruhe, GER
IPTG	Sigma Aldrich, Taufkirchen, GER
Isopropanol	Merck, Darmstadt, GER
KCl	Merck, Darmstadt, GER
KOH	Merck, Darmstadt, GER
Lysozyme	Carl Roth GmbH, Karlsruhe, GER
$MgCl_2 \cdot 6\,H_2O$	Merck, Darmstadt, GER
Methanol	Carl Roth GmbH, Karlsruhe, GER
MonoQ 5/50 column	GE Healthcare Europe, Freiburg, Germany
MOPS	Carl Roth GmbH, Karlsruhe, GER
NaCl	Merck, Darmstadt, GER
NeutrAvidin	Thermo Fisher Scientific, Waltham, MA, USA
*n*OG	Carl Roth GmbH, Karlsruhe, GER

Nycodenz	Axis-shield Alere Technologies AS, Oslo, NOR
Oregon Green 488-DHPE	Thermo Fisher Scientific, Waltham, USA
Oxygen	Air Liquide Deutschland GmbH, Düsseldorf, GER
Parafilm	Pechiney Plastic Packaging, Chicago, USA
Pierce TM BCA Protein Assay	Thermo Fisher Scientific, Waltham, USA
Polycarbonate membrane	Avestin, Ottawa, CAN
POPE	Avanti Polar Lipids, Alabaster, USA
POPS	Avanti Polar Lipids, Alabaster, USA
Pyranine	Acros Organics, New Jersey, USA
SDS	AppliChem GmbH, Darmstadt, GER
Sodium azide	Merck, Darmstadt, GER
TALON Metal Affinity Resin	Clontech, Takara Bio Europe, Saint-Germain-en-Laye, FRA
TEMED	Sigma Aldrich, Taufkirchen, GER
Texas Red DHPE	Sigma Aldrich, Taufkirchen, GER
Tryptone	Carl Roth GmbH, Karlsruhe, GER
Valinomycine	Sigma Aldrich, Taufkirchen, GER
Yeast extract	Carl Roth GmbH, Karlsruhe, GER

8.5 Devices

Protein isolation

ÄKTA Purifier 10	GE Healthcare Europe, Freiburg, GER
Centrifuge Allegra™ X-22R	Beckmann Coulter, Krefeld, GER
Centrifuge Sigma 3K30	Sigma Laborzentrifugen GmbH, Osterode am Harz, GER

Incubator shaker Innova 44	New Brunswick Scientific, Enfield, USA
Microfluidizer LM10	Microfluidics, Westwood, USA
Stuart Tube roller SRT 6	Cole-Parmer, Stone, UK
Thermomixer Compact	Eppendorf AG, Hamburg, GER
Microplate reader Biochrom® Anthos 2010	Anthos Mikrosysteme GmbH, Krefeld, GER
PerfectBlue™ Doppel-Gelsystem Twin S	Peqlab Biotechnologie GmbH, Erlangen, GER
power supply PowerPac 200	Bio-Rad Laboratories GmbH, München, GER

Protein reconstitution and characterization

LiposoFast-Basic	Avestin, Ottawa, CAN
Hamilton syringes	HAMILTON Bonaduz AG, Bonaduz, CHE
Zetasizer NanoS	Malvern Instruments, Herrenberg, GER
Ultracentrifuge Centrikon T-1065	Kontron Instruments, Rossdorf, GER
fluorescence spectrometer FP-6500	JASCO Germany GmbH, Groß-Umstadt, GER

PEGylation of glass slides

plasma cleaner Zepto LF PC	Diener electronic, Ebhausen, GER
Thermomixer Compact	Eppendorf AG, Hamburg, GER
Drying oven VWR Dry-Line	VWR International, Darmstadt, GER

Confocal laser scanning microscopy

BX60 WI, FluoView FV1200 confocal microscope	Olympus Deutschland GmbH, Hamburg, GER
sCMOS camera Zyla 5.5	Andor Technology Ltd., Belfast, UK

Spinning disc confocal laser microscopy

spinning disc unit: Yokogawa CSU-X	Rota Yokogawa GmbH &Co. KG, Wehr, Germany
AOTF: TF525-250-6-3-GH18A	Gooch & Housego PLC, Ilminster , UK

stand: custom, based on ix73	Olympus, Tokyo, JAP
piezo: P-721-CDQ	Physik Instrumente, Karlsruhe, GER
EM-CCD camera iXON 897Ultra	Andor Technology Ltd., Belfast, UK
Laser iBeam Smart 488-S	Toptica Photonics AG, Gräfeling, GER
Laser Cobolt Jive™	Cobolt AB, Solna, Sweden
filter wheel: Rotr	Andor Technology Ltd., Belfast, UK
filter: 496/LP BrightLine HC	AHF Analysentechnik AG, Tübingen, GER
Objective: UPlanSApo, 60×, 1.2 NA	Olympus, Hamburg, GER
Objective adapters: SM1A3TS and RMSA1	Thorlabs GmbH, Dachau/Munich, GER

8.6 Software

ImageJ	Version 1.45s, W. Rasband, NIH, USA, https://imagej.nih.gov/ij/
OriginPro 8.5G	OriginLab Cooperation, Northampton, USA
Matlab 2014a	MathWorks, Natick, USA

8.7 Calculation of ATPase molecules per vesicle

To estimate the average number of TF_0F_1-ATPase molecules per vesicle N_{ATPase}, the intensity-weighted mean diameter (95 nm, determined by DLS) and the protein/lipid ratio (p/l = 1:20,000, determined by Nycodenz density gradient centrifugation and quantification of lipid concentration) are needed. Furthermore, a bilayer thickness of h_{bilayer} = 4.5 nm, an area of a single ATPase of a_{protein} = 20 nm^2 and an average lipid area of a_{lipid} = 0.62 nm^2 were assumed.[122,134] The average area per lipid of the lipid mixture used was calculated from the individual areas per lipid, which were obtained from the CHARMM-GUI Membrane builder.[204]

$$N_{\mathrm{ATPase}} = N_{\mathrm{lipid}} \cdot \frac{p}{l}$$

Table 8-1. The average area per lipid of the lipid mixture used was calculated from the individual areas per lipid, which were obtained from the CHARMM-GUI Membrane builder.[204]

Lipid	Area/lipid
DOPC (50%)	69.7 Å^2
POPE (20%)	58.8 Å^2
POPS (10%)	60.4 Å^2
Cholesterol (20%)	40.0 Å^2
Average:	61.6 Å^2

The number of lipids per vesicle (N_{lipid}) is calculated with Eq. (S1), with A_{lipids} being the total area of all lipids contained in a vesicle and a_{lipid} being the average area of a single lipid. For calculation of A_{lipids}, the total protein area (A_{proteins}) is subtracted from the sum of the outer ($A_{\text{outer surface}}$) and the inner ($A_{\text{inner surface}}$) vesicle surface area.

$$N_{\text{lipid}} = \frac{A_{\text{lipids}}}{a_{\text{lipid}}} = \frac{A_{\text{outer surface}} + A_{\text{inner surface}} - A_{\text{proteins}}}{a_{\text{lipid}}} \tag{S1}$$

The outer vesicles surface is defined by $A_{\text{outer surface}} = \pi \cdot d_{\text{LUV}}^2$ and the inner surface by $A_{\text{inner surface}} = \pi \cdot \left(d_{\text{LUV}} - 2h_{\text{bilayer}}\right)^2$, with d_{LUV} being the diameter of the vesicle and h_{bilayer} the bilayer thickness.

The total protein area A_{proteins} is calculated from the area fraction of protein χ for a protein/lipid ratio of 1:20,000 and the sum of the outer and inner membrane area ($A_{\text{outer surface}}$ + $A_{\text{inner surface}}$).

$$\chi = \frac{a_{\text{protein}}}{a_{\text{protein}} + 20{,}000 \cdot a_{\text{lipid}}}$$

$$A_{\text{proteins}} = \chi \cdot \left(\pi \cdot d_{\text{LUV}}^2 + \pi \cdot \left(d_{\text{LUV}} - 2h_{\text{bilayer}}\right)^2\right)$$

Table 8-2. Results from calculation of TF_0F_1-ATPase molecules per 95 nm diameter vesicle. Four ATPase molecules are reconstituted into an average-sized vesicle.

$A_{\text{outer surface}}$ / nm^2	28,300
$A_{\text{inner surface}}$ / nm^2	23,200
χ	0.15 %
A_{proteins} / nm^2	79,2
A_{lipids} / nm^2	51,400
N_{lipid}	79,100
N_{protein}	4

8.8 Matlab Script

```
% Auswertung, die als input ein tif Bild benötigt, das ein
% Zeitstack ist. Es wird eine Automatische Erkennung der LUVs erstellt,
% welche anschließend durch eine Helligkeitsanalyse gelangt. Die Erkennung
% der LUVs findet im ersten frame statt und dessen Position wird für die
% gesammte Analyse verwedet.


%% Bildeinlesen und verarbeiten

clear

[filenam, newFolder, ~] = uigetfile({'*.tif'}, 'Select a file to analyze.');
filename=[newFolder filenam];
FinalImage=read_tiff(filename);

%%
Threshold=0.08; %Threshold für ROIs
Gausbreite1=1000;


I=FinalImage(:,:,1);
h1=figure(1);
imagesc(I);

h2=figure(2);
If=fftshift(fft2(I));
imagesc(log(abs(If)));

center=(size(I)./2)-0.5;

gm=gauss2d(If,Gausbreite1,center);
% gm2=gauss2d(If,500,center);
% gm=gm-gm2;

h3=figure(3);
imagesc(gm);


Ifg=If.*gm;
h4=figure(4);
imagesc(log(abs(Ifg)));

I2=ifft2(ifftshift(Ifg));
h5=figure(5);
imagesc(real(I2));

I3=real(I2);
I3=I3./max(max(I3));



Vesikelposition = pkfnd(I3,Threshold,5);
```

```
disp('filtered')

%h6=figure(6);
%Ibw=im2bw(I3,0.3);


figure(1)
hold on

plot(Vesikelposition(:,1),Vesikelposition(:,2),'rx')

for k=1:length(Vesikelposition)
    text(Vesikelposition(k,1),Vesikelposition(k,2),num2str(k),'Color','r','Fontsize',11)
end
hold off

%%
oldfolder=cd;
cd(newFolder);
saveas(1,'Positionen_der_Frames.png','png')
%template=imcrop(h5);
%c=normxcorr2(template,I3);
Roigroesse=6;
% Maske erstellen ohne Rois
Maske=ones(size(FinalImage,1),size(FinalImage,2));
for k=1:length(Vesikelposition)
        if Vesikelposition(k,2)<=Roigroesse && Vesikelposition(k,1)<=Roigroesse
            Maske(1:Vesikelposition(k,2)+Roigroesse,1:Vesikelposition(k,1)+Roigroesse)=0;
        elseif Vesikelposition(k,2)<=Roigroesse && Vesikelposition(k,1)>= size(Maske,2)-Roigroesse
            Maske(1:Vesikelposition(k,2)+Roigroesse,Vesikelposition(k,1)-Roigroesse:end)=0;
        elseif Vesikelposition(k,2)>=size(Maske,1)-Roigroesse && Vesikelposition(k,1)>= size(Maske,2)-Roigroesse
            Maske(Vesikelposition(k,2)-Roigroesse:end,Vesikelposition(k,1)-Roigroesse:end)=0;
        elseif Vesikelposition(k,2)>=size(Maske,1)-Roigroesse && Vesikelposition(k,1)<=Roigroesse
            Maske(Vesikelposition(k,2)-Roigroesse:end,1:Vesikelposition(k,1)+Roigroesse)=0;
        elseif Vesikelposition(k,2)<=Roigroesse
            Maske(1:Vesikelposition(k,2)+Roigroesse,Vesikelposition(k,1)-Roigroesse:Vesikelposition(k,1)+Roigroesse)=0;
        elseif Vesikelposition(k,2)>=size(Maske,1)-Roigroesse
            Maske(Vesikelposition(k,2)-Roigroesse:end,Vesikelposition(k,1)-Roigroesse:Vesikelposition(k,1)+Roigroesse)=0;
        elseif Vesikelposition(k,1)<=Roigroesse
            Maske(Vesikelposition(k,2)-Roigroesse:Vesikelposition(k,2)+Roigroesse,1:Vesikelposition(k,1)+Roigroesse)=0;
        elseif Vesikelposition(k,1)>=size(Maske,2)-Roigroesse
            Maske(Vesikelposition(k,2)-Roigroesse:Vesikelposition(k,2)+Roigroesse,Vesikelposition(k,1)-Roigroesse:end)=0;
        else
            Maske(Vesikelposition(k,2)-Roigroesse:Vesikelposition(k,2)+Roigroesse,Vesikelposition(k,1)-Roigroesse:Vesikelposition(k,1)+Roigroesse)=0;
        end
end

%% Auswertung der Rois

Roigroesse=3; % Der Roi ist doppelte Größe +1; Roigroesse bisher=3
Eingabefuerstruck=cell(length(Vesikelposition),1);
for l=1:length(Vesikelposition)
    Eingabefuerstruck{l}=zeros(size(FinalImage,3),1);
end
for l=1:size(FinalImage,3)
    Bild=FinalImage(:,:,l);
    Meanwert=mean(Bild(find(Maske)));
    FinalImage(:,:,l)=Bild-Meanwert;
end
%%
Vesikel=struct('RohIntensity',Eingabefuerstruck,'SGolayIntensity',Eing-
abefuerstruck,'NormIntensity',Eingabefuerstruck,'SGolayNormIntensi-
ty',Eingabefuerstruck,'Positionx',cell(length(Vesikelposition),1),'Posit
iony',cell(length(Vesikelposition),1));
for k=1:length(Vesikelposition)
    for l=1:size(FinalImage,3)
        if Vesikelposition(k,2)<=Roigroesse && Vesikelposi-
tion(k,1)<=Roigroesse
            Vesikel(k).RohIntensity(l,1)=sum(sum(Fi-
nalImage(1:Vesikelposition(k,2)+Roigroesse,1:Vesikelposi-
tion(k,1)+Roigroesse,l)));
        elseif Vesikelposition(k,2)<=Roigroesse && Vesikelposi-
tion(k,1)>= size(FinalImage(:,:,l),2)-Roigroesse
            Vesikel(k).RohIntensity(l,1)=sum(sum(Fi-
nalImage(1:Vesikelposition(k,2)+Roigroesse,Vesikelposition(k,1)-
Roigroesse:end,l)));
        elseif Vesikelposition(k,2)>=size(FinalImage(:,:,l),1)-
Roigroesse && Vesikelposition(k,1)>= size(FinalImage(:,:,l),2)-
Roigroesse
            Vesikel(k).RohIntensity(l,1)=sum(sum(FinalImage(Vesikelposi-
tion(k,2)-Roigroesse:end,Vesikelposition(k,1)-Roigroesse:end,l)));
        elseif Vesikelposition(k,2)>=size(FinalImage(:,:,l),1)-
Roigroesse && Vesikelposition(k,1)<=Roigroesse
            Vesikel(k).RohIntensity(l,1)=sum(sum(FinalImage(Vesikelposi-
tion(k,2)-Roigroesse:end,1:Vesikelposition(k,1)+Roigroesse,l)));
        elseif Vesikelposition(k,2)<=Roigroesse
            Vesikel(k).RohIntensity(l,1)=sum(sum(Fi-
nalImage(1:Vesikelposition(k,2)+Roigroesse,Vesikelposition(k,1)-
Roigroesse:Vesikelposition(k,1)+Roigroesse,l)));
        elseif Vesikelposition(k,2)>=size(FinalImage(:,:,l),1)-
Roigroesse
            Vesikel(k).RohIntensity(l,1)=sum(sum(FinalImage(Vesikelposi-
tion(k,2)-Roigroesse:end,Vesikelposition(k,1)-Roigroesse:Vesikelposi-
tion(k,1)+Roigroesse,l)));
        elseif Vesikelposition(k,1)<=Roigroesse
            Vesikel(k).RohIntensity(l,1)=sum(sum(FinalImage(Vesikelposi-
tion(k,2)-Roigroesse:Vesikelposition(k,2)+Roigroesse,1:Vesikelposi-
tion(k,1)+Roigroesse,l)));
        elseif Vesikelposition(k,1)>=size(FinalImage(:,:,l),2)-
Roigroesse
            Vesikel(k).RohIntensity(l,1)=sum(sum(FinalImage(Vesikelposi-
tion(k,2)-Roigroesse:Vesikelposition(k,2)+Roigroesse,Vesikelposi-
tion(k,1)-Roigroesse:end,l)));
```

```
        else
            Vesikel(k).RohIntensity(1,1)=sum(sum(FinalImage(Vesikelposi-
tion(k,2)-Roigroesse:Vesikelposition(k,2)+Roigroesse,Vesikelposi-
tion(k,1)-Roigroesse:Vesikelposition(k,1)+Roigroesse,1)));
        end
    end
    Vesikel(k).Positionx=Vesikelposition(k,1);
    Vesikel(k).Positiony=Vesikelposition(k,2);
end

%% Darstellen der Vesikel und Bearbeitung der Kurve

clearvars -except Vesikel filenam oldfolder newFolder
Polynomsgol=3;
Bandbreitesgol=5;
Bandbreitemdfilt1=4;
Normierungsbereich=41:42;
for k=1:length(Vesikel)
    Vesikel(k).NormIntensity=Vesikel(k).RohIntensity./mean(Vesi-
kel(k).RohIntensity(Normierungsbereich));
    Vesikel(k).SGolayIntensity=sgolayfilt(Vesikel(k).RohIntensity,Poly-
nomsgol,Bandbreitesgol);
    Vesikel(k).Medfilt1Intensity=medfilt1(Vesikel(k).RohIntensity,Band-
breitemdfilt1);
    Vesikel(k).Medfilt1Intensitynorm=Vesikel(k).Medfilt1Inten-
sity/mean(Vesikel(k).Medfilt1Intensity(Normierungsbereich));
    Vesikel(k).phwert=6.26+log10((Vesikel(k).Medfilt1Intensitynorm-
0.59)./(1.04-Vesikel(k).Medfilt1Intensitynorm));
    Vesikel(k).DELTApH=((Vesikel(k).phwert)-7.3);
    Vesikel(k).Zeitachse=((1:size(Vesikel(k).RohIntensity,1))-41)';
    Vesikel(k).Zeitachse(36:40)=nan;
    Vesikel(k).Zeitachse(89:94)=nan;

    plotfigure=figure(8);
    plot(1:size(Vesikel(k).Zeitachse),Vesikel(k).RohIntensity,'-r')
    hold on
    plot(1:size(Vesikel(k).Medfilt1Intensity,1),Vesikel(k).Medfilt1In-
tensity,'-b')
    hold off
    title([num2str(k,'%4.0f%')],'Fontsize',18);
    set(gca,'FontSize',12)
    xlabel('frame number','Fontsize',14,'FontAngle','italic')
    ylabel('I','Fontsize',14,'FontAngle','italic')
    saveas(plotfigure,['Int_Roi' num2str(k,'%04.0f%') '_' filenam(1:end-
4) '.png'],'png')

    plotfigurenorm=figure(9);
    plot(Vesikel(k).Zeitachse,Vesikel(k).Medfilt1Intensitynorm,'-b')
    title([num2str(k,'%4.0f%')],'Fontsize',18);
    set(gca,'FontSize',12)
    xlabel('frame number','Fontsize',14,'FontAngle','italic')
    ylabel('I/I_0','Fontsize',14,'FontAngle','italic')
    saveas(plotfigurenorm,['Norm_Roi_' num2str(k,'%04.0f%') '_' file-
nam(1:end-4) '.png'],'png')

    plotfigure=figure(10);
    plot(Vesikel(k).Zeitachse,Vesikel(k).DELTApH,'-r')
    title([num2str(k,'%4.0f%')],'Fontsize',18);
    set(gca,'FontSize',12)
    xlabel('frame number','Fontsize',14,'FontAngle','italic')
    ylabel('pH-Value','Fontsize',14,'FontAngle','italic')
    saveas(plotfigure,['pH_Roi_' num2str(k,'%04.0f%') '_' filenam(1:end-
4) '.png'],'png')



    Speicherdaten=[Vesikel(k).Zeitachse,Vesikel(k).RohInten-
sity,Vesikel(k).SGolayIntensity,Vesikel(k).NormIntensity,Vesikel(k).Med-
filt1Intensity,Vesikel(k).Medfilt1Intensitynorm,Vesikel(k).phwert,Vesike
l(k).DELTApH];
    save(['Auswertung_' filenam(1:end-4) '_' num2str(k,'%04.0f%')
'.txt'],'Speicherdaten','-ascii');
end

save(['Auswertung_' filenam(1:end-4) '.mat'],'Vesikel','Poly-
nomsgol','Bandbreitesgol','Bandbreitemdfilt1','Normierungsbereich');


%%
cd(oldfolder);
```

Curriculum vitae

Miriam Schwamborn

Born on January 8th, 1988 in Göttingen

Citizenship: German

Education

since 12/2012	**Ph.D. thesis** at the Institute of Biomolecular und Organic Chemistry, Georg August University Göttingen (Prof. Dr. C. Steinem) Title of thesis: *Establishment of a fluorescence assay for characterization of protein-mediated vesicle fusion and acidification*
10/2010 – 09/2012	**Graduate studies** in chemistry at the Georg August University Göttingen (Prof. Dr. C. Steinem) Title of the Master‘s thesis: *Charakterisierung der Bindung von F-Aktin an Ezrin mittels Oberflächenplasmonenresonanzspektroskopie*
10/2007 – 08/2010	**Undergraduate studies** in chemistry at the Georg August University Göttingen (Prof. Dr. A. Janshoff) Title of the Bachelor’s thesis: *Herstellung und Charakterisierung von großen unilamellaren Vesikeln*
06/2007	Abitur at the Felix-Klein-Gymnasium in Göttingen

Scientific contributions

2016	M. Schwamborn, J. Schumacher, J. Sibold, N. K. Teiwes & C. Steinem, Monitoring ATPase induced pH changes in single proteoliposomes with the lipid-coupled fluorophore Oregon Green 488, A*nalyst* **2017**, accepted, DOI: 10.1039/C7AN00215G.
09/2014	3rd CRC 803 Symposium, Göttingen. *Active proton transport across lipid bilayers: Insertion of ATPase into model membranes by SNARE-mediated fusion*
09/2014	Annual Meeting of the German Biophysical Society, Lübeck. *Generation of proton gradients across lipid bilayers by active transport*

03/2014	Molecular Membrane Biophysics, Hünfeld. *Protein Mediated Proton Transport Across Pore-Spanning Membranes*
07/2013	9th European Biophysics Congress, Lisbon. *Bacteriorhodopsin and ATP-synthase create proton gradients in atto- to picoliter sized compartments*

Danksagung

An erster Stelle bedanke ich mich bei Prof. Dr. Claudia Steinem für die wissenschaftliche Betreuung meiner Doktorarbeit. Die hilfreichen Gespräche und Diskussionen haben mich immer vorangebracht und neu motiviert.

Prof. Dr. Mikael Simons danke ich für die Übernahmen des Korreferats und die guten Ratschläge in den Thesis Committees.

Besonders bedanken möchte ich mich bei Johannes und Jeremias für ihre große Hilfe bei der Etablierung des *Single Vesicle Assays*. Ohne deine Konstruktionsfähigkeiten, Johannes, wären die Messungen niemals innerhalb so kurzer Zeit zustande gekommen. Und ohne deine Matlab Kenntnisse, Jeremias, hätte ich für die Auswertung der Experimente Ewigkeiten gebraucht.

Auch Niko möchte in besonderem Maße danken. Während deiner Praktikums-, Bachelorarbeits- und Hiwi-Zeit sind im Dialog sehr wertvolle Ideen entstanden, die maßgeblich zu dieser Arbeit beigetragen haben.

Nelli, dir danke ich für das Durchhaltevermögen und die Geduld in deiner Bachelorarbeit und dafür, dass wir die ersten Schritte meiner Arbeit quasi zusammen bewältigt haben.

Bei Micha und insbesondere Jutta bedanke ich mich herzlich für die Unterstützung bei all den grundlegenden Laborarbeiten und Experimenten. Ohne euch wäre ein so angenehmes Arbeiten nicht möglich gewesen.

Lando, Raphael und Jan gilt mein Dank für die Bereitstellung der SNARE-Proteine und die Einführung in die Fusionsexperimente.

Martin danke ich für seine wertvolle Hilfe bezüglich der Fluoreszenzmikroskopie und für die oft aufschlussreichen Diskussionen.

Für die angenehme Atmosphäre und kollegiale Unterstützung in den Lehramts- und Mediziner-Praktika bedanke ich mich bei Ole, Markus, Jutta, Micha und Hans-Peter.

Meinen herzlichen Dank an alle Kollegen, die meine Arbeit korrekturgelesen haben und natürlich an den gesamten Arbeitskreis und die Kolleginnen aus dem Sekretariat für die wirklich tolle Atmosphäre und die große Hilfsbereitschaft! Die vielen schönen Stunden außerhalb der Arbeitszeit mit euch haben mich nach Rückschlägen im Laboralltag immer wieder aufgemuntert. An dieser Stelle möchte ich mich auch besonders bei Ingo und seiner Familie bedanken.

Meiner Familie und Jan danke ich von ganzem Herzen dafür, dass ihr mich immer unterstützt und mir mit Rat und Tat bei Seite steht. Es macht mich sehr glücklich zu wissen, dass ihr immer hinter mir steht.